Journal of Volcanology and Geothermal Research 311 (2016) 99–134

Contents lists available at ScienceDirect

Journal of Volcanology and Geothermal Research

journal homepage: www.elsevier.com/locate/jvolgeores

Review

Multi-decadal satellite measurements of global volcanic degassing

S.A. Carn [a,b,*], L. Clarisse [c], A.J. Prata [d]

[a] Department of Geological and Mining Engineering and Sciences, Michigan Technological University, Houghton, MI 49931, USA
[b] Department of Mineral Sciences, National Museum of Natural History, Smithsonian Institution, Washington, DC 20560, USA
[c] Spectroscopie de l'Atmosphère, Service de Chimie Quantique et Photophysique, Université Libre de Bruxelles, Brussels, Belgium
[d] Nicarnica Aviation AS, Kjeller, Norway

ARTICLE INFO

Article history:
Received 4 August 2015
Accepted 4 January 2016
Available online 14 January 2016

Keywords:
Satellite remote sensing
Volcanic SO_2 emissions
Volcanic degassing
Volcanic eruptions
Volcanic plumes
Volcanic clouds

ABSTRACT

Satellite instruments have been providing measurements of global volcanic emissions of sulfur dioxide (SO_2) since 1978, based on observations in the ultraviolet (UV), infrared (IR) and microwave spectral bands. We review recent advances in satellite remote sensing of volcanic gases, focusing on increased instrument sensitivity to tropospheric SO_2 emissions and techniques to determine volcanic plume altitude. A synthesis of ~36 years of global UV, IR and microwave satellite measurements yields an updated assessment of the volcanic SO_2 flux to the upper troposphere and lower stratosphere (UTLS) between 1978 and 2014 (~1–2 Tg/yr). The present availability of multiple UV and IR satellite SO_2 products provides increased confidence in calculated SO_2 loadings for many eruptions. We examine the temporal and latitudinal distribution of volcanic SO_2 emissions and reassess the relationship between eruptive SO_2 discharge and eruption magnitude, finding a first-order correlation between SO_2 emission and volcanic explosivity index (VEI), but with significant scatter. Based on the observed SO_2-VEI relation, we estimate the fraction of eruptive SO_2 emissions released by the smallest eruptions (~0.48 Tg/yr), which is not recorded by satellite observations. A detailed breakdown of the sources of measured SO_2 emissions reveals intuitively expected correlations between eruption frequency, SO_2 loading and volcanic degassing style. We discuss new constraints on e-folding times for SO_2 removal in volcanic plumes, and highlight recent measurements of volcanic hydrogen chloride (HCl) injections into the UTLS. An analysis of passive volcanic emissions of SO_2 detected in Ozone Monitoring Instrument (OMI) SO_2 data since 2004 provides new insight into the location and stability of the dominant sources of volcanic SO_2 over the past decade. Since volcanic SO_2 emissions constitute a random, highly variable perturbation to the atmosphere-climate system, continued monitoring of volcanic SO_2 emissions from space by multiple UV and IR instruments to extend the current multi-decadal record is essential, and near-global, geostationary measurements of SO_2 may be available by the end of the current decade.

Contents

* Corresponding author at: Department of Geological and Mining Engineering and Sciences, Michigan Technological University, Houghton, MI 49931, USA.
E-mail address: scarn@mtu.edu (S.A. Carn).

http://dx.doi.org/10.1016/j.jvolgeores.2016.01.002

1. Introduction

Since the first satellite observation of volcanic sulfur dioxide (SO_2) emissions, made after the major eruption of El Chichón (Mexico) in 1982 (Krueger, 1983; Krueger et al., 2008), satellites have provided unique and critical observations of global volcanic degassing. Prior to the satellite remote sensing era, which for SO_2 measurements began in 1978 with the launch of the first Total Ozone Mapping Spectrometer (TOMS; Krueger, 1983; Krueger et al., 1995) and TIROS Operational Vertical Sounder (TOVS) instruments (Prata et al., 2003), the variability of sulfur emissions from volcanic eruptions was very poorly understood, aside from what could be gleaned from early glaciochemical studies of ice cores (Hammer, 1977; Hammer et al., 1980). Satellite measurements provided unique constraints on the vast SO_2 clouds discharged by the major eruptions of El Chichón in 1982 and Pinatubo (Philippines) and Cerro Hudson (Chile) in 1991 (Krueger, 1983; Doiron et al., 1991; Bluth et al., 1992; Schneider et al., 1999; Constantine et al., 2000; Guo et al., 2004; Krueger et al., 2008), spawning a paradigm shift in our understanding of the petrological origins of 'excess sulfur' emissions (e.g., Luhr et al., 1984; Westrich and Gerlach, 1992; Wallace and Gerlach, 1994; Scaillet et al., 2003; Oppenheimer et al., 2011; Wallace and Edmonds, 2011). More recently, improvements in instrument sensitivity have extended the capabilities of satellite measurements to include smaller eruptions, tropospheric SO_2 emissions (e.g., passive volcanic degassing) and other minor volatile species present in volcanic emissions such as hydrogen sulfide (H_2S), hydrogen chloride (HCl), bromine monoxide (BrO) and chlorine dioxide (OClO) (e.g., Eisinger and Burrows, 1998; Carn et al., 2008b; Theys et al., 2009; Clarisse et al., 2011a,b; Carn et al., 2013; Theys et al., 2014; Carn, 2015a).

Oppenheimer et al. (2011) review the significance of volcanic sulfur emissions for volcano monitoring and their wide-ranging impacts on several facets of the Earth system, including atmospheric chemistry and climate, terrestrial and aquatic environments, and human and animal health. In the context of satellite measurements, which are global in scope and provide unique observations of the largest volcanic SO_2 clouds, the primary motivation for monitoring volcanic SO_2 emissions is their potential impact on atmospheric chemistry and climate (e.g., Robock, 2000). Many of the relevant science questions that we can address using satellite measurements of volcanic degassing have been outlined by the Stratospheric Sulfur and its Role in Climate (SSiRC; http://www.sparc-ssirc.org/) working group, part of the World Climate Research Program's (WCRP's) Stratosphere-Troposphere Processes and their Role in Climate (SPARC) project. Current research foci include: the stratospheric sulfur burden and its partitioning between sulfur species including SO_2, aerosol, H_2SO_4, and OCS, etc.; trends in stratospheric aerosol optical depth (SAOD) and the major SAOD forcing mechanisms; the nature of 'background' stratospheric aerosol (e.g., Deshler et al., 2006; Nagai et al., 2010; Solomon et al., 2011); the role of minor volcanic eruptions in modulating the stratospheric sulfur burden, particularly since the 1991 Pinatubo eruption; trends in emissions of aerosol precursor gases (e.g., SO_2); and the time-constant for SO_2 to H_2SO_4 conversion in SO_2-rich volcanic plumes. In order to address these questions, we require measurements of aerosol precursor gases (including SO_2 and OCS) and analyses of their temporal variability. Monitoring stratospheric injections of sulfur by volcanic eruptions is of prime importance, though quantification of tropospheric volcanic sulfur emissions is also needed since tropospheric sulfur can cross the tropopause via other mechanisms such as deep tropical convection (e.g., Sheng et al., 2015).

Continuous monitoring of volcanic injections of SO_2 into the upper troposphere and lower stratosphere (UTLS) is also required to assess the potential impacts of, and need for, geoengineering of Earth's climate (specifically, the branch of geoengineering referred to as solar radiation management). Injection of sulfate aerosol precursors into the stratosphere, mimicking volcanic forcing of climate, has been proposed to mitigate the impacts of anthropogenic global warming (e.g., Crutzen, 2006; Wigley, 2006; Robock et al., 2009). Accurate characterization of the time-averaged volcanic SO_2 flux into the stratosphere is crucial in this regard, and analyses of volcanic eruptions of varying magnitude provide unique insights into the behavior of SO_2 in the UTLS after injection. Recently, volcanic influence on the post-Pinatubo stratosphere has been scrutinized in considerable detail in order to establish the cause of the reduced rate of global warming observed in global mean surface temperatures over the last decade (dubbed the global warming 'hiatus'). A particular focus has been the role of 'small' volcanic eruptions, or those with a volcanic explosivity index (VEI; Newhall and Self, 1982) below 5. Although alternative causes and even the very existence of the global warming hiatus are subject to ongoing debate (e.g., Schmidt et al., 2014; Steinman et al., 2015; Karl et al., 2015), several studies have concluded that SAOD perturbations by small volcanic eruptions not included in pre-hiatus climate model simulations have likely played a role (e.g., Solomon et al., 2011; Vernier et al., 2011; Neely et al., 2013; Ridley et al., 2014; Santer et al., 2014, 2015). But regardless of the dominant forcing factors influencing recent trends in global warming, it remains crucial to monitor volcanic degassing and quantify SO_2 and other volcanic gas fluxes into the atmosphere.

In this contribution we review the current state of our knowledge of volcanic degassing (primarily focused on SO_2 emissions) based on multi-decadal satellite measurements since 1978, which have been collated in a new volcanic SO_2 emissions database (Carn, 2015c). This review discusses both the volcanological and atmospheric applications of the SO_2 emissions database. We do not offer a detailed overview of any specific volcanic eruptions, but instead synthesize ~36 years of satellite observations and augment previous compilations of satellite SO_2 data for volcanic eruptions (e.g., Bluth et al., 1993, 1997; Carn et al., 2003) and estimates of global volcanic SO_2 emissions (e.g., Kellogg et al., 1972; Cadle, 1975; Berresheim and Jaeschke, 1983; Le Guern, 1982; Stoiber et al., 1987; Spiro et al., 1992; Andres and Kasgnoc, 1998; Halmer et al., 2002; Diehl et al., 2012), incorporating a significant amount of new data on smaller eruptions and passive degassing collected since 2004. The paper is organized as follows. Firstly (Section 2), we briefly review recent developments in satellite remote sensing of volcanic gases, focusing on improvements in instrument sensitivity and in techniques to determine volcanic plume altitude. In Section 3 we describe the ultraviolet (UV), infrared (IR) and microwave satellite datasets used to generate the multi-decadal volcanic SO_2 emissions database. The main results are presented in Section 4, including the temporal and latitudinal distribution of volcanic SO_2 emissions, updated estimates of the annual volcanic SO_2 flux from volcanic eruptions (including the fraction not recorded by satellite

observations) and a reassessment of the relationship between eruptive SO_2 discharge and eruption magnitude (VEI). We also provide a detailed breakdown of the sources of the measured SO_2 emissions and attempt to classify them based on degassing style. New constraints on e-folding times for SO_2 removal in volcanic plumes are discussed, and we also highlight recent measurements of volcanic HCl injections into the UTLS. An analysis of the major sources of passive volcanic emissions of SO_2 detected in satellite data is presented in Section 4.2, followed by a discussion (Section 5) and conclusions.

2. Satellite measurements of volcanic gases

Although to date no satellite instrument has been deployed to specifically target volcanic emissions, passive UV, IR and microwave sensors have been used to measure seven volcanic gas species since 1978 (SO_2, H_2S, HCl, CO, BrO, OClO and CH_3Cl; Table 1). However, SO_2 is by far the most frequently measured volcanic gas, and it is currently not possible to measure other volcanic gases from space with comparable accuracy or frequency to that of SO_2. It is the major target for remote

Table 1
Volcanic gases measured or potentially detectable from space.

	Volatile species										
Sensor[a]	H_2O	CO_2	CO	SO_2	H_2S	HCl	BrO	OClO	CH_3Cl	Timespan	Reference(s)[b]
TOMS*										1978–2005	1, 2
SBUV* (P)										1978–present	3, 4
HIRS*										1978–present	5
GOME										1995–2003	6, 7, 8, 9
MODIS*										1999–present	10, 11
ASTER										1999–present	12, 13, 14
MOPITT										1999–present	15
SCIAMACHY (L)										2002–2012	8, 16, 17, 18
MIPAS (L)										2002–2012	19
AIRS										2002–present	20, 21
ACE (L)										2003–present	22
SEVIRI										2004–present	23
OMI										2004–present	18, 24, 25, 26
MLS* (L)										1991–2001; 2004–present	27, 28, 29, 30
TES (P)										2004–present	31
GOME–2*										2006–present	18, 32, 33, 34
IASI*										2006–present	15, 35, 36
OMPS*										2011–present	37
VIIRS										2011–present	38
CrIS										2011–present	39
AHI										2015–present	40
GOSAT (P)										2009–present	41
OCO–2										2014–present	42

Red = detected in a volcanic cloud; *Light gray* = potentially detectable but not yet proven in a volcanic context and/or not viable for routine volcanic measurements (e.g., due to background interference).

a. Sensor acronyms: TOMS: Total Ozone Mapping Spectrometer; SBUV: Solar Backscatter Ultraviolet Instrument; HIRS: High-resolution Infrared Radiation Sounder; GOME: Global Ozone Monitoring Experiment; MODIS: Moderate resolution Imaging Spectroradiometer; ASTER: Advanced Spaceborne Thermal Emission and Reflection Radiometer; MOPITT: Measurements of Pollution in the Troposphere; SCIAMACHY: Scanning Imaging Absorption Spectrometer for Atmospheric Chartography; MIPAS: Michelson Interferometer for Passive Atmospheric Sounding; AIRS: Atmospheric Infrared Sounder; ACE: Atmospheric Chemistry Experiment; SEVIRI: Spinning Enhanced Visible and Infrared Imager; OMI: Ozone Monitoring Instrument; MLS: Microwave Limb Sounder; TES: Tropospheric Emission Spectrometer; IASI: Infrared Atmospheric Sounding Interferometer; OMPS: Ozone Mapping and Profiler Suite; VIIRS: Visible Infrared Imaging Radiometer Suite; CrIS: Cross-track Infrared Sounder; AHI: Advanced Himawari Imager; GOSAT: Greenhouse Gases Observing Satellite; OCO-2: Orbiting Carbon Observatory 2.

* = Sensor flown (or to be flown) on multiple satellites; P: nadir profiling and/or pointable instrument (limited mapping capability); L: limb instrument (vertical profiling); all other instruments provide some spatial mapping capability (SCIAMACHY provided nadir and limb observations).

b. 1. Krueger et al. (1995); 2. Krueger et al. (2000); 3. McPeters et al. (1984); 4. McPeters (1993); 5. Prata et al. (2003); 6. Eisinger and Burrows (1998); 7. Thomas et al. (2005); 8. Afe et al. (2004); 9. Noël et al. (1999); 10. Watson et al. (2004); 11. Corradini et al. (2009); 12. Urai (2004); 13. Pugnaghi et al. (2006); 14. Campion et al. (2010); 15. Martínez-Alonso et al. (2012); 16. Noël et al. (2004); 17. Lee et al. (2008); 18. Theys et al. (2014); 19. Höpfner et al. (2013); 20. Carn et al. (2005); 21. Prata and Bernardo (2007); 22. Doeringer et al. (2012); 23. Prata and Kerkmann (2007); 24. Krotkov et al. (2006); 25. Yang et al. (2007); 26. Carn et al. (2013); 27. Read et al. (1993); 28. Prata et al. (2007); 29. Pumphrey et al. (2015); 30. W.G. Read, pers. Comm.; 31. Clerbaux et al. (2008); 32. Noël et al. (2008); 33. Rix et al. (2009); 34. Theys et al. (2009); 35. Clarisse et al. (2008); 36. Clarisse et al. (2011a,b); 37. Carn et al. (2015); 38. V.J. Realmuto, pers. Comm.; 39: Gambacorta and Barnet (2013); 40. Carn (2015a); 41. Schwandner and Carn (2011); 42. Schwandner et al. (2015).

sensing due to its ease of measurement relative to the dominant volcanic volatile species, which are typically water vapor (H_2O) and carbon dioxide (CO_2). The characteristics of SO_2 that enable space-based measurements over at least 5 orders of magnitude in atmospheric column amount (without spatial or temporal data averaging) are its relative abundance in volcanic emissions (typically 2nd or 3rd after H_2O and CO_2; e.g., Oppenheimer et al., 2011), low background SO_2 concentrations away from strong anthropogenic point sources (power plants and metal smelters; Carn et al., 2007), and the accessibility of absorption bands for remote sensing in the UV, IR and microwave spectral regions. The relatively high emission altitude (cf. anthropogenic sources) and consequent atmospheric lifetime of volcanic SO_2 (typically hours to days) is also conducive to satellite measurements, the latter being sufficiently long to enable detection and tracking of volcanic SO_2 plumes despite the large spatial scale of satellite sensor footprints, but short enough to prevent significant accumulation in the atmosphere and interference with fresh emissions (in contrast to CO_2). To date, the only point sources of anthropogenic SO_2 emissions observed to rival volcanic SO_2 plumes in terms of signal strength have been metal smelters (e.g., Khokhar et al., 2005; Carn et al., 2007; Walter et al., 2012; Bauduin et al., 2014) and rare sulfur fires (Carn et al., 2004; Kearney et al., 2009), although, on a global scale, estimated total anthropogenic sulfur emissions may exceed volcanic sulfur emissions by up to an order of magnitude, with significant uncertainty (e.g., Chin and Jacob, 1996; Graf et al., 1997; Andres and Kasgnoc, 1998). The main impediment to detection of volcanic CO_2 and H_2O emissions from space is the small volcanic contributions relative to the ambient atmospheric concentrations of these molecules (e.g., Gerlach, 2011). Whilst the detection of volcanic CO_2 from space has not yet been conclusively demonstrated, it is likely to occur as more data from instruments providing CO_2 retrievals, including GOSAT, OCO-2, SCIAMACHY, AIRS and IASI (Table 1), are analyzed (e.g., Schwandner and Carn, 2011; Schwandner et al., 2015). But, although several operational sensors retrieve profiles of atmospheric water vapor (Table 1), satellite detection of volcanic H_2O is extremely unlikely due to even greater background interference than for CO_2, with the possible exception of volcanic H_2O injections into the dry stratosphere.

Satellite remote sensing of SO_2 exploits the molecule's absorption bands at UV, IR and microwave wavelengths (e.g., Carn, 2015a). Somewhat fortuitously, the overlap of SO_2 absorption features in the UV and IR with spectral regions used to retrieve higher priority measurements or atmospheric constituents (e.g., ozone, water vapor, clouds and surface temperature) has ensured that most operational satellite instruments have included channels suitable for SO_2 detection. UV measurements utilize SO_2 absorption bands at wavelengths of 300–340 nm, in the Huggins ozone absorption band; hence ozone and SO_2 must be retrieved simultaneously and large column amounts of ozone can impact the sensitivity of UV measurements to lower tropospheric or boundary layer SO_2 (e.g., Krotkov et al., 2008). IR measurements of SO_2 can exploit three vibrational absorption bands in the thermal IR at ~4 μm ($\nu_1 + \nu_3$-band), ~7.3 μm (ν_3-band) and ~8.6 μm (ν_1-band). Of these, the 7.3 μm band is most often used since it is the stronger band (providing greater sensitivity), is less susceptible to interference by volcanic ash (e.g., Corradini et al., 2009), and provides sensitive measurements of SO_2 in the upper troposphere and above (e.g., Rinsland et al., 1995; Prata et al., 2003; Carn et al., 2005; Prata and Bernardo, 2007; Clarisse et al., 2008, 2012; Doeringer et al., 2012; Höpfner et al., 2013). It lacks sensitivity to lower tropospheric SO_2 (<3–5 km altitude; i.e., small eruptions and passive degassing) notwithstanding relatively rare coincidences of surface temperature inversions, extreme pollution levels and low humidity (e.g., Boynard et al., 2014; Bauduin et al., 2014). The typically poor sensitivity to lower tropospheric SO_2 at 7.3 μm is due to interference from water vapor absorption, but this also simplifies retrievals somewhat since the background 7.3 μm radiation originates from relatively homogeneous (on the scale of a volcanic cloud) lower tropospheric water vapor. The 4 μm and 8.6 μm bands are weaker but are situated in atmospheric windows, allowing retrieval of lower tropospheric SO_2, but with the added complexity of dependence on variable background emissivity, especially over land (e.g., Realmuto et al., 1994, 1997; Teggi et al., 1999; Realmuto, 2000; Watson et al., 2004; Prata and Bernardo, 2007; Prata and Kerkmann, 2007; Kearney et al., 2008), atmospheric water vapor (Realmuto and Worden, 2000), daytime solar reflection at 4 μm, and interference from volcanic ash at 8.6 μm (Corradini et al., 2009). Microwave limb sounding of SO_2 in the UTLS by the Microwave Limb Sounder (MLS) instruments has exploited rotational absorption bands of the molecule at frequencies of 200–240 GHz (Read et al., 1993; Pumphrey et al., 2015).

The era of satellite observations of volcanic degassing (primarily SO_2) can be broadly divided based on sensor specifications (mainly spectral and spatial resolution), which directly impact sensitivity to SO_2 abundance and altitude and hence to different styles of volcanic activity. Between October 1978 and December 2005, four TOMS missions provided near-continuous multi-spectral, global, nadir UV observations at low spatial resolution (39–50 km at nadir), with occasional small data gaps and a major 19-month gap in 1995–96 between the Meteor-3 and Earth Probe (EP) TOMS missions (Krueger et al., 1995, 2000; Fig. 1). The limited number of TOMS wavelengths restricted measurements to larger volcanic eruptions and extreme levels of passive SO_2 degassing (e.g., Bluth et al., 1993; Carn et al., 2003; Carn, 2004). SBUV (flown since 1978; Table 1) has also provided nadir UV observations of volcanic SO_2 clouds, albeit with poorer spatial sampling than TOMS, but only for the largest eruptions (McPeters et al., 1984; McPeters, 1993; Schnetzler et al., 1995). Coincident with TOMS, the High-resolution Infrared Radiation Sounder and subsequent iterations (HIRS, HIRS/2, HIRS/3, etc.), flown as part of the TIROS Operational Vertical Sounder (TOVS) package on NOAA polar-orbiters since October 1978, provide multi-spectral, global IR SO_2 measurements at 7.3 μm (Prata et al., 2003). The HIRS SO_2 data provide coverage of the 1995–96 TOMS data gap and also offer nighttime and high-latitude winter measurements, unlike TOMS.

Hyperspectral UV measurements, offering increased sensitivity to lower tropospheric SO_2 due to optimized spectral resolution (Krueger et al., 2009), began with the Global Ozone Monitoring Experiment (GOME) in July 1995 (Burrows et al., 1999). GOME provided some of the first satellite observations of lower tropospheric SO_2 from volcanic and anthropogenic sources despite its low spatial resolution (40 × 320 km at nadir; Eisinger and Burrows, 1998), and detected numerous volcanic eruptions during its operational lifetime (1995–2003; e.g., Afe et al., 2004; Thomas et al., 2005; Khokhar et al., 2005). However, a GOME inventory of volcanic SO_2 mass loading has not been widely reported to date and hence GOME SO_2 data are not included in the database presented here (Fig. 1). GOME was superseded by the Scanning Imaging Absorption Spectrometer for Atmospheric Chartography (SCIAMACHY; Bovensmann et al., 1999), launched on Envisat in March 2002 and operational from 2002 to 2012. SCIAMACHY provided increased sensitivity to tropospheric SO_2 over GOME due to higher spatial resolution (30 × 60 km at nadir), and also detected many volcanic SO_2 emissions (e.g., Afe et al., 2004; Lee et al., 2008, 2009; Penning de Vries et al., 2014) and provided the first satellite observation of volcanic OClO (Theys et al., 2014), but its spatial coverage was limited by alternation between nadir and limb mode observations. Thus, SCIAMACHY-derived volcanic SO_2 mass loadings have also not been widely reported and are not used herein, although there is potential for further analysis of the SCIAMACHY limb mode data archive to constrain volcanic plume altitudes (e.g, Penning de Vries et al., 2014). The Ozone Monitoring Instrument (OMI), launched on NASA's Aura satellite in July 2004, has provided operational, hyperspectral nadir UV SO_2 measurements with a nadir spatial resolution of 13 × 24 km since September 2004 (Fig. 1; Krotkov et al., 2006; Yang et al., 2007). OMI SO_2 measurements have been the primary source of data for continuation of the TOMS record of volcanic SO_2 emissions, but with increased sensitivity to small eruptions and passive degassing (Carn et al., 2008b; Carn and Prata, 2010; McCormick et al., 2012, 2013; Campion et al., 2012; Carn et al., 2013).

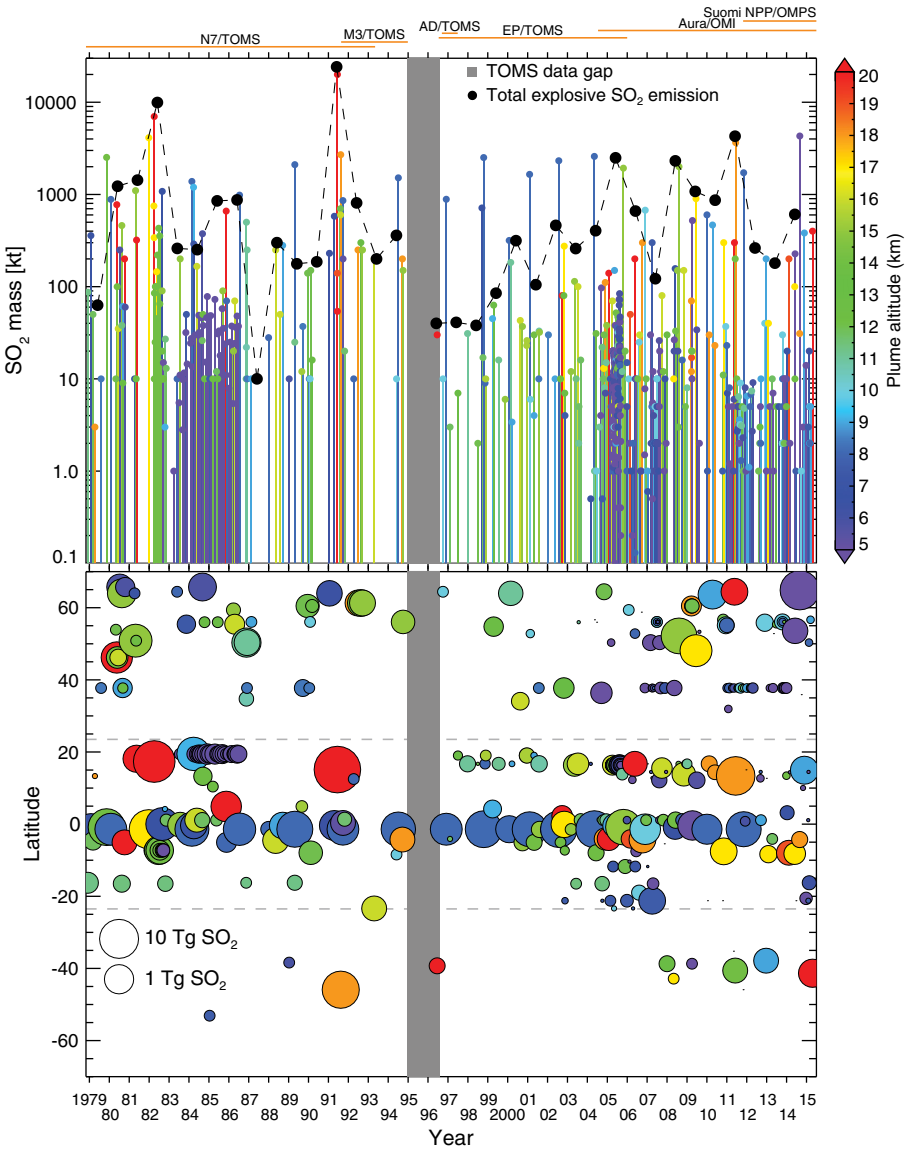

Fig. 1. Satellite measurements of SO_2 emissions by volcanic eruptions between October 1978 and April 2015. Measurements are primarily based on UV TOMS, OMI and OMPS data, supplemented by IR data from TOVS, AIRS and IASI. Eruptions are color-coded by estimated plume altitude, derived from a variety of sources, including Smithsonian Institution Global Volcanism Program volcanic activity reports, volcanic ash advisories, and satellite data (e.g., CALIOP lidar for eruptions since 2006). *Upper panel* shows SO_2 mass loading against time, with annual total explosive volcanic SO_2 production (omitting SO_2 discharge from effusive eruptions) shown in *black*. *Orange lines* above the plot indicate the operational lifetimes of the UV satellite instruments: Nimbus-7 (N7), Meteor-3 (M3), ADEOS (AD), and Earth Probe (EP) TOMS, OMI (currently operational) and OMPS (currently operational). The TOMS data gap in 1995–96 is shown in *gray* (but note that TOVS SO_2 data provide coverage during this time). *Lower panel* shows eruption latitude against time, with symbol size proportional to SO_2 mass loading. *Horizontal dashed lines* delineate the tropics. The charts only depict SO_2 emissions from discrete volcanic eruptions; continuous emissions from passive degassing and some smaller eruptions are not included. Over 600 eruptions are shown, releasing a total of ~100 Tg of SO_2. The database shown in this plot will soon be available from the NASA Goddard Earth Sciences (GES) Data and Information Services Center (DISC) as a level 4 MEaSUREs (Making Earth System Data Records for Use in Research Environments) data product.

Overlap between EP/TOMS in OMI in 2004–2005 provides opportunities for comparison of multi-spectral and hyperspectral SO_2 retrievals for several eruptions (Fig. 1; Table 2), to assess continuity between satellite missions. Second generation GOME (GOME-2) instruments were launched on the MetOp-A and MetOp-B satellites in October 2006 (Munro et al., 2006) and September 2012, respectively, offering higher spatial resolution than GOME (80 × 40 km) and high sensitivity to volcanic SO_2 and BrO emissions (e.g., Theys et al., 2009; Nowlan et al., 2011; Rix et al., 2012; Theys et al., 2013), but lower sensitivity to passive SO_2 degassing than OMI due to OMI's higher spatial resolution. However, as for GOME and SCIAMACHY, we have not made extensive use of GOME-2 data in this study. A further hyperspectral UV sensor, the Ozone Mapping and Profiler Suite (OMPS), was launched on the Suomi National Polar-orbiting Partnership (SNPP) satellite in October 2011 and will be flown on future NOAA Joint Polar Satellite System (JPSS) polar-orbiters beginning in 2017. OMPS has variable spatial resolution (50 × 50 km in standard mode and 10 × 10 km in zoom mode, currently used once weekly on Saturdays) and comparable sensitivity to volcanic SO_2 to SCIAMACHY, OMI and GOME-2 (e.g., Yang et al., 2013) and is also being used to extend the UV volcanic SO_2 measurements in conjunction with OMI (Carn et al., 2015; Fig. 1).

IR satellite sensors have shown a similar evolution to UV instruments. Following on from TOVS/HIRS, multi-spectral TIR observations from the Moderate resolution Imaging Spectroradiometer (MODIS) and Advanced Spaceborne Thermal Emission and Reflection radiometer (ASTER) began following the launch of Terra in December 1999, and a second MODIS instrument was deployed on Aqua in May 2002. Both Terra and Aqua MODIS and ASTER continue to operate at the time of writing. MODIS and ASTER data can be used for IR SO_2 retrievals at moderate-to-high spatial resolution (90 m to 1 km) using channels at

Table 2
SO_2 mass loadings for selected volcanic eruptions (1978–2014).

Volcano	Eruption date(s)	Total SO_2 loading (Tg)	Sensor(s)	Reference
Nyamuragira	1979–2004	~25[a]	TOMS	Bluth and Carn (2008)
Hekla	17 Aug. 1980	0.6 ± 0.1	TOMS	Carn et al. (2008a)
El Chichón	28 Mar. 1982	1.6	TOMS	Krueger et al. (2008)
	3–4 Apr. 1982	5.9	TOMS	Krueger et al. (2008)
Galunggung	Apr 1982–Jan. 1983	2.03	TOMS	Bluth et al. (1994)
Nevado del Ruiz	13 Nov. 1985	0.66	TOMS	Krueger et al. (1990)
Redoubt	15 Dec. 1989	0.18	TOMS	Schnetzler et al. (1994)
Hekla	17 Jan. 1991	0.4 ± 0.1	TOMS	Carn et al. (2008a)
Pinatubo	15 Jun. 1991	18 ± 4	TOMS	Guo et al. (2004)
		19 ± 4	HIRS/2	Guo et al. (2004)
		17	MLS	Read et al. (1993)
		12–15	SBUV/2	McPeters (1993)
Hudson	8–12 Aug. 1991	4	TOMS	Constantine et al. (2000)
Mt. Spurr	27 Jun. 1992	0.25	TOMS	Bluth et al. (1995)
	18 Aug. 1992	0.3	TOMS	Bluth et al. (1995)
	17 Sep. 1992	0.25	TOMS	Bluth et al. (1995)
Ruapehu	17 Jun. 1996	0.08	HIRS/2	Prata et al. (2003)
Hekla	26 Feb. 2000	0.2	TOMS/HIRS	Rose et al. (2003)
Miyakejima	18 Aug. 2000	0.043	Multiple	McCarthy et al. (2008)
Popocatepetl	23 Jan. 2001	0.017	MODIS 7.3 μm	Matiella Novak et al. (2008)
Nyiragongo	17 Jan. 2002	0.03	TOMS	Carn (2004)
Etna	30 Oct. 2002	0.025	AIRS	Carn et al. (2005)
		0.022	AIRS	Prata et al. (2007)
Anatahan	10–12 May 2003	0.11	TOMS	Wright et al. (2005)
Soufriere Hills	13 Jul. 2003	0.10	TOMS	Carn and Prata (2010)
		0.13	MODIS 7.3 μm	Carn and Prata (2010)
		0.12	AIRS	Carn and Prata (2010)
Soputan	Oct 2004–Oct. 2008	0.11[b]	OMI	Kushendratno et al. (2012)
Manam	28 Jan. 2005	0.14	TOMS	*This study*
		0.14	OMI	*This study*
		0.13	AIRS	Prata and Bernardo (2007)
Anatahan	6 Apr. 2005	0.070	TOMS	*This study*
		0.075	OMI	*This study*
		0.077	AIRS	Prata and Bernardo (2007)
Sierra Negra	22 Oct. 2005	1.74	OMI	Yang et al. (2009a)
		0.33	TOMS	Thomas et al. (2009)
		1.27	MODIS 8.6 μm	Thomas et al. (2009)
Karthala	24 Nov. 2005	0.08	SEVIRI	Prata and Kerkmann (2007)
Soufriere Hills	20 May 2006	0.22	OMI	Carn and Prata (2010)
		0.23	AIRS	Carn and Prata (2010)
		0.18	SEVIRI	Prata et al. (2007)
P. Fournaise	4–9 Apr. 2007	0.23	OMI	Tulet and Villeneuve (2011)
Manda Hararo	12 Aug. 2007	0.03	OMI	Ferguson et al. (2010)
Jebel al-Tair	30 Sep. 2007	0.08 ± 0.02	Multiple	Eckhardt et al. (2008)
		0.05	IASI	Clarisse et al. (2008)
Chaitén	2–8 May 2008	0.01	OMI	Carn et al. (2009a)
Okmok	12 Jul. 2008	0.12	OMI	Spinei et al. (2010)
		0.3	AIRS	Prata et al. (2010)
		0.09	IASI	This study
Kasatochi	7 Aug. 2008	1.7	IASI	Karagulian et al. (2010)
		1.2	AIRS	Prata et al. (2010)
		1.7	Multiple	Kristiansen et al. (2010)
		2.2	OMI	Krotkov et al. (2010)
		0.9 ± 0.2	MODIS 7.3 μm	Corradini et al. (2010)
		2.7 ± 0.8	MODIS 8.6 μm	Corradini et al. (2010)
		1.6	IASI	Clarisse et al. (2012)
		1.6	GOME-2	Nowlan et al. (2011)
Dalafilla	3 Nov. 2008	0.23	IASI	*This study*
Redoubt	23 Mar.–12 Jun. 2009	0.54–0.61[c]	OMI	Lopez et al. (2013a)
Sarychev Peak	15–16 Jun. 2009	1.2	IASI	Haywood et al. (2010)
Manda Hararo	28 Jun. 2009	0.03	OMI	Ferguson et al. (2010)
Eyjafjallajökull	1–12 May 2010	0.17	IASI + Model	Boichu et al. (2013)
	5–18 May 2010	1.2 ± 0.5	GOME-2	Rix et al. (2012)
	7 May 2010	0.18	IASI	Carboni et al. (2012)
Manda Hararo	21 May 2010	0.001	GOME-2+OMI	Barnie et al., 2015
Merapi	26 Oct.–4 Nov. 2010	0.44	Multiple	Surono et al. (2012)
Kizimen	13–31 Dec. 2010	0.06	IASI	*This study*
Kirishima	26 Jan. 2011	0.03	IASI	*This study*
Grimsvötn	21 May 2011	0.38	OMI + IASI	Sigmarsson et al. (2013)
Cordon Caulle	4–6 Jun. 2011	0.2	IASI	Theys et al. (2013)
Nabro	12–28 Jun. 2011	4.5	Multiple	Theys et al. (2013)
Nyamuragira	6 Nov.–6 Dec. 2011	~1	OMI	Theys et al. (2013)
Tolbachik	27 Nov. 2012	0.09	IASI	*This study*
	Nov 2012–Aug. 2013	0.2	Multiple	Telling et al. (2015)
Copahue	22 Dec. 2012	0.5	IASI	*This study*
Paluweh	2 Feb. 2013	0.03	Multiple	Carn et al. (2015)
Kelut	14 Feb. 2014	0.2	OMI	*This study*
		0.19	IASI	*This study*

[a] Total SO_2 release for 14 effusive eruptions.
[b] Total SO_2 release for 9 explosive eruptions.
[c] Total SO_2 release for several UTLS injections.

7.3 μm (MODIS) or 8.6 μm (MODIS and ASTER); these sensors have typically been used for specific volcanic eruption or degassing case studies that exploit their higher spatial resolution rather than the production of long-term volcanic SO_2 emissions inventories (e.g., Rose et al., 2003; Watson et al., 2004; Urai, 2004; Pugnaghi et al., 2006; Kearney et al., 2008; McCarthy et al., 2008; Matiella Novak et al., 2008; Corradini et al., 2009, 2010; Campion et al., 2010, 2012; Henney et al., 2012). This is largely due to the difficulty of processing the larger data volumes associated with high spatial resolution data, the limited spatial coverage of ASTER (a result of the trade-off between spatial resolution and swath width), plus the aforementioned interference from volcanic ash at 8.6 μm. Although high-resolution IR spectra were acquired from space as early as 1969 (Clarisse et al., 2011a), global, nadir hyperspectral IR measurements began from orbit in earnest with the launch of the Atmospheric Infrared Sounder (AIRS) on Aqua in 2002 (Chahine et al., 2006), which provides robust retrievals of volcanic SO_2 in the UTLS using the 7.3 μm band (Carn et al., 2005; Prata and Bernardo, 2007; Prata et al., 2007, 2010). AIRS spectra also cover the 4 μm band and part of the 8.6 μm SO_2 band but these data have not been widely exploited to date (Prata and Bernardo, 2007). AIRS SO_2 measurements provide particularly valuable observations of volcanic eruptions between 2002 and the beginning of OMI measurements in September 2004 (Fig. 1), in addition to ongoing complementary coverage of nighttime and high-latitude winter events. Hyperspectral IR measurements of SO_2 were augmented by the Infrared Atmospheric Sounding Interferometer (IASI), first launched on MetOp-A with GOME-2 in 2006 and followed by a second IASI instrument on MetOp-B in 2012. In addition to providing high-quality UTLS volcanic SO_2 measurements (e.g., Clarisse et al., 2008, 2012, 2014; Karagulian et al., 2010; Theys et al., 2013), IASI has provided new observations of other volcanogenic gas and aerosol species including hydrogen sulfide (H_2S; Clarisse et al., 2011a,b) and sulfate aerosol (Clarisse et al., 2010; Karagulian et al., 2010).

In tandem with the advent of hyperspectral measurements, a key advance in satellite remote sensing that has occurred in the past decade, and one that is particularly relevant to volcanic eruption detection, is the availability of altitude information for SO_2 (and other trace gases) and aerosols to complement measurements of SO_2 mass loading by the nadir UV and IR imagers and sounders describe above. Although it has long been possible to estimate the altitude of a volcanic cloud by comparing observed SO_2 or ash cloud transport and winds aloft (e.g., from a radiosonde), by using IR cloud-top brightness temperatures for optically thick plumes, or by using trajectory models (e.g., Schoeberl et al., 1993; Carn et al., 2008a; Krotkov et al., 2010), there are now multiple sources of altitude information, with variable accuracy. Altitude information can be derived directly from satellite instruments in several ways including: active LiDAR or radar remote sensing of volcanic aerosols and hydrometeors (Fig. 2; e.g., Cloud-Aerosol Lidar with Orthogonal Polarization (CALIOP) or CloudSat data; Carn et al., 2009a, 2015; Spinei et al., 2010; Lopez, 2011; Winker et al., 2012; Fromm et al., 2014; Prata et al., 2015); passive multi-angle imaging (e.g., the Multi-angle Imaging Spectroradiometer [MISR]; Kahn et al., 2007; Kahn and Limbacher, 2012); passive limb sounding of volcanic gases and aerosols in the UV, IR or microwave (e.g., MLS, OSIRIS, MIPAS, SCIAMACHY, ACE, OMPS; Read et al., 1993; Bourassa et al., 2010, 2012, 2013; Doeringer et al., 2012; Höpfner et al., 2013, 2015; Penning de Vries et al., 2014; Pumphrey et al., 2015); solar occultation measurements of volcanic aerosols (e.g., SAGE); or SO_2 altitude retrievals using passive nadir hyperspectral UV or IR measurements (e.g., OMI, GOME-2, IASI; Yang et al., 2009a,b, 2010; Nowlan et al., 2011; Rix et al., 2012; Clarisse et al., 2014). Information on the SO_2 vertical profile can also be gleaned from inverse trajectory modeling of satellite measurements (e.g., Eckhardt et al., 2008; Kristiansen et al., 2010; Hughes et al., 2012) or by comparisons of simultaneous UV and IR measurements, exploiting their different vertical sensitivity (e.g., Fig. 2; Carn et al., 2009b). Whilst it is rare to possess all the above information for a given volcanic eruption, the redundancy offered by multiple techniques means that some altitude information is nearly always available. The operation of polar-orbiting satellites in close formation along the same orbit track, such as NASA's A-Train afternoon constellation (http://atrain.nasa.gov/; including OCO-2, Aqua, CALIPSO, CloudSat and Aura), providing near-coincident passive and active measurements from multiple platforms, has greatly facilitated analysis of volcanic cloud altitude (e.g., Fig. 2; Carn et al., 2009a, 2009b).

To summarize, there have been many improvements in satellite remote sensing of volcanic gases since 1978, largely due to the advent of hyperspectral UV and IR sensors and satellite constellations. Currently (June 2015), as several operational sensors continue to exceed their intended lifetimes, our capabilities for monitoring volcanic SO_2 emissions from space have reached a zenith, with up to ~18 daily SO_2 observations potentially available from nadir imagers and sounders. In chronological order, these are: AIRS and MODIS (Aqua; equator crossing at 1:30 am local time (LT)); VIIRS and CrIS (SNPP; 1:30 am LT), GOME-2B and IASI-B (MetOp-B; 9:00 am LT); GOME-2 A and IASI-A (MetOp-A; 9:30 am LT); MODIS (Terra; 10:30 am LT); AIRS and MODIS (Aqua; 1:30 pm LT); OMPS, VIIRS and CrIS (SNPP; 1:30 pm LT); OMI (Aura; 1:45 pm LT); IASI-B (9:00 pm LT); IASI-A (9:30 pm LT); and MODIS (Terra; 10:30 pm LT). This sequence does not include further observations from multiple consecutive overpasses for high latitude regions (e.g., Kamchatka, Iceland, Alaska), daily SO_2 observations from TOVS/HIRS, limb observations of SO_2 and HCl from MLS on Aura and occasional SO_2 observations by ASTER and the geostationary SEVIRI (for eruptions in Europe, Africa and the eastern Americas). Note that the times listed above are equatorial crossing times (ascending or descending nodes) and the gap between local satellite overpass times may be substantially longer at higher latitudes, although this is offset by the convergence of polar orbits towards the poles. But at low latitudes the maximum data gap between volcanic SO_2 measurements (UV or IR) is currently ~7.5 h (1:30 am–9:00 am and 1:30 pm–9:00 pm), which is useful for near real-time (NRT) monitoring applications (e.g., Brenot et al., 2014) and ensures that very few, if any, volcanic eruptions emitting significant SO_2 go undetected. Having numerous satellite SO_2 measurements available also permits inter-comparisons between UV and IR data and increases confidence in calculated SO_2 mass loadings. Furthermore, the recently launched Earth Polychromatic Imaging Camera (EPIC) on the NOAA Deep Space Climate Observatory (DSCOVR) will soon provide the first volcanic SO_2 measurements from the L_1 Earth-Sun. Lagrange point (http://www.nesdis.noaa.gov/DSCOVR/). Beginning in 2016, EPIC will provide multi-spectral UV SO_2 measurements of the sunlit Earth disk several times per day, with spatial resolution similar to OMI, offering improved temporal resolution over LEO UV sensors. The L_1 orbit offers a unique perspective of Earth, distinct from a geostationary orbit (GEO). Like GEO, year-round L_1 observations will be best suited to eruptions at low- to mid-latitudes, but whereas GEO observations are always limited at high latitudes, EPIC will provide good coverage of the high latitude summer hemisphere as the Earth's axis tilts towards the Sun.

3. Satellite instruments and data

Here, we describe the specific datasets used in the multi-decadal analysis of volcanic SO_2 emissions in chronological order of sensor deployment, namely TOMS, TOVS/HIRS, AIRS, OMI, MLS, IASI and OMPS. We do not provide detailed descriptions of retrieval algorithms, since these have been extensively reported elsewhere and the focus of this review is interpretation of the measurements. Limitations and uncertainties in SO_2 retrievals will be acknowledged as appropriate, but we will also demonstrate broad agreement between SO_2 retrievals from independent UV and IR sensors (especially for the larger volcanic eruptions), providing confidence in the measurements. However, we also note that retrieval algorithms are likely to improve in the future due to continued improvements in spectroscopic data, additional constraints from ancillary data and better characterization of uncertainties.

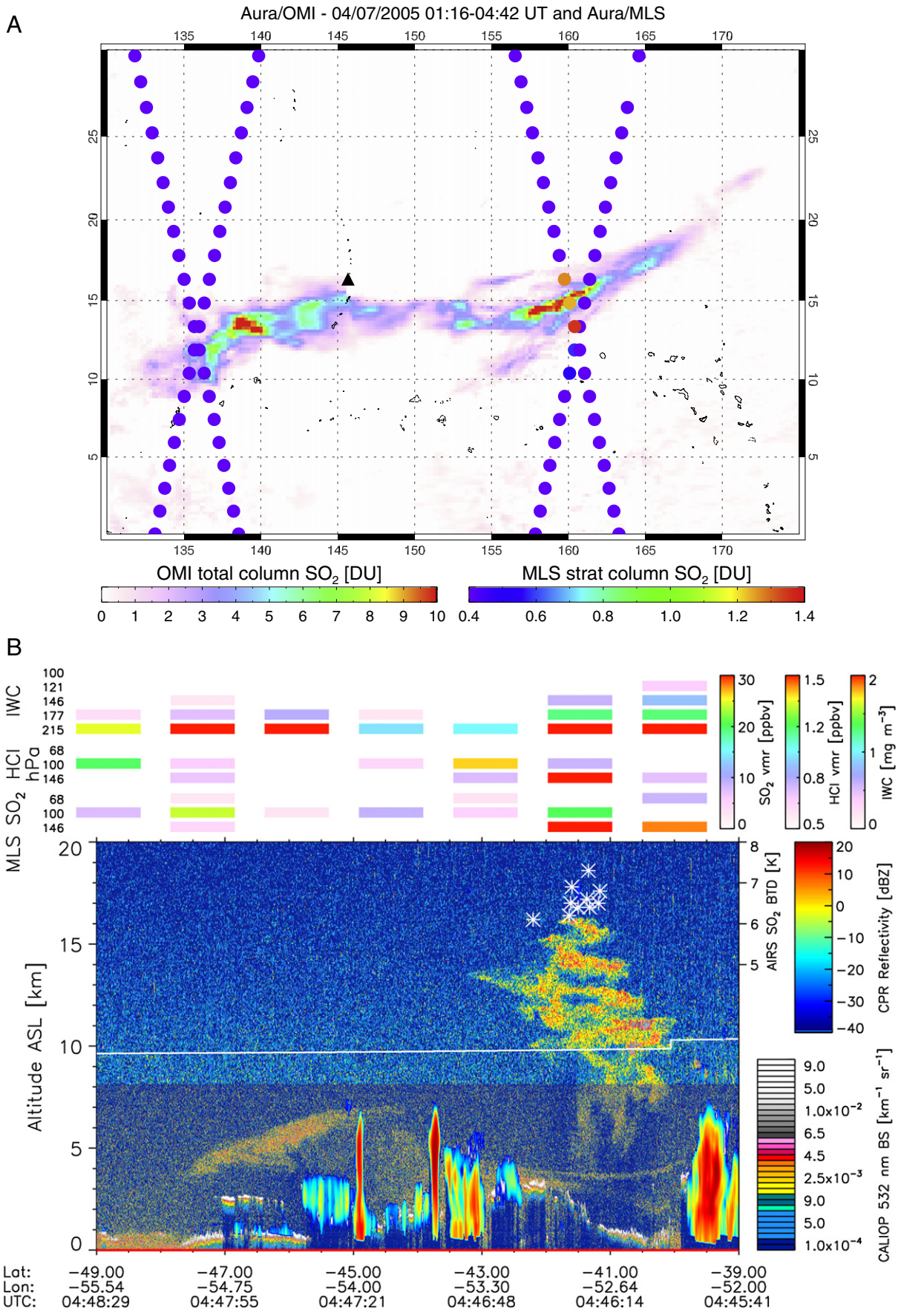
A
Aura/OMI - 04/07/2005 01:16-04:42 UT and Aura/MLS
OMI total column SO2 [DU]
MLS strat column SO2 [DU]
B
IWC
HCl
MLS SO2
hPa
SO2 vmr [ppbv]
HCl vmr [ppbv]
IWC [mg m-3]
Altitude ASL [km]
AIRS SO2 BTD [K]
CPR Reflectivity [dBZ]
CALIOP 532 nm BS [km-1 sr-1]
Lat:
Lon:
UTC:

Thomas and Watson (2009) and Carn (2015a) provide recent tabulations of satellite sensor specifications.

3.1. TOMS (UV)

A TOMS instrument was first deployed on the Nimbus-7 (N7) satellite that was operational between October 1978 and May 1993, and N7/TOMS provided the first satellite observation of volcanic SO_2 after the 1982 El Chichón eruption (Krueger, 1983; Krueger et al., 2008). Subsequently, three similar 6-channel TOMS sensors were launched on the Meteor-3 (M3; August 1991–December 1994), ADEOS (AD; September 1996–June 1997) and Earth Probe (EP; July 1996–December 2005) spacecraft. Following the 1982 El Chichón SO_2 cloud sighting, algorithms were developed for quantitative retrievals of SO_2 column amounts (Krueger et al., 1995, 2000). The N7, M3, AD and EP/TOMS instruments differed in their channel placement (after discovery of the volcanic SO_2 mapping capability, AD/TOMS and EP/TOMS wavelengths were optimized for SO_2 measurements; Gurevich and Krueger, 1997) and spatial resolution (24–50 km nadir footprint size), which impacts SO_2 sensitivity: the estimated volcanic SO_2 cloud detection limit ranges from ~2–4 kt (EP/TOMS) to ~11 kt (N7/TOMS; Carn et al., 2003). There was a TOMS data gap of ~19 months in 1995–96 between the M3 and EP/TOMS missions, but we use IR TOVS SO_2 measurements to cover this time period (Prata et al., 2003). The Solar Backscatter Ultraviolet (SBUV or SBUV/2) instruments flown on the N7 satellite with TOMS and later on NOAA polar-orbiting satellites could also detect volcanic SO_2 (e.g., McPeters et al., 1984; McPeters, 1993; Schnetzler et al., 1995), but with limited mapping ability (Table 1), and to date have only been applied to the largest eruptions (El Chichón and Pinatubo).

Most TOMS volcanic SO_2 data reported here have been produced using the iterative 4-band matrix inversion retrieval technique described by Krueger et al. (1995, 2000), using Sun.-normalized radiances produced by the TOMS ozone data production algorithm as input, and effective optical paths derived from a UV radiative transfer model. Krueger et al. (1995) report errors of ±10–30% for TOMS SO_2 retrievals, highest at large solar zenith angles near the swath edge. Previous TOMS volcanic SO_2 analyses used TOMS production data version 6 (e.g., Bluth et al., 1992, 1993, 1997) or version 7 (Carn et al., 2003), whereas more recent analyses have used version 8 (the current TOMS ozone algorithm is version 9). Some, though not all, older eruptions have been reanalyzed using version 8 TOMS data, with little change from previously reported results (e.g., Krueger et al., 2008). TOMS production algorithm updates are largely focused on improving the accuracy of total ozone retrievals by correcting for the effects of aerosols, clouds and ozone profile variability (e.g., Bhartia and Wellemeyer, 2002), and hence small improvement in SO_2 retrievals may also result. TOMS SO_2 column retrievals are not publicly available at present, but will be released following a major reprocessing of the TOMS data archive that is expected to be complete by 2018 (in the meantime, TOMS SO_2 retrievals are available from the first author upon request). Currently, N7/TOMS and EP/TOMS level 2 (L2) ozone data (version 8) are publicly available from the NASA Goddard Earth Sciences (GES) Data and Information Services Center (DISK; http://disc.sci.gsfc.nasa.gov/), and the L2 TOMS ozone data files contain a SO_2 index (SOI) indicating contamination of ozone retrievals by volcanic SO_2.

As is the case for all satellite-based volcanic SO_2 measurements, opportunities to validate TOMS SO_2 data were rare and opportunistic, relying on the chance overpass of a volcanic cloud over a ground measurement site. The best validation data have been obtained using ground-based UV Brewer spectrophotometers, which can be used to measure total column SO_2 and are operated as networks in several countries (e.g., Fioletov et al., 1998). A Brewer instrument in Toronto (Canada) detected SO_2 (column amounts up to ~100 DU) in the May 1980 Mt. St. Helens (WA, USA) eruption cloud as it drifted east, with general agreement between TOMS and Brewer SO_2 columns (Kerr and Evans, 1987). In 1984, a Brewer in Sweden detected SO_2 (>40 DU) emitted by the September 5, 1984 effusive eruption of Krafla (Iceland); in this case significant disagreement between Brewer and TOMS SO_2 observations was attributed to lower tropospheric SO_2 which was not detected by TOMS (Kerr and Evans, 1987). Perhaps the most robust TOMS SO_2 validation occurred when the Toronto Brewer measured SO_2 in a drifting volcanic cloud from Mt. Spurr (Alaska) in September 1992, with coincident N7/TOMS and Brewer SO_2 columns (~40–50 DU) agreeing to within 20% (Fioletov et al., 1998; Krueger et al., 2000). Attempts to compare TOMS SO_2 mass measurements with ground-based UV correlation spectrometer (COSPEC) SO_2 emission rates were made for the first time during the 1982 Galunggung eruption (Java, Indonesia; Bluth et al., 1994). In this case TOMS and COSPEC observed different emissions (eruptive and non-eruptive, respectively), precluding validation but demonstrating the complementarity of the satellite and ground-based measurements.

3.2. TOVS/HIRS (IR)

The High-resolution Infrared Radiation Sounder (HIRS/2) was first launched as part of the TOVS package on the TIROS-N satellite in October 1978, and subsequent iterations of the HIRS instrument (HIRS/3, HIRS/4) have been flown on all NOAA polar-orbiters and more recently on the European MetOp satellites, providing continuous coverage to the present. Prata et al. (2003) provide further details on TOVS/HIRS and describe a technique for retrieving UTLS SO_2 column amounts from HIRS/2 L1b radiance data, which we use to analyze volcanic eruptions that occurred during the 1995–96 TOMS data gap. However, the full HIRS/2 SO_2 dataset could potentially be used to generate a long-term volcanic SO_2 climatology for 1978-present, with greater temporal sampling than UV sensors, but reduced sensitivity to tropospheric SO_2. Prata et al. (2003) and Carn et al. (2008a) show good agreement between TOMS and HIRS/2 SO_2 retrievals for a small subset of eruptions that have been analyzed to date with both instruments (e.g., Table 2).

3.3. AIRS (IR)

AIRS, in Sun.-synchronous orbit on Aqua in the A-Train, provides hyperspectral IR measurements using 2378 channels at IR wavelengths between ~3.3–16.7 μm (Chahine et al., 2006). This wavelength range covers SO_2 absorption bands at 4 and 7.3 μm, and part of the 8.6 μm band (there is a gap from ~8.2–8.8 μm). The primary goal of AIRS is to provide global atmospheric soundings of temperature, moisture and other gases for numerical weather prediction and climate, but Carn et al. (2005) and Prata and Bernardo (2007) have shown that AIRS can be used to retrieve volcanic SO_2 at altitudes above ~3–5 km using the 7.3 μm band. AIRS scans a swath of ±49° from nadir and the sensor's elliptical footprint dimensions vary from 15 × 15 km at nadir to

Fig. 2. Examples of A-Train synergy for characterizing volcanic cloud altitude. (A) OMI total column SO_2 and MLS UTLS column SO_2 (W. Read, *pers. Comm.*) for the April 6, 2005 eruption of Anatahan (CNMI; *triangle*). MLS retrievals are shown as *filled circles* along the Aura satellite daytime and nighttime overpass tracks; note that circle size is not representative of the MLS field-of-view. Whilst the nadir OMI measurements detect SO_2 east and west of Anatahan, MLS only detects UTLS SO_2 to the east, confirming the variable altitude of the mapped SO_2. (B) Composite of nighttime A-Train measurements of the Chaitén volcanic plume on May 7, 2008 at ~4:47 UTC. Main panel shows 532 nm total attenuated backscatter (km^{-1} sr^{-1}) from CALIOP, clearly showing aerosol in the layered volcanic cloud, overlain with reflectivity from the CloudSat Cloud Profiling Radar (CPR), which in this case only detects hydrometeors in the tropospheric meteorological clouds (indicating that the volcanic aerosol particle size is below the radar detection limit, i.e., sub-mm). *White stars* show locations of SO_2 detection by AIRS based on a 2-channel brightness temperature difference (BTD in K). The *sub-horizontal white line* indicates the tropopause altitude. MLS retrievals of SO_2 (ppbv), HCl (ppbv) and ice-water content (IWC; mg m^{-3}) for several pressure levels (indicated top left in hPa) are plotted above the CALIOP data; these show clear enhancements in the volcanic cloud above 215 hPa.

18 × 40 km at the swath edge. A full description of the AIRS instrument and operational data processing can be found at http://airs.jpl.nasa.gov.

IR AIRS SO_2 retrievals used here are derived using the Level 1B AIRS IR geolocated and calibrated radiance product (AIRIBRAD version 5) and the Prata and Bernardo (2007) algorithm. AIRIBRAD data granules are publicly available from the NASA GES DISK (http://disc.sci.gsfc.nasa.gov/). The Prata and Bernardo (2007) algorithm is also used to produce NRT AIRS SO_2 products for aviation hazard mitigation, which can be obtained via the NASA GES DISK (http://disc.sci.gsfc.nasa.gov/nrt/data-holdings/airs-nrt-products) and viewed on the Support to Aviation Control Service (SACS) website (http://sacs.aeronomie.be/nrt; Brenot et al., 2014). Prata and Bernardo (2007) quote a retrieval accuracy (or detection limit) of 6 DU SO_2 (~1.6×10^{17} molecules cm^{-2}) for a single AIRS pixel retrieval, mostly due to errors in accounting for background atmospheric water vapor and clouds. Thomas et al. (2011) report a similar AIRS SO_2 detection limit of 5 DU. A detection limit of 6 DU equates to ~30–100 tons of SO_2 within a single AIRS footprint, depending on swath position, and assuming that a cluster of ~10 pixels would constitute a statistically significant volcanic cloud yields a minimum detectable SO_2 mass of ~0.3–1 kt (kt) in the UTLS. In practice, minimum reported volcanic SO_2 mass loadings derived from AIRS (for SO_2 clouds consisting of multiple pixels) are ~0.3–10 kt depending on eruption latitude (e.g., Prata and Bernardo, 2007; Carn and Prata, 2010; Bonny et al., in preparation), indicating slightly higher sensitivity to UTLS SO_2 than EP/TOMS in the 2002–2004 period of overlap between AIRS and TOMS. We also exploit the synergy between near-coincident AIRS 7.3 μm partial column SO_2 retrievals and OMI total column retrievals from the A-Train to infer volcanic SO_2 altitude, where OMI ≈ AIRS > 0 implies UTLS SO_2, OMI > AIRS > 0 implies a vertically extensive SO_2 cloud straddling the lower troposphere and UTLS (or alternatively, a multi-layered volcanic cloud with layers residing at multiple altitudes), and OMI > AIRS ≈ 0 implies SO_2 confined to the lower troposphere (e.g., Carn et al., 2009b).

To date, efforts to validate AIRS SO_2 measurements have focused on inter-comparisons with UV SO_2 retrievals from TOMS, OMI and OMPS. Good correlations have been found between AIRS and UV SO_2 burdens for volcanic clouds at high altitude (>8 km; e.g., Fig. 3; Prata and Bernardo, 2007; Carn and Prata, 2010; Thomas et al., 2011; Carn et al., 2015). The weak sensitivity of AIRS to lower tropospheric SO_2, along with incomplete coverage by the AIRS swath for some eruptions, results in a poorer correlation for eruptions to lower altitudes (Prata and Bernardo, 2007). As yet there have been few detailed comparisons between IR and UV SO_2 column retrievals at the pixel scale, principally due to problems with spatial and temporal collocation and typically non-uniform SO_2 distributions in volcanic clouds (e.g., Kearney et al., 2009; Carn et al., 2015).

3.4. OMI (UV)

OMI is a hyperspectral UV–Visible spectrometer (270–500 nm) using a two-dimensional charge-coupled device (CCD) detector to collect simultaneous spectral and spatial measurements of backscattered solar radiation across a 2600 km swath (Levelt et al., 2006). Spatial resolution is 13 × 24 km (along-track × across-track) at nadir, increasing to ~28 × 160 km at the swath edge. The OMI UV-2 channel (307–383 nm) used for SO_2 retrievals has an average spectral resolution of 0.45 nm (Levelt et al., 2006), and this high spectral resolution coupled with the small OMI footprint size provides unprecedented SO_2 sensitivity for a satellite instrument, permitting detection of passive volcanic degassing and anthropogenic pollution (e.g., Carn et al., 2007, 2008b, 2013). OMI became fully operational in September 2004 and provided daily contiguous, global daytime mapping of ozone, SO_2 and other trace gases (NO_2, BrO, HCHO) until May 2008, when a blockage appeared in the sensor's field of view. This 'row anomaly' evolved dynamically (generally worsening) over time to obscure a significant proportion of the OMI swath from nadir to the east (see: http://www.knmi.nl/omi/research/product/rowanomaly-background.php), ending daily contiguous coverage at low latitudes, although data unaffected by the anomaly remain of high quality. Future evolution of the row anomaly is hard to predict.

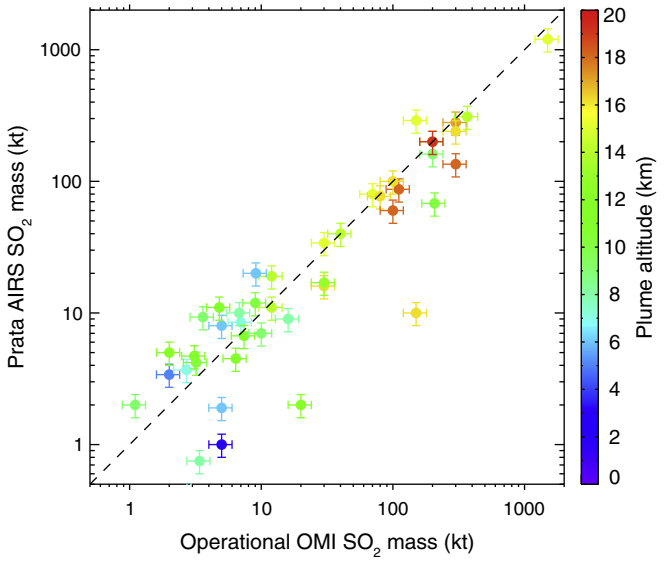

Fig. 3. SO_2 mass loadings (kilotons; log scale) derived from the operational OMI Linear Fit SO_2 algorithm (Yang et al., 2007) against those derived from the Prata and Bernardo (2007) AIRS SO_2 algorithm for selected volcanic eruptions in the 2004–2014 period. Eruptions are color-coded by estimated plume altitude (see text for discussion of sources) and 20% error bars are shown. *Dashed line* is the 1:1 line. Note broad correlation between OMI and AIRS SO_2 retrievals with greater scatter for smaller eruptions and/or lower altitude plumes, as expected.

Several algorithms have been used to retrieve SO_2 from OMI UV radiances, with some differences in SO_2 column sensitivity and retrieval dynamic range (e.g., Krotkov et al., 2006; Yang et al., 2007, 2009a,b, 2010; Lee et al., 2009; Li et al., 2013; Carn et al., 2013; Theys et al., 2015). Most of the volcanic SO_2 measurements in the current inventory are derived from the Linear Fit (LF) algorithm (Yang et al., 2007), which has been used to generate the operational, publicly available OMI SO_2 product (OMSO2 collection 3; available from the NASA GES DISC). The LF algorithm uses 10 OMI wavelengths at 310–360 nm, covering regions of strong (shorter wavelengths) and weak (longer wavelengths) SO_2 absorption, to retrieve SO_2 column amounts (Yang et al., 2007). By using longer UV wavelengths, the LF algorithm avoids some of the non-linear saturation effects that limit algorithms using shorter wavelengths to lower SO_2 column amounts (~10–20 DU; Krotkov et al., 2006). However, the use of a zero SO_2 a-priori constraint as a linearization point also limits the LF algorithm to column amounts of ~100 DU (Yang et al., 2007), and hence offline iterative algorithms have been developed to retrieve higher SO_2 columns (Yang et al., 2009a). Such high SO_2 column amounts (>100 DU) are typically only encountered in very fresh volcanic eruption clouds (<1 day old), after which SO_2 columns are rapidly depleted by upper atmospheric wind shear (e.g., Krueger et al., 2008), or close to the vent during SO_2-rich effusive eruptions (e.g., Yang et al., 2009a). With the exception of highly concentrated SO_2 plumes from effusive eruptions (>1000 DU; Yang et al., 2009a), the highest SO_2 columns detected from space in UTLS volcanic clouds to date were measured by N7/TOMS ~6 h after the April 4, 1982 El Chichón eruption (~600 DU; Krueger et al., 2008) and ~21 h after the paroxysmal June 15, 1991 eruption of Pinatubo (~540 DU; Guo et al., 2004). No explosive eruption comparable in SO_2 release to El Chichón or Pinatubo has occurred during the OMI mission, but iterative SO_2 retrieval techniques (e.g., Yang et al., 2009) would certainly be required for accurate SO_2 mass estimation in such cases. For comparison, peak SO_2 column amounts of 200–300 DU were measured by OMI in the August 2008 Kasatochi volcanic cloud, among the largest to have occurred since Pinatubo (Krotkov et al., 2010). In the current

volcanic SO_2 inventory, most eruptions have been analyzed using the operational LF algorithm, with several of the larger explosive eruptions (e.g., Okmok and Kasatochi in 2008; Nabro and Grimsvötn in 2011) also analyzed using offline algorithms to check for SO_2 column saturation. Other consistency checks, such as monitoring the temporal evolution of SO_2 loading in the days following an eruption, checking coincident ozone fields for artifacts (anomalies in ozone retrievals indicate that SO_2 absorption has been incorrectly accounted for), and comparing with IR SO_2 retrievals (e.g., Fig. 3), are also routinely used.

SO_2 retrieval algorithms require specification of SO_2 altitude due to the temperature- and pressure-dependence of SO_2 absorption and the air mass factor (the ratio of slant to vertical column density). In the LF algorithm, and others, this is achieved by retrieving separate SO_2 column amounts for three prescribed SO_2 vertical profiles representing different volcanic degassing styles (e.g., Yang et al., 2007; Rix et al., 2012; Carn et al., 2013; Theys et al., 2015). The vertical profiles used are (Carn et al., 2013): SO_2 in the lower troposphere (TRL; 0–5 km altitude with center of mass altitude (CMA) of 2.5 km); SO_2 in the mid-troposphere (TRM; 5–10 km altitude, CMA = 7.5 km) and SO_2 in the lower stratosphere (STL; 15–20 km altitude; CMA = 17 km). Corresponding styles of volcanic degassing are passive emissions in the lower troposphere (TRL), high-altitude volcanic degassing and/or small-to-moderate eruptions (TRM) and large eruptions with stratospheric injection (STL). Our approach for volcanic eruption analysis is to use available information on plume altitude (see Section 2, and below) to select the appropriate SO_2 CMA, or interpolate between CMAs for intermediate altitudes. Information on altitude can include direct SO_2 altitude retrievals using OMI measurements (e.g., Yang et al., 2009b, 2010). Provided that SO_2 column saturation is avoided and the assumed SO_2 vertical profile is approximately correct, LF SO_2 retrievals have an uncertainty of ~20% (Yang et al., 2007).

In addition to SO_2 mass, we also use an OMI SO_2 index (OSI) calculated from OMI ozone algorithm (OMTO3) residuals (Krotkov et al., 2006) to identify volcanic SO_2 emissions (e.g., Fig. 4). We use the OSI as a proxy for volcanic SO_2 to avoid complications related to calculation of SO_2 mass when SO_2 from multiple sources at different altitudes may be present (due to the difficulty of isolating SO_2 at different altitudes), a common problem in UV measurements which are sensitive to SO_2 anywhere in the atmospheric column in cloud-free conditions (e.g., Yang et al., 2007). This is less of an issue with IR SO_2 retrievals using the 7.3 μm band since these effectively screen out any lower tropospheric SO_2.

OMTO3 residuals are calculated using scaled, normalized reflectances (N-values) where N-values are defined as:

$$N_\lambda = -100 \ \log\left(\frac{I_\lambda}{F_\lambda}\right) \tag{1}$$

where I is the backscattered Earth radiance and F is the solar irradiance at wavelength λ. N-value residuals for a pair of wavelengths (res_j) are computed thus:

$$res_j = N_j^{measured} - N_j^{calculated} \tag{2}$$

$$N_j = N\left(\lambda_j^{short}\right) - N\left(\lambda_j^{long}\right) \tag{3}$$

where calculated N-values are derived from a forward radiative transfer model, accounting for Rayleigh scattering, ozone absorption, Ring effect (Raman scattering) and surface reflectivity, but not SO_2 absorption. The subscript j ($j = 1, 2, 3$) denotes wavelength pairs where pairs 1, 2 and 3 (P1, P2 and P3) correspond to wavelengths of 311.9–310.8 nm, 313.2–311.9 nm and 314.4–313.2 nm, respectively. These wavelength pairs represent maxima and minima in the UV SO_2 absorption cross-section (Krotkov et al., 2006; Carn et al., 2013) and this wavelength placement permits detection of SO_2 contamination (independent of SO_2 column retrieval) if the following relationships are simultaneously satisfied (Carn et al., 2013):

$$\begin{aligned} res_{P1} &> 0 \\ res_{P2} &< 0 \\ res_{P3} &> 0 \end{aligned} \tag{4}$$

The OSI is defined using the N-value pair residuals as follows:

$$OSI = res_{P1} + abs(res_{P2}) + res_{P3} \tag{5}$$

The value of the OSI thus increases with the severity of SO_2 contamination (higher SO_2 column amount and/or SO_2 altitude), but since it uses short UV wavelengths it also saturates at a certain point for large eruptions. Here, we use the OSI as a semi-quantitative indication of volcanic SO_2 emissions and also to detect sources of passive volcanic degassing. In the latter case saturation is not an issue due to the much lower SO_2 column amounts and plume altitudes involved.

There have been several efforts to validate OMI SO_2 retrievals, including inter-comparisons with IR satellite measurements (e.g., Carn and Prata, 2010), ground-based SO_2 measurements (e.g., Spinei et al., 2010; Lopez, 2011; Theys et al., 2015; Ialongo et al., 2015) and airborne in-situ measurements (e.g., Krotkov et al., 2008; Carn et al., 2011). Results suggest that OMI SO_2 measurements are generally consistent with independent retrievals in dilute (aged) volcanic clouds, but validation of the very high SO_2 column amounts present in fresh volcanic eruption clouds remains a challenge, mainly due to the absence of ground-based or in-situ data in such situations.

To detect sources of passive SO_2 degassing using the OSI we have adopted the following procedure, which exploits the fact that the locations of all subaerial volcanoes (i.e., the sources of passive SO_2 emissions) are known and cataloged in the VOTW database. Detection and attribution of small, non-eruptive volcanic SO_2 plumes also requires sufficient spatial resolution to identify the source, which OMI provides in most cases although ambiguity can still arise in regions with several actively degassing volcanoes. For each day of global OMI SO_2 measurements, all pixels with identifiable SO_2 contamination (based on Eq. (4) above) are extracted from the OMSO2 data products and ranked based on their OSI values. In doing this, we attempt to exclude pixels affected by the South Atlantic radiation Anomaly (SAA) over South America (which have distinctive N-value residuals) and also exclude pixels with solar zenith angles >65° to reduce noise. Then, for each pixel we identify the closest active volcano within a 50 km radius of the pixel center coordinates using a modified version of the VOTW catalog, which is assigned as the presumed source of the detected SO_2; the 50 km distance threshold is arbitrary, but further afield the source of detected SO_2 becomes increasingly ambiguous. We acknowledge that there are uncertainties associated with this approach (e.g., the possible presence of more than one volcano within 50 km of the anomaly), but we attempt to mitigate these by cross-checking with available activity reports to exclude unlikely sources. Also, the modified volcano list used here includes the most likely potential sources of SO_2 emissions based on historical activity, and is necessary to facilitate source attribution in some regions (note that this modification does not impact SO_2 detection, only source identification). Once sources have been assigned to all the SO_2 contaminated pixels, the unique sources are identified (eliminating multiple detections of the same SO_2 plume; e.g., where multiple SO_2 contaminated pixels occur within a SO_2 plume from a single source volcano) and cataloged for each day. By repeating this process for the lifetime of the OMI mission we acquire an inventory of the dominant sources of passive SO_2 emissions detected from space. The analysis presented here is based on OMI SO_2 observations from the beginning of the mission (6 September, 2004) to the end of 2014, or ~3700 days of SO_2 measurements.

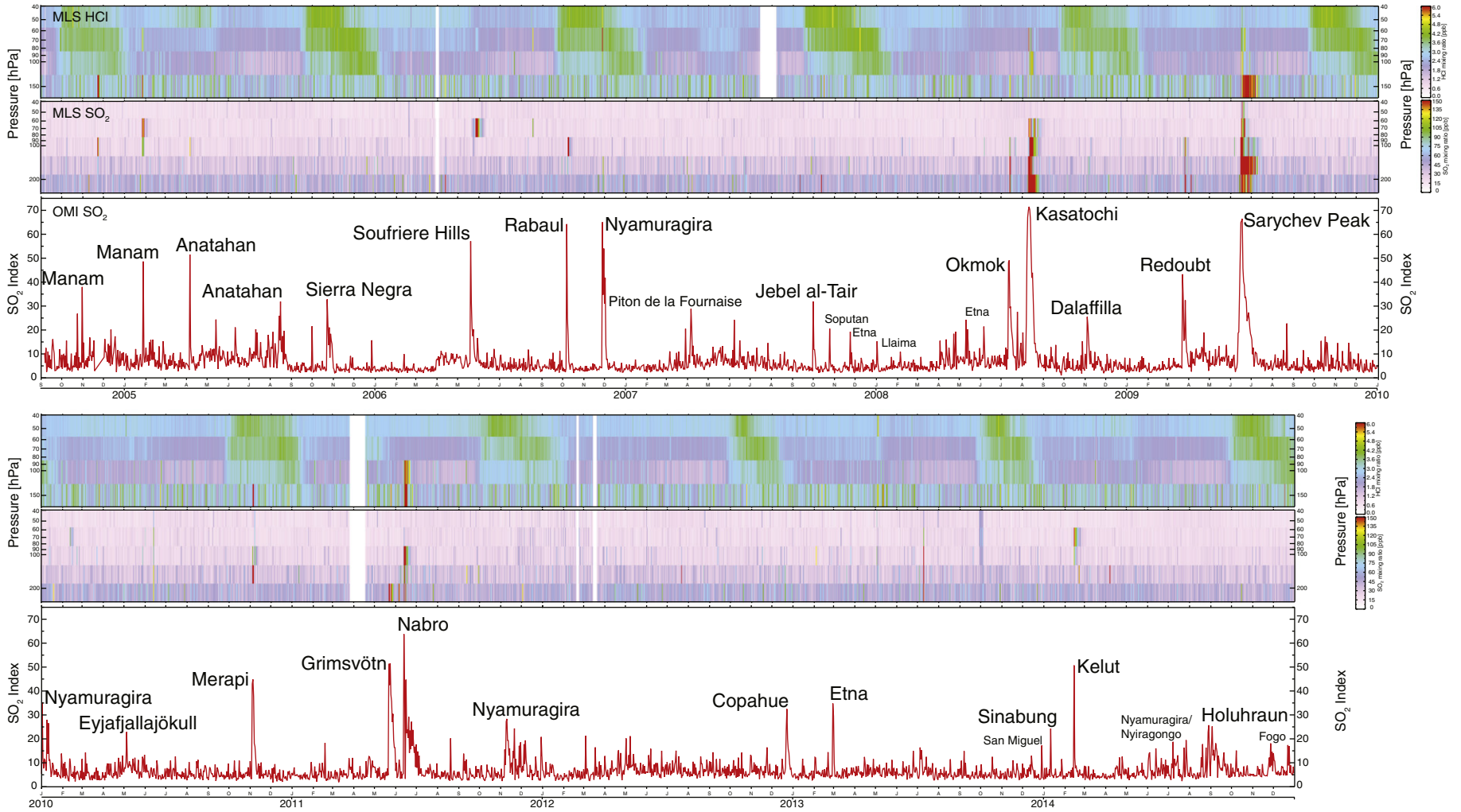

Fig. 4. Time-series of maximum daily OMI SO_2 index (OSI) and MLS UTLS SO_2 and HCl measurements from September 2004 to December 2014. OMI panels (*red curve*) show the maximum daily value of the OSI recorded in global OMI measurements. The OSI is sensitive to SO_2 loading and altitude (see text for definition). Some of the prominent volcanic eruptions responsible for OSI excursions are labeled. MLS panels show the maximum retrieved UTLS SO_2 and HCl mixing ratios on a pressure grid extending from 215 hPa (~11 km altitude) to 40 hPa (~20–21 km altitude) for SO_2 and from 150 hPa (~14 km altitude) to 40 hPa for HCl (note that although MLS HCl measurements are deemed invalid for scientific use below 100 hPa (Livesey et al., 2011), and clearly biased high at 147 hPa, it is clear that volcanic HCl is detected at this level). Note that noise in MLS measurements increases with pressure (i.e., towards lower altitudes) and the data shown here do not represent the full vertical extent of MLS measurements. *Blank regions* are MLS data gaps. MLS data have been screened using the criteria recommended by Livesey et al. (2011).

3.5. MLS (microwave) and IR limb sounders

The first MLS instrument was deployed on NASA's Upper Atmosphere Research Satellite (UARS) in September 1991, shortly after the Pinatubo and Cerro Hudson eruptions, and continued to operate until August 2001 but with only intermittent measurements after December 1993 (http://mls.jpl.nasa.gov/uars/). UARS MLS detected the tropical stratospheric SO_2 veil produced by the Pinatubo eruption (Read et al., 1993) and the large April 1993 eruption of Lascar volcano (Chile; http://mls.jpl.nasa.gov/joe/so2_lascar.html). UARS MLS data were used to constrain the altitude (~26 km), SO_2 decay e-folding time (~29–41 days) and total SO_2 mass (~17 Tg) of the Pinatubo SO_2 cloud (Read et al., 1993). However, UARS MLS data have not been analyzed in detail for this work. The second MLS was launched on Aura (with OMI) in July 2004 (Waters et al., 2006) and continues to operate at the time of writing. Aura/MLS measures microwave thermal emission from Earth's limb to retrieve vertical profiles of trace gas mixing ratios in the UTLS; its great value for volcanic gas detection is its ability to provide vertical profiles of SO_2 and HCl (and also ice water content; e.g., Fig. 2) coincident with nadir OMI and AIRS measurements from the A-Train. Hence we use daily Aura/MLS limb soundings of SO_2 and HCl to pinpoint UTLS injections of these species since September 2004 (e.g., Figs. 2, 4; Pumphrey et al., 2015). The main weakness of MLS is poor spatial sampling: profiles (with vertical resolution of ~3 km) are retrieved only along the sub-satellite Aura orbit track with horizontal spacing of ~167 km (Pumphrey et al., 2015). Hence smaller volcanic eruptions may not be sampled, but these are also less likely to reach the UTLS. We use version 3.3 of the level 2 MLS Daily SO_2 and HCl products, collection 3 (ML2SO2.003 and ML2HCL.003; Froidevaux et al., 2008). ML2SO2 and ML2HCL data products are available from the NASA GES DISK (http://disc.sci.gsfc.nasa.gov/). Further details on MLS and SO_2 retrieval procedures are given by Pumphrey et al. (2015), and Livesey et al. (2011) provide information on the precision, accuracy and useful vertical range of MLS SO_2 and HCl retrievals, which are 3 ppbv, 5–20 ppbv and 215–10 hPa for SO_2 and 0.2–0.6 ppbv, 0.2–0.4 ppbv and 100–0.32 hPa for HCl, respectively. We note, however, that the very strong perturbations to SO_2 and HCl mixing ratios caused by volcanic eruptions can permit detection in MLS data at pressure levels outside the stated useful range.

In addition to MLS data, information on SO_2 vertical profiles in volcanic clouds for some eruptions has also been supplied by other limb sounding instruments (Table 1) such as MIPAS (2002–2012; Höpfner et al., 2013, 2015) and ACE (2003-present; Doeringer et al., 2012), and by Aura/TES (a nadir hyperspectral sounder; Clerbaux et al., 2008). MIPAS and ACE are both Fourier Transform Spectrometer (FTS)-based sensors operating in the TIR using the 7.3 μm SO_2 band, but MIPAS detected limb thermal emission whilst ACE uses solar occultation twice daily (sunrise and sunset). Both MIPAS and ACE data can suffer from poor spatial and temporal sampling (hence identification of the source of volcanic SO_2 perturbations can be ambiguous; e.g., Brühl et al., 2015); for example, Höpfner et al. (2013) analyzed monthly mean MIPAS limb spectra binned within 10°-wide latitude bands in order to detect small amounts of SO_2 in the upper stratosphere. Höpfner et al. (2015) analyzed single MIPAS limb scans and identified over 30 volcanic SO_2 injections into the UTLS between 2002 and 2012, some of which were from unidentified sources. However, our database of global volcanic SO_2 emissions based on nadir satellite observations can be used to pinpoint these sources: e.g., tropical UTLS injections of SO_2 from an unidentified source detected by MIPAS in July–August 2005 (Höpfner et al., 2015) can be confidently ascribed to eruptions of Anatahan (CNMI; Fig. 4).

3.6. IASI (IR)

IASI is a nadir-viewing Fourier-transform IR (FTIR) spectrometer first launched on the polar-orbiting MetOp-A satellite on 19 October 2006 (Clerbaux et al., 2007; Phulpin et al., 2007). A second, identical IASI instrument was launched on MetOp-B on 17 September 2012. Both IASI instruments provide global coverage twice a day, with a nadir footprint size of 12 km (diameter) and a full swath width of 2200 km. The MetOp satellites are operational platforms; hence the IASI measurements are available in near real time. The IASI spectrometer provides continuous spectral coverage from 645 cm^{-1} to 2760 cm^{-1} (~3.6–15.5 μm) with no gaps (in contrast to AIRS), with full coverage of the ν_1, ν_3 and $\nu_1 + \nu_3$ SO_2 absorption bands. IASI measurement noise is also lower than AIRS; the IASI noise-equivalent temperature change (NEΔT) at 280 K is estimated to be 0.05 K in the ν_3 band and 0.12 K in the ν_1 band, significantly better than the expected 0.2–0.35 K. For comparison, the AIRS NEΔT is ~0.2 K (but note that this is at a scene temperature of 250 K; at the warmer temperature of 280 K quoted for IASI the AIRS NEΔT will be higher) and it only partially covers the ν_1 band (Carn et al., 2005).

IASI SO_2 retrievals (Figs. 7, 8) employ the technique described by Clarisse et al. (2012), using an SO_2 altitude retrieval algorithm (Clarisse et al., 2014) to derive accurate plume altitudes and hence more reliable estimates of SO_2 mass loadings. Inaccurate SO_2 loadings may still result if the plume altitude is incorrectly retrieved. Furthermore, as for most IR 7.3 μm SO_2 retrievals, the IASI SO_2 measurements are only reliable for SO_2 at altitudes above ~5 km (in mid-latitudes) or ~7 km (in the tropics) due to water vapor interference. SO_2 plumes at lower altitudes will be missed or mass loading will be underestimated (this could be mitigated in the future by exploitation of IASI data in the ν_1 SO_2 band). This is a pertinent issue for relatively long-lived eruptions with temporally variable plume altitudes, such as the 2010 Eyjafjallajökull, 2011 Nabro and 2014–15 Holuhraun eruptions.

3.7. Volcanic activity and eruption altitude information

Information on eruption occurrence, timing and VEI is derived from the Volcanoes of the World (VOTW) database curated by the Smithsonian Institution Global Volcanism Program (GVP; http://www.volcano.si.edu; Global Volcanism Program, 2013). The VOTW database is updated frequently (see http://www.volcano.si.edu/gvp_votw.cfm for latest updates) but for this analysis we have used VOTW v4.3.0, which includes eruptions through June 2014 (Global Volcanism Program, 2013). It is important to note that VEIs provided in the VOTW database (particularly for more recent eruptions) are assigned based on the best available information at the time (e.g., plume altitude, estimated eruption volume) and hence are subject to some uncertainty. Furthermore, a single VEI cannot capture any variability of explosive activity during long-lived eruptions; in such cases the assigned VEI corresponds to the largest event recorded in given time period.

The altitude of volcanic SO_2 injection determines its climate impact, and hence our database includes estimates of SO_2 altitude for all eruptions (Fig. 1). As discussed above, altitude estimates can be derived from several sources, with more frequent measurements of volcanic plume altitude available since 2002 (MIPAS), 2004 (MLS) and particularly since June 2006 (CALIOP and CloudSat). CALIOP, launched in April 2006 on the Cloud-Aerosol Lidar and Infrared Pathfinder Satellite Observations (CALIPSO) satellite (Winker et al., 2009), has been of tremendous value to the volcano remote sensing community with its ability to determine precisely the altitude of aerosols and clouds (e.g., Vaughan et al., 2009). CALIOP browse and expedited browse imagery products produced at NASA Langley Research Center (http://www-calipso.larc.nasa.gov/products/) are routinely checked during eruptions for evidence of plume detection. Lidar backscatter data in conjunction with depolarization ratios (indicating aerosol phase) and color ratios (indicating relative particle size) can be used to confidently distinguish volcanic plumes from meteorological clouds (e.g., Winker et al., 2012), especially when matched with coincident nadir satellite observations from the A-Train (e.g., OMI or AIRS SO_2 data; Carn et al., 2009a, 2009b; Vernier et al., 2013). Although CALIOP detects aerosol particles and not SO_2 gas, it is often assumed that aerosols and SO_2 will be

approximately collocated (horizontally and vertically). Clarisse et al. (2014) found good agreement (within ~2 km in the vertical) between IASI SO_2 altitude retrievals and CALIOP aerosol layer altitudes for the 2011 Nabro eruption cloud. However, collocation may not always be a valid assumption and some separation between gas and aerosol phases is expected due to different sedimentation rates. The poor spatial sampling of CALIOP along the A-Train orbit track often precludes detection of fresh volcanic eruption plumes (~1–3 h old; where ash and hydrometeors may dominate; e.g., Rose et al., 2000) until they expand in size in subsequent days, although the February 2014 eruption of Kelut (Java, Indonesia) provided a rare CALIOP profile through an explosive eruption column only ~2 h after emission (Kristiansen et al., 2015). The Cloud-Profiling Radar (CPR) on the CloudSat satellite complements CALIOP with millimeter-wave (W-band; 3.2 mm wavelength) observations of larger cloud particles and precipitation, but is only sensitive to very fresh volcanic eruption clouds with high loadings of coarse ash and hydrometeors; to date very few confirmed CPR detections of volcanic clouds have been reported but there is evidence that a young plume (~4 h old) from Redoubt (Alaska) was detected on March 26, 2009 (*S.A. Carn*, unpublished data). Unfortunately, no CloudSat data are available for the February 2014 Kelut eruption. More typically, CALIOP samples volcanic plumes several hours after eruption at the earliest, but for the larger eruptions CALIOP observations can continue for many days or weeks as SO_2 gradually converts to sulfate aerosol and/or fine volcanic ash persists (e.g., Eckhardt et al., 2008; Shibata and Kouketsu, 2008; Carn et al., 2009a, 2009b; Spinei et al., 2010; Tulet and Villeneuve, 2011; Lopez, 2011; Vernier et al., 2011; Winker et al., 2012; Wang et al., 2013; Fromm et al., 2014; Clarisse et al., 2014; Carn et al., 2015). CALIOP observations of volcanic clouds since 2006 have also revealed the complex, multi-layered structure of some plumes (Fig. 2; e.g., Carn et al., 2009a), which has implications for the altitude assumptions made in nadir satellite SO_2 retrievals.

SO_2 altitude retrievals from nadir UV or IR satellite observations (e.g., Yang et al., 2009b, 2010; Nowlan et al., 2011; Rix et al., 2012; Carboni et al., 2012; Clarisse et al., 2014) offer the advantage of much better spatial sampling than CALIOP, although nadir-viewing satellite measurements are sensitive to a range of altitudes rather than a specific level; hence the retrieved SO_2 altitude typically represents the peak of a larger vertical distribution. SO_2 altitude retrievals require a minimum SO_2 column amount but are now routinely performed using IASI data (Fig. 7; e.g., Clarisse et al., 2014), although to date UV SO_2 altitude retrievals have only been applied to a small subset of eruptions (Yang et al., 2009b, 2010; Rix et al., 2012).

Prior to 2004–2006, and for many smaller eruptions since then which go undetected by CALIOP and/or provide insufficient signal for SO_2 altitude retrievals, the main sources of information on eruption altitude are Smithsonian GVP volcanic activity reports (which include pilot reports, satellite observations, and ground-based observations) and trajectory modeling.

4. Results and discussion

In presenting the results of our analysis, it is important to stress the ephemeral nature of any database pertaining to active volcanic processes. In essence, this work provides a snapshot of a dynamic inventory that is being continually revised as new eruptions occur or old events are reanalyzed (Carn, 2015c). We stress however, and demonstrate below, that the largest eruptions have been subject to greater scrutiny and are well-characterized using numerous satellite instruments; it is the smaller eruptions that are the source of most uncertainty. For larger eruptions, it may be possible to validate satellite SO_2 measurements using the mass of sulfate aerosol produced; e.g., for the 1982 El Chichón eruption the TOMS estimate of SO_2 loading is consistent with independent estimates of the mass of sulfate aerosol produced by SO_2 oxidation (Krueger et al., 2008). However, this is not possible for smaller eruptions. Although many eruptions are analyzed in close to real-time as they occur, providing preliminary estimates of SO_2 loading, post-analysis of eruptions may continue many years or decades after the event as new retrieval algorithms are developed (e.g., Guo et al., 2004; Krueger et al., 2008). Table 2 lists many of the eruptions that have been subject to more detailed analysis (typically the larger events); this invariably results in more accurate estimates of SO_2 loadings and uncertainties. We therefore acknowledge that significant uncertainty remains on SO_2 loadings for some eruptions; estimates could potentially change by 50–100% in some cases though order of magnitude changes are considered extremely unlikely.

4.1. Eruptive degassing

4.1.1. General trends in eruptive degassing

An overview of the entire eruptive volcanic SO_2 inventory (Carn, 2015c) is given in Fig. 1, with more detailed time-series of OMI (September 2004–December 2014), AIRS (January 2003–December 2014) and IASI (October 2007–December 2014) SO_2 data shown in Figs. 4, 5, 6 and 7, and a map of average IASI SO_2 columns depicting the geographical extent of detected volcanic SO_2 plumes shown in Fig. 8. Fig. 9 shows a plot of cumulative SO_2 emissions against time for different eruption styles. In total, the database currently contains SO_2 measurements for ~700 eruptions or eruptive events, with a cumulative SO_2 emission of ~101 Tg. Figs. 1 and 9 display the main trends in eruptive SO_2 emissions observed since 1978, namely the large perturbations associated with the 1982 El Chichón and 1991 Pinatubo eruptions, a significant decline after Pinatubo until the late 1990s, followed by a general increase throughout the 2000s, with peaks in 2005, 2008 and 2011, and reduced emissions in 2012–14. Fig. 9 shows possible evidence for an increase in the rate of SO_2 production (primarily from explosive eruptions) beginning in 2004–2005, after a lull between the mid-1990s and early 2000s, although we interpret this cautiously since the change in slope corresponds to the onset of more sensitive SO_2 measurements by OMI, and hence may simply reflect an increased rate of eruption detection (the mean detection rate increases from 8 eruptions/year in 1978–2004 to ~40 eruptions/year in 2004–2014). In contrast, the time-averaged flux of SO_2 from effusive eruptions has been less variable over the past 3–4 decades, although a possible change in slope occurred in the early 2000s (Fig. 9), which may be partly related to an increased magma output rate at Nyamuragira (DR Congo) in this timeframe (e.g., Wadge and Burt, 2011).

No major eruptions were reported during the 1995–96 TOMS data gap (Fig. 1), but we have assessed several smaller events for SO_2 emissions using HIRS/2 data. An effusive eruption of Fernandina (Galápagos Islands) in January–March 1995 was not detected by HIRS/2 (Head, 2005), indicating that SO_2 emissions were confined to the lower troposphere. Some of the largest eruptions of the 1995–96 period occurred at Ruapehu (New Zealand), with significant SO_2 degassing suggested by ground-based COSPEC measurements (Christenson, 2000) and eruption plume altitudes of up to ~9 km (Prata and Grant, 2001), which is close to the tropopause in the mid-latitude southern hemisphere winter. However, Prata et al. (2003) report relatively minor SO_2 loadings of ~0.01–0.03 Tg for the June 17, 1996 eruptions. Analysis of HIRS/2 data for other eruptions in 1995–96 has not revealed any significant UTLS SO_2 emissions. We therefore conclude that the apparent decline in total volcanic SO_2 emissions between 1994 and 1996 (Fig. 1) is genuine; an inference that is also supported by the lack of major SAOD perturbations in that period (Fig. 9).

The latitudinal distribution of eruptive SO_2 emissions in 1978–2014 (Fig. 1) simply reflects the geographic distribution of active volcanoes, which has clusters at 0°–10°S (including Ecuador, the Galapagos islands, DR Congo, Indonesia and Papua New Guinea), 10°–20°N (including Mexico, central America, the West Indies, Afar, the Philippines, the Marianas, and Hawaii), and 50°–60°N (including Kamchatka, the northern Kuriles and the Aleutian islands), with a smaller peak at 30°–40°N (including Sicily, Italy and Japan; Siebert et al., 2010). Regular eruptive activity in the equatorial region is evident, largely due to frequent

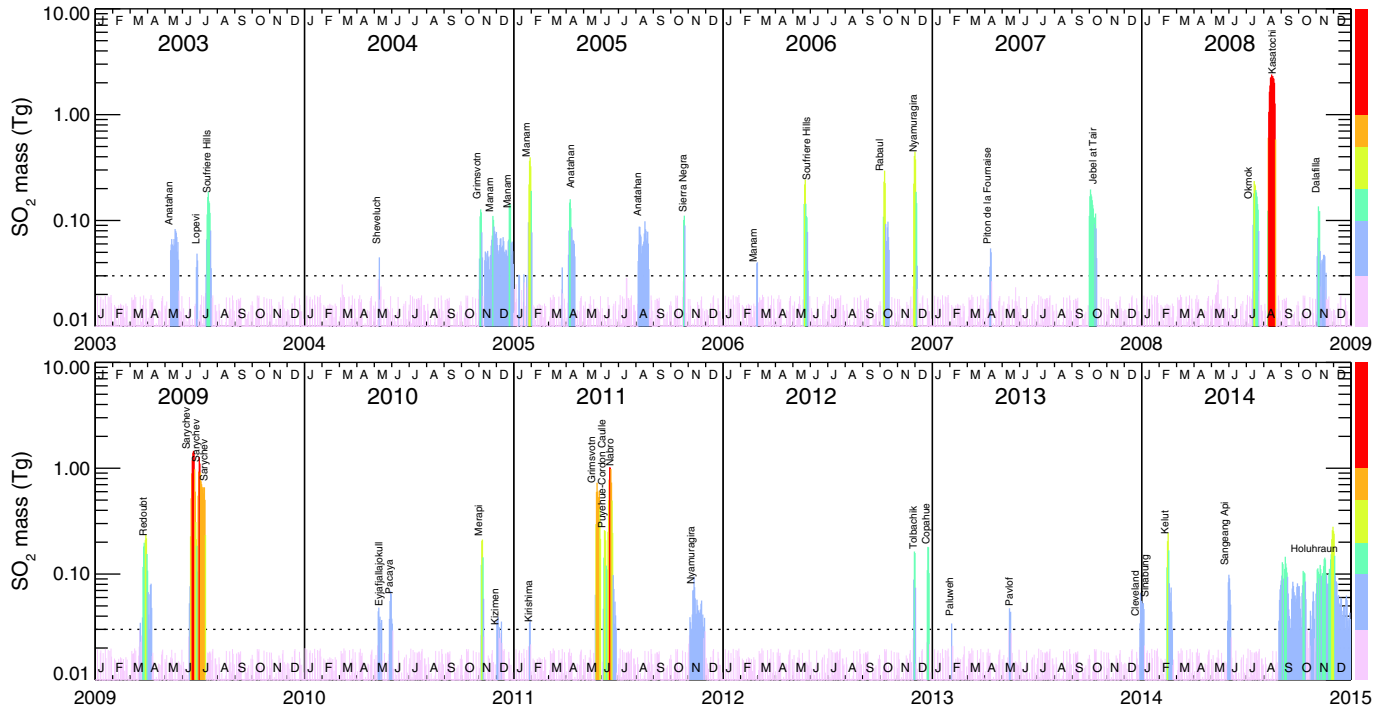

Fig. 5. Time-series of UTLS SO_2 emissions (Tg, log scale) detected by AIRS in 2003–2014 using the Prata and Bernardo (2007) SO_2 retrieval technique. Sources of the observed SO_2 emissions are indicated. SO_2 loadings are also colored based on the *color bar* to the right of the plot.

effusive eruptions of Nyamulagira (DR Congo; Carn and Bluth, 2003; Bluth and Carn, 2008; Smets et al., 2014) and the Galápagos Islands volcanoes (Head, 2005; Carn, 2015b). The spate of increased activity in southern Chile since 2008 (eruptions of Llaima, Chaitén, Cordon-Caulle, Copahue, and Calbuco) is also noteworthy in the otherwise less active extra-tropical southern hemisphere. The general dearth of southern hemisphere eruptions contrasts with the high-latitude northern hemisphere, where there have been relatively frequent eruptions in the Kuriles, Kamchatka, Alaska and Iceland, particularly since 2008 (Figs. 1, 6, 8).

The more sensitive SO_2 measurements by OMI since 2004 (Fig. 4) and IASI since 2007 (Fig. 7) provide more detailed insight into volcanic SO_2 emissions in the last decade. As previously discussed, use of the maximum daily OSI to detect volcanic SO_2 emissions in a continuous daily time-series (Fig. 4) avoids complications when SO_2 from multiple sources at different altitudes is present (accurate SO_2 loadings are shown in Fig. 1). Spikes in the OSI correlate with known eruptions as indicated on Fig. 4, with the OSI value roughly proportional to the maximum SO_2 column amount and altitude on a given day, and the larger (or longer-lived) eruptions have distinctive OSI tails due to the persistence of SO_2 in the atmosphere for days or weeks as it converts to sulfate aerosol. Comparison of the OSI with coincident maximum daily SO_2 and HCl mixing ratios measured by MLS (Fig. 4) clearly indicates the major UTLS injections (e.g., Manam in February 2005, Soufriere Hills in May 2006, Rabaul in October 2006, Kasatochi in August 2008, Redoubt in March 2009, Sarychev Peak in June 2009 (see animation provided as Supplementary Material), Merapi in November 2010, Nabro in June 2011 and Kelut in February 2014; Table 2), although many smaller injections are also apparent upon closer inspection (see also Pumphrey et al., 2015). The significance of the observed HCl emissions will be discussed later (Section 4.1.6). The advantage of SO_2 measurements from multiple platforms is also demonstrated by the large eruption of Manam on November 24, 2004: this occurred during an OMI data gap but the corresponding UTLS SO_2 and HCl injection was detected by MLS (Fig. 4) and the SO_2 cloud was measured by AIRS (Fig. 5), though it was not detected by MIPAS (Höpfner et al., 2015).

Much of the background variation in the OSI time-series in periods devoid of large eruptions is due to smaller eruptions or very high passive SO_2 emissions from volcanoes such as Nyiragongo (DR Congo; 2004–2005; Carn, 2004), Ambrym (Vanuatu; 2005; e.g., Bani et al., 2009, 2012), and Kilauea (Hawaii; strong summit degassing from March 2008), or extended periods of unrest at volcanoes such as Anatahan (CNMI; April–September 2005; see animation provided as Supplementary Material) and Kliuchevskoi (Kamchatka; May–July 2007). Section 4.2 discusses observed sources of passive SO_2 degassing in more depth. It is also likely that some seasonally variable anthropogenic SO_2 emissions are detected by the OSI: for example, the strong SO_2 emissions from the Norilsk metal smelter (Siberia, Russia; e.g., Walter et al., 2012) produce a strong signal in the OMI data in the northern hemisphere spring (March–April) each year (Fig. 4), due to the presence of SO_2 above highly-reflective snow-covered ground.

The AIRS and IASI measurements of UTLS SO_2 emissions and altitude (Figs. 5, 6, 7) are broadly consistent with the OMI SO_2 data, and also with MIPAS SO_2 observations (Höpfner et al., 2015) with the 2008 Kasatochi, 2009 Sarychev Peak and 2011 Nabro eruptions dominating the time-series in terms of SO_2 loading (Table 2). IASI SO_2 altitude retrievals for these eruptions indicate injection of SO_2 to a range of altitudes in the UTLS (Fig. 7), which is consistent with MLS data (Fig. 4). These vertical profiles contrast with the more localized UTLS SO_2 injections associated with the tropical eruptions of Soufriere Hills in May 2006, Rabaul in October 2006, Merapi in November 2010 and Kelut in February 2014 (Figs. 4, 7); this may be a consequence of variable eruption magnitude and style, or of diverse atmospheric dynamics in the tropics and mid-latitudes. An advantage of IASI and AIRS is that they provide robust measurements of high-latitude winter eruptions, such as the December 2010 eruption of Kizimen (Kamchatka; which was incorrectly ascribed to Shiveluch by Höpfner et al. (2015)), the November 2012 eruption of Tolbachik (e.g., Telling et al., 2015), and the 2014 eruption of Holuhraun (Bardabunga, Iceland; Figs. 5, 7). Long-range dispersal of SO_2 emitted by the June 2011 eruption of Cordon Caulle (Chile), which occurred in the southern hemisphere winter, was also tracked more effectively by the IR sensors (Figs. 6, 8). Average SO_2 columns

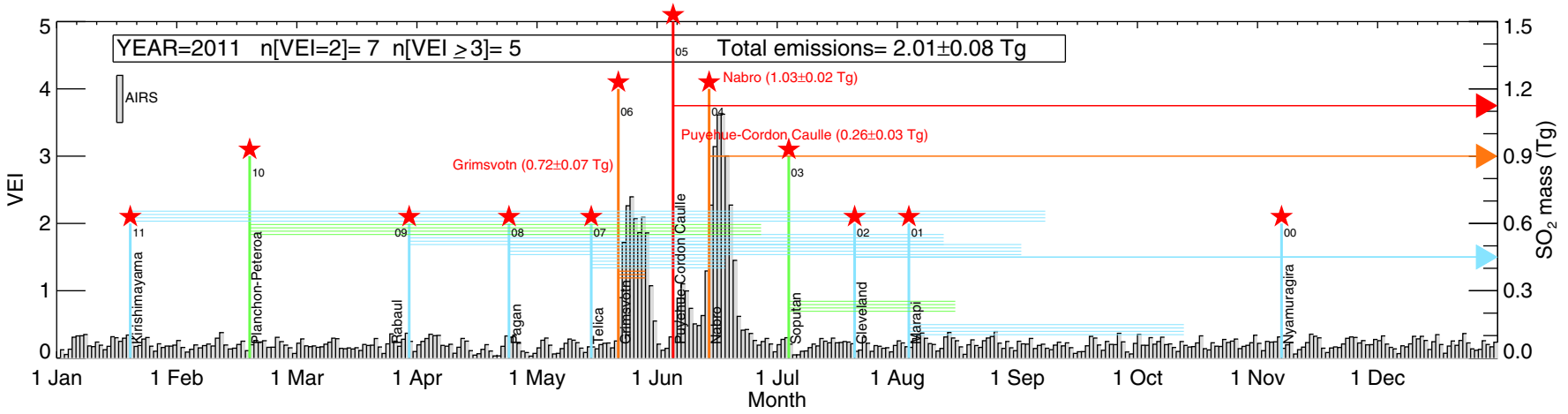
YEAR=2011 n[VEI=2]= 7 n[VEI ≥3]= 5
Total emissions= 2.01±0.08 Tg
AIRS
Nabro (1.03±0.02 Tg)
Puyehue-Cordon Caulle (0.26±0.03 Tg)
Grimsvotn (0.72±0.07 Tg)
VEI
SO2 mass (Tg)
Month
1 Jan
1 Feb
1 Mar
1 Apr
1 May
1 Jun
1 Jul
1 Aug
1 Sep
1 Oct
1 Nov
1 Dec
Kirishimayama
Planchon-Peteroa
Rabaul
Pagan
Telica
Grimsvotn
Puyehue-Cordon Caulle
Nabro
Soputan
Cleveland
Marapi
Nyamuragira

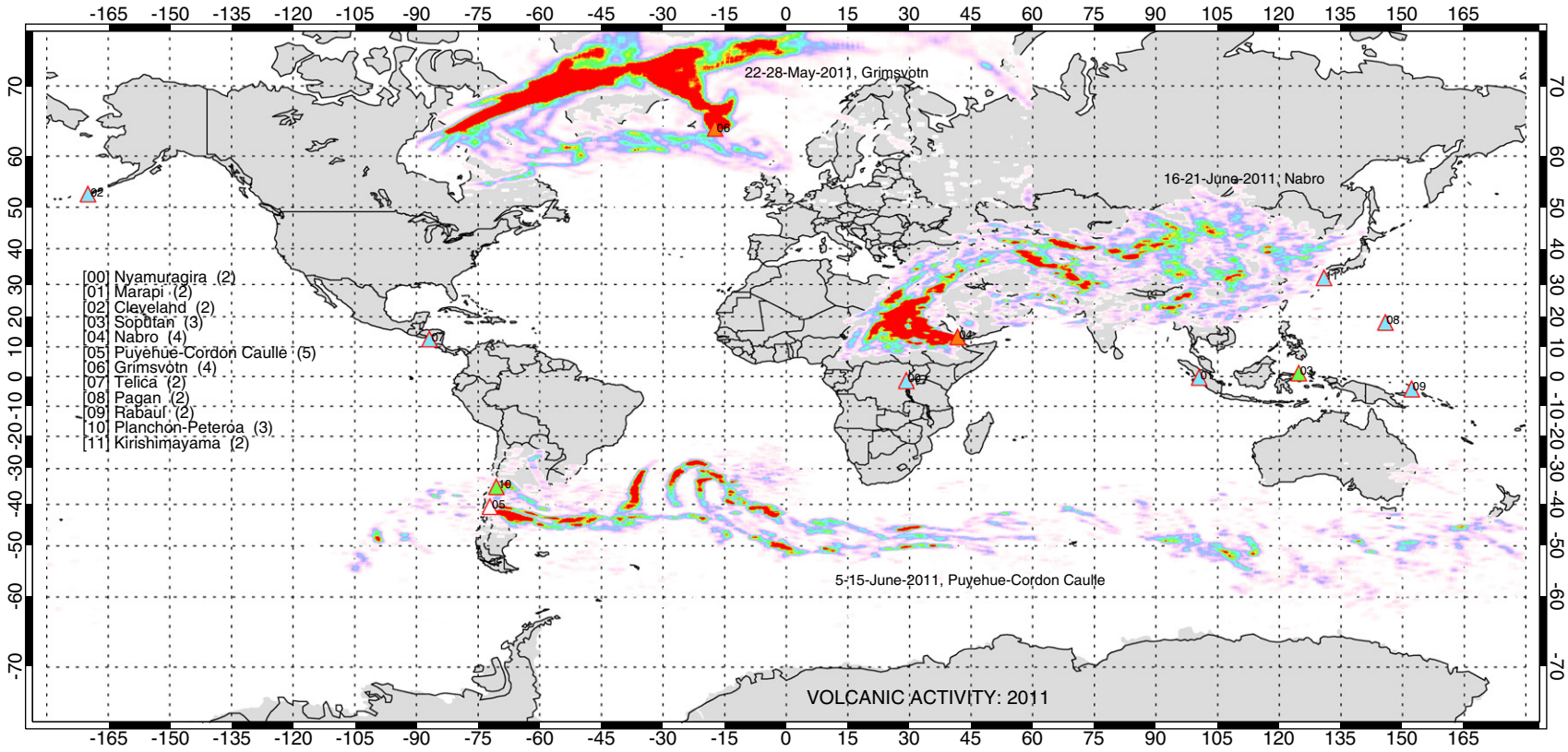
22-28-May-2011, Grimsvotn
16-21-June-2011, Nabro
5-15-June-2011, Puyehue-Cordon Caulle
VOLCANIC ACTIVITY: 2011
[00] Nyamuragira (2)
[01] Marapi (2)
[02] Cleveland (2)
[03] Soputan (3)
[04] Nabro (4)
[05] Puyehue-Cordon Caulle (5)
[06] Grimsvotn (4)
[07] Telica (2)
[08] Pagan (2)
[09] Rabaul (2)
[10] Planchon-Peteroa (3)
[11] Kirishimayama (2)

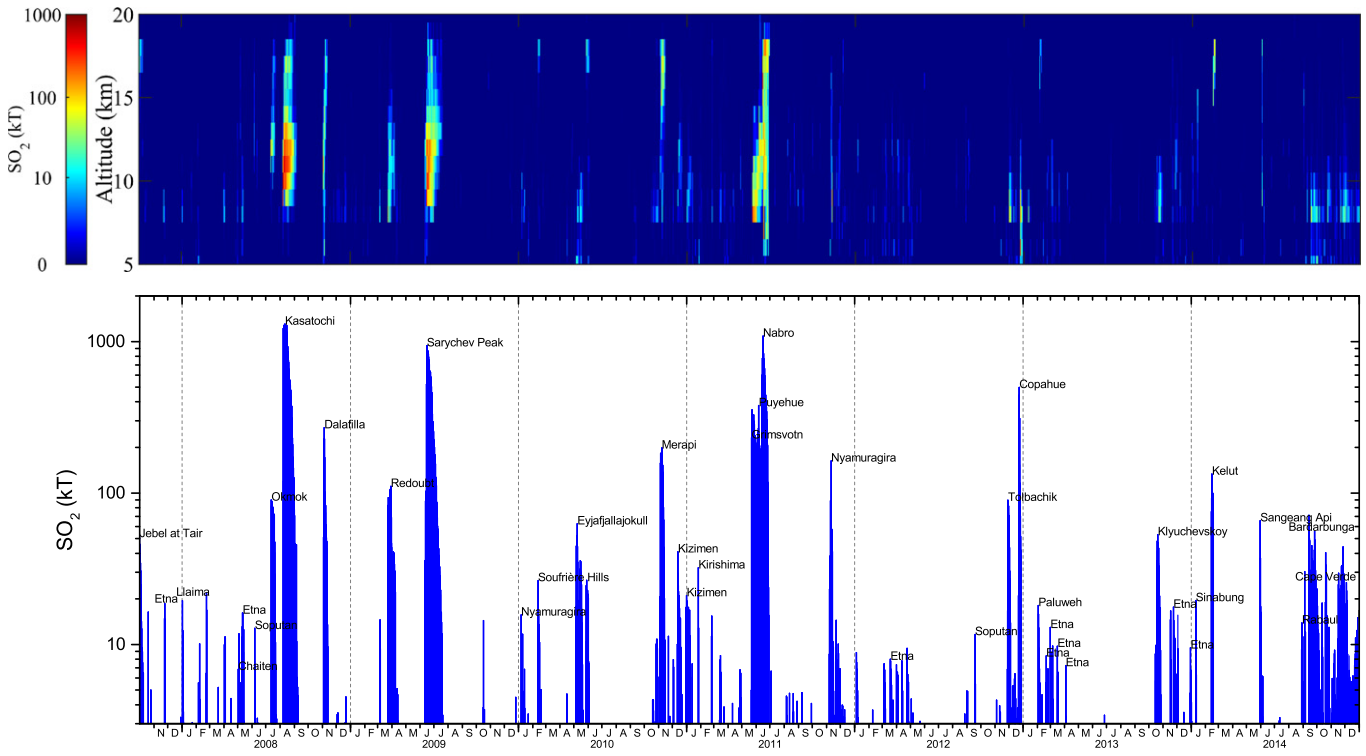

Fig. 7. Time-series of IASI total SO_2 mass (*lower panel*; logarithmic scale in kilotons) and altitude-binned SO_2 mass (*upper panel*; for altitudes >5 km only) measurements from October 2007 to December 2014, derived using the retrieval techniques described by Clarisse et al. (2012, 2014). Prominent volcanic eruptions are labeled in the lower panel.

detected by IASI clearly show the imbalance between northern and southern hemisphere SO_2 emissions since 2007, and long-range tracking of SO_2 from several eruptions made possible by sensitivity to low SO_2 column amounts (Fig. 8). During a two-month period in May–June 2011, large eruptions occurred in Iceland (Grimsvötn), Chile (Cordon Caulle) and Eritrea (Nabro), resulting in UTLS SO_2 emissions spread over an unusually large latitudinal range (Fig. 6).

Comparisons between satellite SO_2 measurements in the overlap periods between missions provide confidence in the data for larger eruptions and in the multi-decadal continuity of the volcanic SO_2 database (e.g., Table 2). TOMS, MODIS, AIRS and MIPAS measured very similar SO_2 amounts (~0.1–0.12 Tg) in the July 2003 Soufriere Hills eruption cloud, which reached 16 km altitude (Table 2; Prata and Bernardo, 2007; Carn and Prata, 2010; Höpfner et al., 2015). The UTLS SO_2 injection from Anatahan on April 6, 2005 was observed by TOMS, OMI, AIRS and MIPAS, with each sensor measuring ~70–80 kt SO_2 (Table 2; Höpfner et al., 2015), with similar agreement observed for most other UTLS SO_2 emissions. Other eruptions, such as the October 2005 effusive eruption of Sierra Negra (Galapagos Islands) show discrepancies between satellite measurements (Table 2) but often there are good reasons for this; in this case a significant fraction of the emitted SO_2 was lower tropospheric, preventing detection by TOMS, which also had some data gaps. Variable spatial coverage of volcanic clouds can also produce differences (e.g., Prata and Bernardo, 2007), hence in general the largest SO_2 mass measured by any sensor is assumed to provide the best estimate.

The August 2008 eruption of Kasatochi, one of the largest explosive eruptions since Pinatubo, is a good example of an event that has been subject to detailed analysis with encouraging convergence of total SO_2 loading estimates from multiple satellite instruments and analysis techniques (Table 2). Contemporary eruption reports suggested ash emissions to at least 11–14 km altitude during the Kasatochi eruption on August 7, 2008 (Global Volcanism Program, 2008). Multiple satellite instruments observed the emitted SO_2 cloud. Kristiansen et al. (2010) used SO_2 measurements from OMI, GOME-2 and AIRS in an inversion scheme to derive a total SO_2 discharge of 1.7 Tg, and a co-eruptive vertical SO_2 profile extending from 7 to 20 km altitude with a major peak at 12 km. They also estimated that ~1 Tg SO_2 (i.e., ~60% of the total SO_2 discharge) was injected into the local stratosphere (>10 km altitude), although this is dependent on the tropopause definition (Kristiansen et al., 2010; Clarisse et al., 2014; similarly, Eckhardt et al. (2008) estimated ~10–60% of SO_2 emitted by the October 2007 eruption of Jebel al-Tair (Yemen) was injected into the stratosphere, depending on tropopause definition). Kristiansen et al. (2010)'s SO_2 loading estimate for Kasatochi could be regarded as robust since the inversion technique includes multiple UV and IR satellite datasets. Individual satellite datasets yield similar results: Karagulian et al. (2010) report 1.7 Tg SO_2 based on IASI measurements using both the 7.3 μm and 4 μm SO_2 bands. A subsequent, improved analysis of IASI data by Clarisse et al. (2012) found a maximum of 1.6 Tg SO_2 measured on Aug. 11, 2008; in agreement with the 1.6 Tg SO_2 measured by GOME-2 (Nowlan et al., 2011). Prata et al. (2010) retrieved a total of ~1.2 Tg SO_2 using AIRS data, with the lower SO_2 amount detected perhaps due to lower sensitivity to low SO_2 columns and incomplete cloud coverage by AIRS. Krotkov et al. (2010) report a slightly higher value of ~2.2 Tg SO_2, injected to 10–12 km altitude, based on OMI measurements and trajectory modeling; in this case the estimated SO_2 loading was derived from extrapolation of the SO_2 decay trend back to the eruption time. This procedure is subject to some uncertainty as the prevailing SO_2 removal processes may not be the same in the early and aged volcanic plume, plus

Fig. 6. Time-series (*upper panel*) and cumulative map (*lower panel*) of SO_2 emissions detected by AIRS in 2011 (data for other years in 2003–2014 are provided as Supplementary Material). *Upper panel* shows daily SO_2 amounts (Tg) retrieved by AIRS using the Prata and Bernardo (2007) algorithm (*gray bars*) and reported volcanic eruptions (*colored bars* and *stars*; color denotes VEI). *Horizontal bars* indicate eruption duration reported by the Smithsonian GVP; *horizontal arrows* indicate eruptions or activity continuing into the following year. Note that not all the indicated eruptions produced SO_2 detected by AIRS. *Lower panel* shows cumulative SO_2 column amounts retrieved by AIRS with major eruptions indicated.

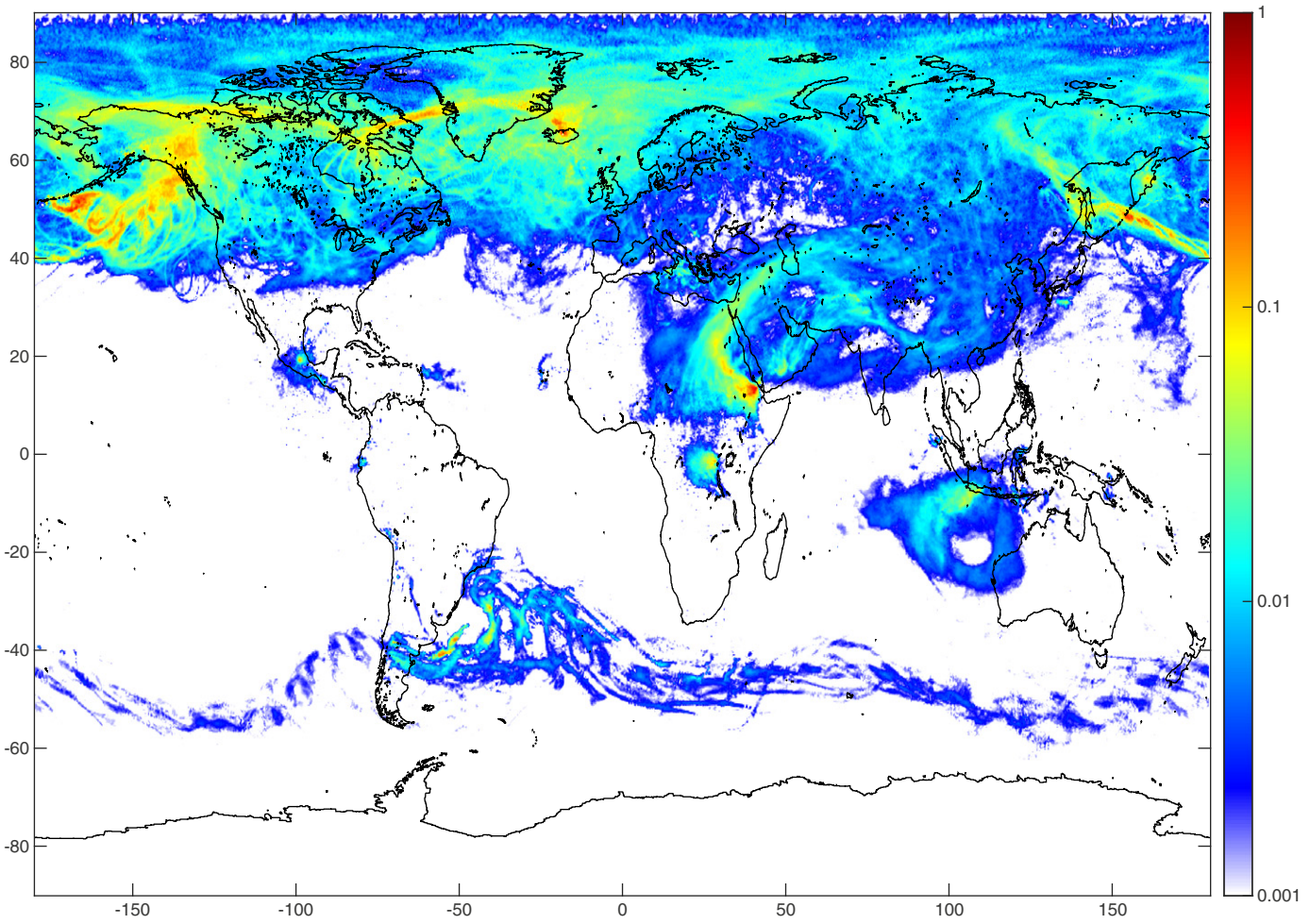

Fig. 8. Average SO_2 columns measured by IASI over ~7 years (October 2007–December 2014). The scale is logarithmic (log[1 + (mean SO_2 column in DU)]). The more prominent eruptions evident in this map include Kasatochi (Alaska; August 2008), Sarychev Peak (Kurile Islands; June 2009), Merapi (Indonesia; November 2010), Grimsvötn (Iceland; May 2011), Cordón Caulle (Chile; June 2011), Nabro (Eritrea; June 2011) and Copahue (Chile; December 2012).

the observed e-folding time for SO_2 removal was relatively short (~9 days; Krotkov et al., 2010), possibly due to proximity to the tropopause (e.g., Campbell et al., 2012), and this impacts the extrapolated SO_2 mass estimate. Note that the largest SO_2 mass measured by OMI in a single, coherent cloud was 1.8 Tg on August 10 (Krotkov et al., 2010). MODIS SO_2 retrievals for Kasatochi, including 8.6 μm data corrected for ash interference (Corradini et al., 2010), are broadly consistent with the other estimates within stated uncertainties (Table 2). Thus, when all UV and IR satellite measurements are considered we find general convergence on a total SO_2 emission of ~2 Tg for the 2008 Kasatochi eruption, a value that can be considered very robust.

4.1.2. Eruptive SO_2 flux

Knowledge of the time-averaged flux of volcanic SO_2 into the UTLS is crucial for interpretation of trends in SAOD and assessment of the impact of volcanic activity on climate. Using TOMS SO_2 data for 1978–1993, Bluth et al. (1993) estimated an annual volcanic SO_2 flux from explosive volcanism of ~4 Tg, clearly influenced by the large El Chichón and Pinatubo eruptions in that era. Pyle et al. (1996) calculated a medium-term (~100 year) flux of ~1 Tg/yr. volcanic SO_2 to the stratosphere (0.3–3 Tg/yr. range), and a short-term (10–20 year) flux due to small eruptions (10^{10}–10^{12} kg or VEI 3–5) of ~0.4 Tg/yr. Here, we provide updated estimates of the volcanic SO_2 flux to the UTLS based on recent satellite measurements, with improved data for smaller eruptions.

Table 3 reports the total annual SO_2 emissions measured by satellites from 1978 to 2014 for all detected eruptions and for explosive eruptions only (i.e., excluding effusive eruptions; also plotted in Fig. 1). The latter have greater potential to reach the UTLS and impact climate. Our distinction between explosive and effusive eruptions in the SO_2 emissions database (Carn, 2015c) is based on the dominant style of activity; we define effusive eruptions as those dominated by effusion of basaltic lava flows (typically in intraplate settings). Eruptions involving extrusion of silicic lava domes (e.g., Soufriere Hills, Montserrat) are categorized as 'explosive' since it is the discrete, explosive emissions from these eruptions that are most effectively measured from space. To estimate total SO_2 emissions from effusive eruptions we have used the procedure described by Bluth and Carn (2008), which accounts for rapid, daily removal of SO_2 in lower tropospheric plumes.

A notable feature of the volcanic SO_2 data is significant inter-annual variability, with total explosive SO_2 emissions varying from 10 kt (in 1987) to ~24 Tg (in 1991; Table 3). On average, ~50% of annual measured SO_2 emissions have been sourced from explosive eruptions (Table 3), indicating the important contribution of sulfur-rich effusive basaltic eruptions to the global flux. The mean annual SO_2 fluxes from all detected eruptions and explosive eruptions are 2.8 Tg (range = 0.04–26 Tg) and 1.6 Tg (range = 0.01–24 Tg), respectively; the latter can be considered an estimate of the SO_2 flux to the UTLS, and if we assume that ~60% of this SO_2 enters the stratosphere (based on detailed analyses of the 2008 Kasatochi and 2007 Jebel al-Tair eruptions; Eckhardt et al., 2008; Kristiansen et al., 2010) then the stratospheric flux is ~1 Tg/yr. SO_2, similar to earlier estimates of medium-term and longer-term (~10^3 years) fluxes (Pyle et al., 1996). We can

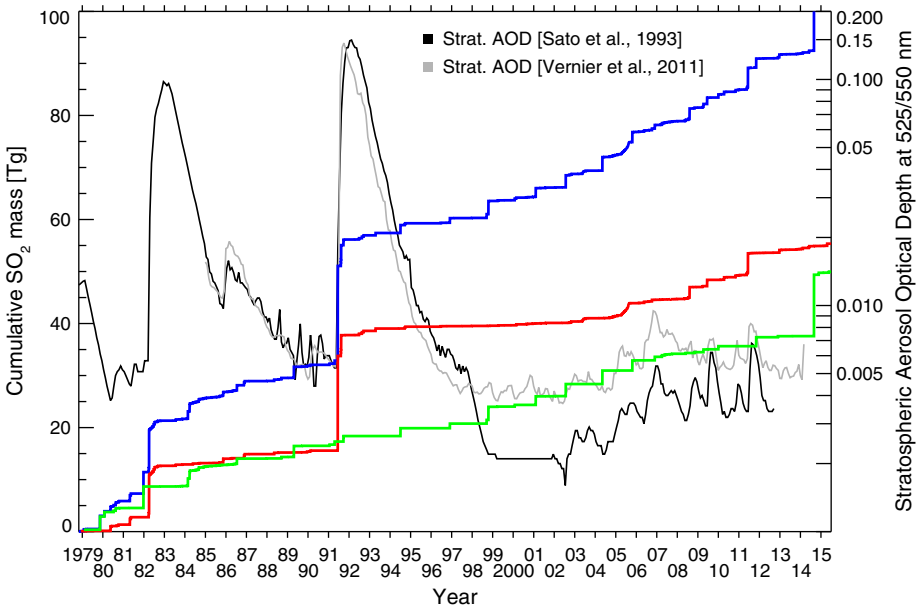

Fig. 9. Cumulative SO_2 emissions from volcanic eruptions against time for 1978–2015, showing emissions for all eruptions detected from space (*blue line*), explosive eruptions only (*red line*) and effusive eruptions only (*green line*). *Black line* shows global stratospheric aerosol optical depth (SAOD) at 550 nm for 1978–2012 from Sato et al. (1993) and recent updates through December 2012 (http://data.giss.nasa.gov/modelforce/strataer/); *gray line* shows the tropical (30°S–30°N) SAOD at 525 nm data of Vernier et al. (2011; with recent updates) for 1985–2014 based on SAGE II, GOMOS and CALIPSO observations of aerosol between 15 and 40 km altitude. Differences in the SAOD datasets arise from different sources of SAOD observations, interpolation methods, latitude range (the Sato et al. (1993) data plotted are global whereas the Vernier et al. (2011) data are for the tropics; thus high-latitude eruptions produce a weaker signal in the latter) and altitude ranges (the Vernier et al. (2011) data cover altitudes of 15–40 km and hence includes part of the tropical upper troposphere, resulting in larger AODs in some periods).

conclude that the flux of volcanic SO_2 to the stratosphere in the past 3–4 decades has not been abnormally high or low. The relationship between SO_2 emission and eruption magnitude is explored in more detail in Section 4.1.3.

The exact proportion of emitted SO_2 that enters the stratosphere during an explosive eruption will vary with eruption magnitude, location and style. Although we attempt to separate volcanic SO_2 injected into the UTLS from that injected into the stratosphere sensu stricto, volcanic SO_2 injected into the upper troposphere below the tropopause also has the potential to impact the stratosphere. Effusive eruptions are not generally regarded as significant sources of stratospheric pollution, notwithstanding large-volume fissure eruptions with high eruption rates (e.g., Stothers et al., 1986), yet they frequently emit prodigious quantities of SO_2 into the upper troposphere (e.g., Krueger et al., 1996; Carn and Bluth, 2003; Head, 2005; Bluth and Carn, 2008; Hughes et al., 2012; Höpfner et al., 2015) where it has the potential to cross the tropopause. MIPAS detected SO_2 in the UTLS (at altitudes of up to 18–22 km) after several eruptions of Nyamuragira (in 2002, 2006 and 2010) and the 2009 Fernandina eruption (Galápagos Islands; Höpfner et al., 2015), suggesting that such eruptions should not be neglected as a possible source of stratospheric SO_2. The June 12, 2011 eruption of Nabro, which was initially (and, it transpired, incorrectly) reported as tropospheric but produced a significant SAOD anomaly (e.g., Sawamura et al., 2012; Uchino et al., 2012; Bourassa et al., 2012; Mateshvili et al., 2013), ignited a debate over the relative roles of direct injection and cross-tropopause transport by other processes such as deep convection or isentropic ascent in lofting volcanic SO_2 into the stratosphere (Bourassa et al., 2012; Fromm et al., 2013; Vernier et al., 2013; Bourassa et al., 2013; Fairlie et al., 2014; Fromm et al., 2014; Penning de Vries et al., 2014; Clarisse et al., 2014). In addition to the evidence presented in these works, which indicate that both early direct injection and subsequent slow ascent of SO_2 and sulfate aerosol contributed to Nabro's stratospheric impact, daily MLS SO_2 retrievals (Fig. 10) also show SO_2 close to or above the tropopause (at 68 hPa) as early as June 13–14 plus a slower ascent of SO_2 (up to ~46 hPa or 19–20 km altitude) in the subsequent two weeks. Interestingly, MLS data do not show the same evidence for substantial stratospheric HCl input (Fig. 10), likely due to more efficient HCl removal processes in the troposphere. Overall, the Nabro eruption demonstrates that volcanic eruptions can be complex, multifaceted events and require analysis on a case-by-case basis to unravel their stratospheric impact. The Nabro eruption displayed characteristics of both explosive and effusive eruptions in that it initially produced an energetic eruption column (e.g., Fee et al., 2013) that penetrated the UTLS, yet it did not produce a substantial ash cloud and emitted a long lava flow, with tropospheric SO_2 emissions continuing for several weeks after the initial paroxysm (e.g., Theys et al., 2013; Goitom et al., 2015). It can thus be considered a relatively rare, hybrid event sharing features of two 'end-member' eruptions: a sulfur-rich, effusive eruption injecting SO_2 predominantly into the troposphere (e.g., similar to Nyamuragira) and an explosive eruption with direct stratospheric injection (e.g., the January 2005 Manam eruption; Fig. 4).

4.1.3. VEI-SO_2 loading relationships

Analysis of the relationship between SO_2 production and eruption magnitude (VEI) can inform studies of the atmospheric and climate impact of eruptions prior to the satellite measurement era. In comparing measured SO_2 emissions with reported eruption VEIs, we extend earlier work based on TOMS SO_2 data by Schnetzler et al. (1997) with the addition of many more observations of smaller eruptions due to improved satellite data quality. We also attempt to estimate how much volcanic SO_2 could elude detection from space based on VEI-SO_2 mass relationships. We note that more precise (i.e., continuous) measures of eruption size, such as magnitude and intensity, are more useful for such analyses than the more limited cardinal (or discrete) VEI scale, since each VEI category encompasses a significant range of eruption size (e.g., Pyle, 1995, 2015). However, magnitudes and intensities are only available for a relatively small number of eruptions, and here we use the Smithsonian GVP database of VEIs from VOTW 4.3.0. Some small modifications to the VOTW database were necessary to account for long-duration eruptions assigned a single VEI; hence continuous activity at Anatahan in 2005, included as a single VEI 3 eruption in the VOTW catalog, was

Table 3
Total annual eruptive volcanic SO_2 emissions, 1978–2014.

Year	Total SO_2 emissions (kt)	Explosive SO_2 emissions (kt)	Explosive/Total SO_2 (%)
1978[a]	87	87	100
1979	2945	63	2.1
1980	2882	1228	43
1981	5562	1430	26
1982	11,033	9950	90
1983	348	260	75
1984	3957	252	6.4
1985	1241	852	69
1986	2086	872	42
1987	38	10	26
1988	580	300	52
1989	2329	177	7.6
1990	186	186	100
1991	26,082	24,214	93
1992	810	810	100
1993	450	450	100
1994	1874	360	19
1995[a]	TOMS data gap		
1996[a]	987	100	10
1997	41	41	100
1998	3265	38	1.2
1999	130	85	65
2000	653	336	51
2001	1783	122	6.8
2002	2626	271	10
2003	679	679	100
2004	2997	410	14
2005	4634	2501	54
2006	1347	661	49
2007	712	122	17
2008	2625	2318	88
2009	1934	1379	71
2010	1470	867	59
2011	6030	4310	71
2012	763	563	74
2013	185	180	97
2014	5296	608	11
Total	**100,646**	**57,090**	
Mean[b]	**2873**	**1629**	**57**
1σ[b]	**4621**	**4317**	

[a] Denotes incomplete year or data gap.
[b] Excluding 1978 and 1995.

subdivided into discrete VEI 2 and 3 events based on reported plume altitudes.

As pointed out by Pyle (2015), there are few metrics other than VEI, magnitude and intensity that are routinely used to describe eruption size. However, we contend that SO_2 measurements are the most accurate way of quantifying the impact of an eruption on climate (and atmospheric composition generally), which is ultimately among the main goals of any eruption magnitude scale, given that volcanic ash has only minor climate impacts (e.g., Robock, 2000). Since SO_2 emissions are not clearly linked to other magnitude scales (which are more relevant to impacts determined by emissions of solid ejecta such as volcanic ash and lava, e.g., on aviation or the environment), except in the broadest sense (e.g., Schnetzler et al., 1997; Blake, 2003; Scaillet et al., 2003), there may be a need for multiple measures of eruption magnitude and impact. Intensity (which determines eruption column altitude) may be a more relevant metric than magnitude or VEI for assessment of climate impacts.

Tables 4 and 5 summarize the measured SO_2 emissions per VEI category for explosive eruptions and all detected eruptions, respectively, and the data for individual eruptions are plotted in Fig. 11. Fig. 11 indicates that, when effusive eruptions (as defined in Section 4.1.2) are excluded, there is a broad correlation between VEI and SO_2 emission; i.e., there is roughly an order of magnitude increase in mean SO_2 discharge with increasing VEI (Table 4). A similar correlation was found by Schnetzler et al. (1997) using a smaller dataset. Based on the mean SO_2 loading for each VEI (Table 4) we find the following relationship:

$$\log_{10}(SO_2, \mathrm{Tg}) = 0.71VEI - 3.15 \quad (1)$$

Cross-checking with the VOTW database shows that SO_2 emissions by all reported eruptions with VEI ≥ 4 have been quantified (consisting of 26, 4, and 1 eruptions of VEI 4, 5, and 6, respectively, reported in the VOTW database), confirming that satellite measurements provide excellent constraints on SO_2 emissions by the largest eruptions. Note that some eruptions are assigned high VEIs due to large cumulative erupted volumes over long periods (years), but may not feature any discrete large eruptive events; e.g., activity at Kliuchevskoi (Kamchatka) in 1986–1990 (where SO_2 was occasionally detected by TOMS), or long-term dome-building eruptions at Shiveluch (Kamchatka) in 1999–2014, during which time a few relatively small SO_2 emissions have been detected. In such cases we include these eruptions as 'detected' if any SO_2 emissions were measured at any time during the reported eruption period, although the total eruptive SO_2 emissions may be poorly constrained. Emissions from such continuous eruptions are more akin to passive volcanic degassing, with similar challenges for detection from space.

For eruption magnitudes below VEI 4, the SO_2 emission record becomes increasingly incomplete. Based on reported VEIs, around 50% of VEI 3 eruptions (n = 162) have been detected by satellite SO_2 measurements (Tables 4, 5). The VEI 3 category likely includes some phreatic or phreatomagmatic eruptions that may generate substantial eruption columns (>3 km altitude required for VEI 3) but which would not emit large quantities of SO_2. Some VEI 3 events also correspond to extended periods of volcanic unrest, often with continuous SO_2 emissions (e.g., Ambrym, Vanuatu). Other VEI 3 eruptions only appear to produce ash, with no detectable SO_2; e.g., many eruptions of Bezymianny (Kamchatka) produce little measurable SO_2, but based on Smithsonian GVP reports it appears that the larger explosive eruptions are detected. However, Bezymianny clearly does not appear to be a major source of SO_2 emissions based on detected events. We also stress that, for the lower magnitude eruptions, not all satellite data has been analyzed in detail due to the increasingly large number of events. However, it is likely that any significant SO_2 emissions would have been noticed and recorded.

At magnitudes of VEI ≤ 2, it is clear that the majority of eruptions (87% or more) are not detected (Tables 4, 5), most likely due to insufficient SO_2 release. However, it is also certain that not all the >1000 reported VEI 0–2 eruptions have been checked for SO_2 emissions in satellite data. By definition, non-explosive, effusive eruptions (e.g., in Hawaii, DR Congo, the Galápagos Islands and Iceland) are generally assigned a VEI of 0–2, but these are all detected due to their typically SO_2-rich emissions (e.g., Carn and Bluth, 2003; Sharma et al., 2004; Head, 2005; Bluth and Carn, 2008; Carn, in press), which obfuscate any relationship between SO_2 emission and VEI (e.g., Fig. 11). In fact, the only VEI 0 eruptions with confirmed SO_2 emissions are effusive eruptions (Tables 4, 5; Fig. 11). Although the undetected, explosive VEI 0–2 eruptions are unlikely to be significant from a climate perspective (due to low column heights and/or low SO_2 amounts), quantifying their emissions may be important for the global sulfur budget and sulfur cycle, and for the budgets of other, longer-lived volcanic gases such as CO_2, but would require more extensive ground-based measurements of this class of eruption. Indeed, at the lower end of the VEI scale the distinction between continuous, passive degassing and frequent small eruptions becomes tenuous.

Despite the poor sampling of low magnitude eruptions, a notable feature of the SO_2 data is the high variability of SO_2 emissions from eruptions of intermediate size (VEI 2–4), with standard deviations similar to or exceeding the mean SO_2 loading for each VEI (Tables 4, 5; Fig. 11). The range of SO_2 emissions for intermediate VEIs is larger than reported by Schnetzler et al. (1997) due to improved data for

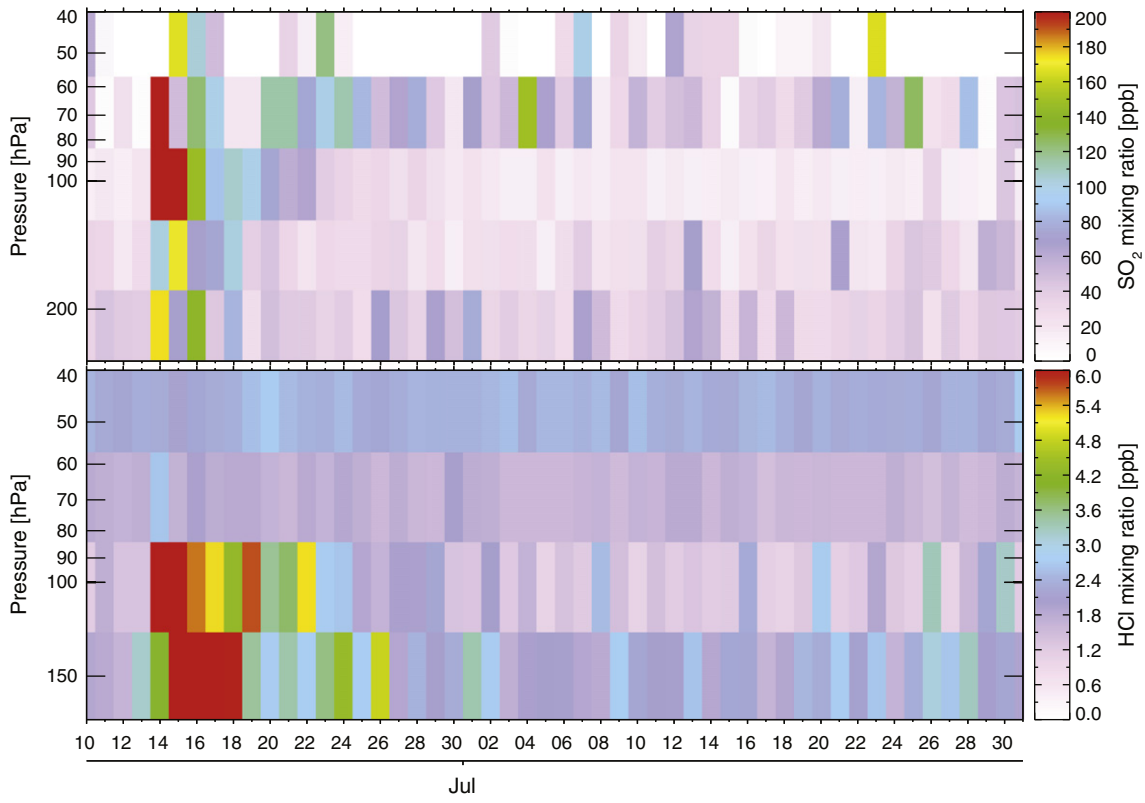

Fig. 10. Daily maximum UTLS mixing ratios of SO_2 (*upper panel*) and HCl (*lower panel*) measured by MLS between June 10 and July 30, 2011, showing the impact of the June 12, 2011 eruption of Nabro (Eritrea).

smaller eruptions; thus the increased variability may reflect sampling of eruptions with a larger range of magmatic sulfur contents. Since all VEI 4 eruptions since 1978 have been detected, we have good constraints on the variability of SO_2 discharge from this magnitude class, which covers ~2–3 orders of magnitude. The greatest variability is found for VEI 3 eruptions (Tables 4, 5), which range over ~3 orders of magnitude (Fig. 10). The actual variability may be even greater, since only 50% of VEI 3 eruptions have been detected (likely the more SO_2-rich ones). This extreme variability makes it challenging to estimate SO_2 emissions from past eruptions based on VEI alone, but this analysis at least provides some potential error bars on such predictions. One likely cause of the observed variability is that some VEIs may be inaccurate, which relates to our earlier point that SO_2 emissions offer a useful alternative indication of eruption magnitude. For example, both the 2011 Nabro and 2008 Kasatochi eruptions were assigned a VEI of 4, but their total SO_2 emissions (~2–4 Tg) are the highest in this VEI class and are similar to or greater than the mean SO_2 loading for VEI 5 eruptions. Indeed, for Nabro, Goitom et al. (2015) estimate a magnitude of 5.1 based on total observed SO_2 emissions (Theys et al., 2013) and magmatic sulfur content. Similarly, the magnitude of the Kasatochi eruption has been estimated as 4.5–4.7 (Pyle, 2015), although we note that the 2008 Chaitén eruption (which produced <20 kt of detectable SO_2) was also a magnitude 4.7–5 event. Nevertheless, refinement of eruption magnitudes would likely improve the correlation between SO_2 emission and VEI shown in Fig. 11, and the SO_2 measurements provide perhaps the most robust basis for adjusting VEIs for recent eruptions. Finally, we note that Scaillet et al. (2003) also found an increased spread of estimated SO_2 yield with decreasing eruption magnitude based on petrological data, which they attributed to the variability in bulk sulfur contents of magmas. Thus the variability in observed SO_2 loadings for smaller eruptions (Fig. 10) may represent sampling of magmas with different bulk sulfur content.

Table 4
Explosive volcanic SO_2 emissions per Volcanic Explosivity Index (VEI) class.

VEI	Eruptions[a]	Detected (%)	Measured SO_2				Est. undetected SO_2	
			Mass (Tg)	Flux (Tg/yr)[b]	Mean (Tg)	1σ (Tg)	Mass (Tg)	Flux (Tg/yr)[b]
0	222	0	–	–	–	–	0.22	0.006
1	507	4	0.26	0.007	0.006	0.006	2.9	0.081
2	479	13	3.22	0.09	0.02	0.02	8.35	0.23
3	162	50	8.18	0.23	0.05	0.11	5.67	0.16
4	26	100	13.05	0.36	0.45	0.75	0	0
5	5	100	11.28	0.31	2.26	2.82	0	0
6	1	100	20	0.56	20	–	0	0
Total	1402		55.97				17	0.48

[a] Extracted from the Global Volcanism Program Volcanoes of the World 4.3.0 database (accessed 19 Sept. 2014) for Oct. 1978–Sep. 2014. Listed eruptions without an assigned VEI (75 eruptions) were ignored.
[b] Mean annual SO_2 flux for the ~36 year period of observations.

Table 5
Total volcanic SO_2 emissions per Volcanic Explosivity Index (VEI) class.

VEI	Eruptions[a]	Detected (%)	Measured SO_2			
			Mass (Tg)	Flux (Tg/yr)[b]	Mean (Tg)	1σ (Tg)
0	222	5	6.6	0.18	0.6	1.28
1	507	4	4.6	0.13	0.05	0.15
2	479	13	21.4	0.59	0.07	0.3
3	162	50	22.4	0.62	0.14	0.45
4	26	100	13.2	0.37	0.44	0.74
5	5	100	11.3	0.31	2.26	2.82
6	1	100	20	0.56	20	–
Total	1402		99.6			

[a] Extracted from the Global Volcanism Program Volcanoes of the World 4.3.0 database (accessed 19 Sept. 2014) for Oct. 1978–Sep. 2014. Listed eruptions without an assigned VEI (75 eruptions) were ignored.
[b] Mean annual SO_2 flux for the ~36 year period of observations.

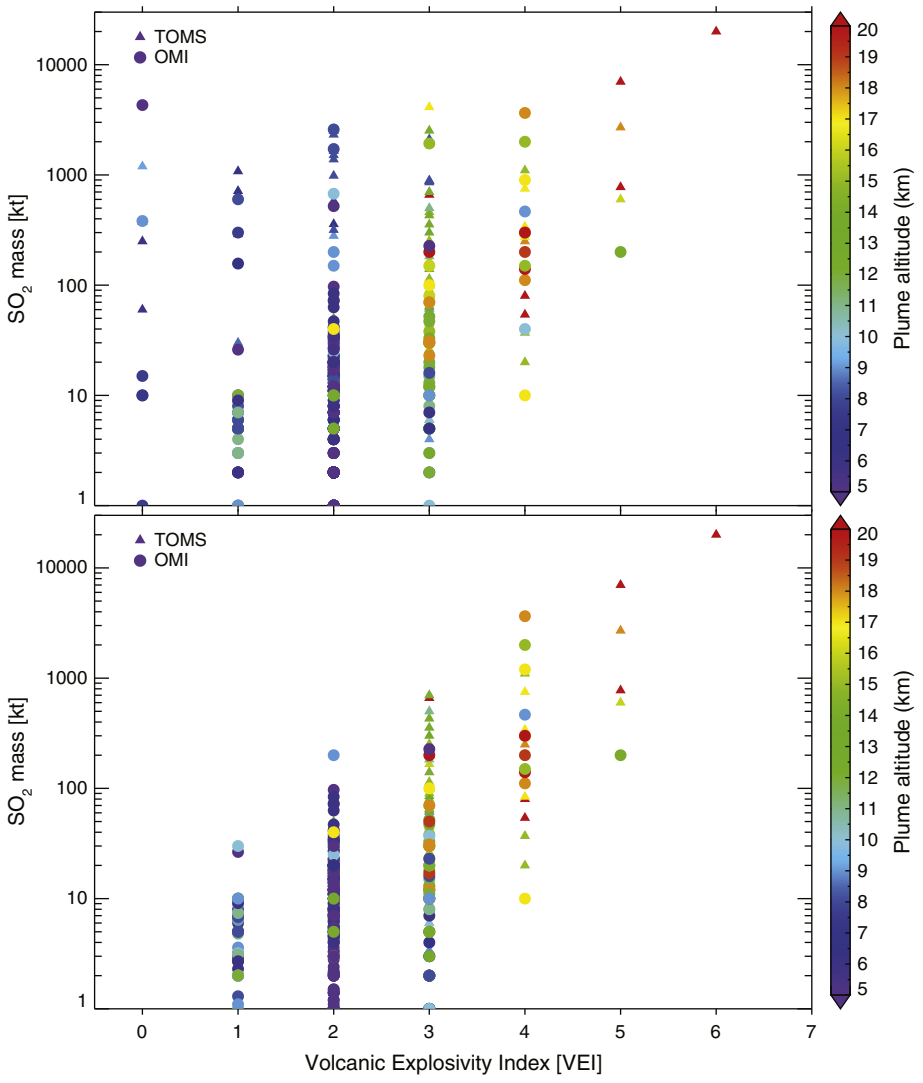

Fig. 11. *Upper panel*: SO_2 mass loading against Volcanic Explosivity Index (VEI) for all measured eruptions (1978–2014). *Triangles* and *circles* denote eruptions detected by TOMS (i.e., in 1978–2004) and OMI (i.e., in 2004–2014), respectively. *Lower panel*: SO_2 mass loading against VEI for explosive eruptions only (i.e., excluding effusive eruptions regardless of VEI). VEIs are derived from the Smithsonian Global Volcanism Program (GVP) database (VOTW 4.3.0).

To assess the SO_2 emissions from low-magnitude explosive eruptions that elude detection from space, we can use the mean SO_2 loading for detected eruptions, the VEI-SO_2 regression (Eq. (1)), or an estimate of the sensor detection limit. For example, the VOTW 4.3.0 catalog includes 507 eruptions with VEI 1, of which only 4% have detected SO_2 emissions (Table 4), i.e., 487 eruptions are unaccounted for. Using the mean SO_2 emission for detected VEI 1 eruptions (excluding effusive eruptions) of 0.006 Tg SO_2 yields an estimated SO_2 emission of $487 \times 0.006 = 2.9$ Tg SO_2 from undetected eruptions (Table 4). Using Eq. (1) yields an estimated SO_2 loading of 0.004 Tg per eruption and a total undetected amount of 1.9 Tg SO_2. We consider these upper limits, since it is likely that the larger SO_2 emissions in each VEI category would be detected, and hence the mean SO_2 mass may be biased high, and some eruptions are known to have produced only ash emissions and/or no measurable SO_2 (e.g., phreatic or phreatomagmatic eruptions, submarine eruptions). Using the same logic for all VEI categories with missing data (VEI 0–3) we calculate the estimates of undetected SO_2 emissions and equivalent annual mean fluxes for the ~36 years of satellite measurements listed in Table 4. Hence, the total estimated unmeasured SO_2 discharge for VEI 0–3 eruptions is ~0.48 Tg/yr. SO_2, or ~17 Tg SO_2 in total (Table 4), i.e., equivalent to a single Pinatubo-scale event, or ~20% of the ~100 Tg total measured SO_2 emissions. Most of the undetected SO_2 is sourced from VEI 2 eruptions (~50%; Table 4). Again, we consider these estimates to be upper bounds for the reasons mentioned above. The undetected SO_2 emissions are commensurate with one VEI 4 eruption per year, or a single VEI 6 eruption, but although this appears significant we stress that the unquantified SO_2 is sourced from low-magnitude eruptions and hence is unlikely to significantly impact the stratosphere or climate. However, the emissions will impact the tropospheric SO_2 budget and the budgets of other volcanic gases (e.g., CO_2). Due to variable eruption rates, the unmeasured fraction may be more significant in some years than others, but we find an overall uncertainty of ~20% on total eruptive SO_2 emissions to be very acceptable. A further consideration in calculating the mean SO_2 emission for each VEI category is whether the probability density function (PDF) of SO_2 loading for measured eruptions is Gaussian or lognormal, since this affects calculation of the mean. Although data are limited, the PDF appears approximately Gaussian for some VEIs (VEI 4), but may be more lognormal for lower VEIs. Further statistical analysis of the database is encouraged.

In summary, we conclude that the flux to the stratosphere (or UTLS) from VEI 4+ eruptions is very well constrained (Tables 4, 5), but significant uncertainty remains on the flux from smaller eruptions (as for passive volcanic degassing). However, more eruptions of low VEI eluded detection during the TOMS missions (1978–2004) than since 2004 with the onset of more sensitive OMI and IASI SO_2 measurements, so

the uncertainty on SO_2 emissions from small eruptions is lower for the last decade.

4.1.4. Sources of eruptive volcanic SO_2 emissions

In total, around 110 volcanoes are responsible for the eruptive SO_2 emissions detected from space in the current database (Fig. 12). With the exception of Antarctica and the South Sandwich Islands, at least one eruption has been detected in each of the 19 volcanic regions defined by the Smithsonian GVP (Siebert et al., 2010; Fig. 12). A further ~30 volcanoes have produced passive (non-eruptive) SO_2 emissions detected in satellite data (see later discussion), resulting in a total of ~140 global volcanoes with detectable SO_2 emissions since 1978. This is only ~9% of the 1545 volcanoes with known or inferred Holocene eruptions, or ~17% of the 858 volcanoes with dated Holocene eruptions, listed in the Smithsonian GVP catalog (Siebert et al., 2010). Table 6 lists the sources of detected eruptive SO_2 emissions over 10 kt between 1978 and 2014 in decreasing order of total measured SO_2 production, along with the number of eruptions generating the observed SO_2 emissions, and a qualitative assessment of degassing style. Only eruptive SO_2 emissions are reported in Table 6, i.e., passive degassing from volcanoes with variable degassing styles such as Etna and Kilauea is excluded. The global distribution of eruptive SO_2 sources is shown in Fig. 12.

The sources in Table 6 highlight the significant contribution of effusive volcanic eruptions to the eruptive volcanic SO_2 flux (e.g., Nyamuragira, Sierra Negra, Holuhraun, Fernandina, Cerro Azul, Mauna Loa, Wolf), though the SO_2 emitted by these events is mostly tropospheric and less significant for climate. However, effusive eruptions have the potential to inject SO_2 at or above tropopause altitudes, particularly at higher latitudes (e.g., Stothers et al., 1986; Krueger et al., 1996), and have been linked to SAOD perturbations in the past (e.g., a SAOD disturbance in 1979 was partly attributed to the 1979 Sierra Negra eruption; Fig. 13; Rosen and Hofmann, 1980). Hence, given the frequency of these eruptions (e.g., Figs. 1, 9), they constitute an important source of SO_2 in the UTLS. Otherwise, the dominant eruptive SO_2 emissions (>2 Tg SO_2) have been produced by the first recorded eruptions of previously dormant volcanoes (mostly in subduction zones), typically after centuries or more of quiescence (e.g., 1991 Pinatubo: previous dated eruption in 1450; 1982 El Chichón: previous known eruption in 1360 or 1850; 2011 Nabro: first known eruption; 2008 Kasatochi: previous confirmed minor eruption in 1760; 2003 Anatahan: first documented eruption; Siebert et al., 2010). However, there are exceptions: the large 1991 eruption of Cerro Hudson followed relatively recent, albeit smaller, eruptions in 1891 and 1971 (Siebert et al., 2010), although in this case the large SO_2 emission in 1991 may have been supplied by a large basaltic dyke intrusion that triggered the eruption (e.g., Kratzmann et al., 2009). One possible explanation for the broad correlation between inter-eruptive quiescence and SO_2 emission is that it reflects the accumulation of a vapor phase in long-lived magma chambers during repose (e.g., Wallace and Gerlach, 1994; Scaillet et al., 2003; Wallace, 2005). Although many of the dominant sources have limited data on inter-eruptive degassing (no significant SO_2 emissions have been detected from space, but weak, fumarolic emissions would not be measured), they appear to release the vast majority of their SO_2 during eruptions. Whether this SO_2 originates from a stored vapor phase or syn-eruptive melt degassing is an open question that requires more extensive petrological studies. However, the behavior of other volatile species such as CO_2 may be different (e.g., there could be substantial inter-eruptive outgassing of CO_2 exsolved at depth), but would require extensive ground-based CO_2 flux measurements to resolve.

After the dominant explosive SO_2 sources, which tend to produce single, large injections of SO_2 into the UTLS, there are a number of volcanoes that produce smaller but more frequent emissions. The latter include Rabaul, Manam, Ulawun, Soputan, Kelut, Soufriere Hills, Sarychev Peak and Hekla (Table 6), which generally produce <1 Tg SO_2 per eruption but erupt relatively frequently (e.g., Tupper and Kinoshita, 2003; Tupper et al., 2004, 2007; Carn and Prata, 2010; Kushendratno et al., 2012) and in some cases may be persistently active between larger eruptions (e.g., Rabaul, Manam). Some volcanoes, such as Manam and Soputan, are prolific SO_2 emitters with 100% eruption detection rates where explosive degassing appears to dominate the total SO_2 flux, whereas passive SO_2 emissions appear more significant at others (e.g., Tungurahua (Ecuador) and Nevado del Ruiz (Colombia)). Soufriere Hills volcano (SHV) is unusual in that the SO_2 emissions listed in Table 6 are all associated with lava dome collapses or explosive events during a single, long-lived dome-forming eruption (Carn and Prata, 2010); these events trigger the release of a deep, SO_2-rich vapor phase (e.g., Christopher et al., 2010) and are not supplied by syn-eruptive degassing. Although these are not explosive eruptions in the conventional sense, they are still capable of injecting SO_2 into the UTLS and impacting SAOD (e.g., the July 2003, May 2006 and February

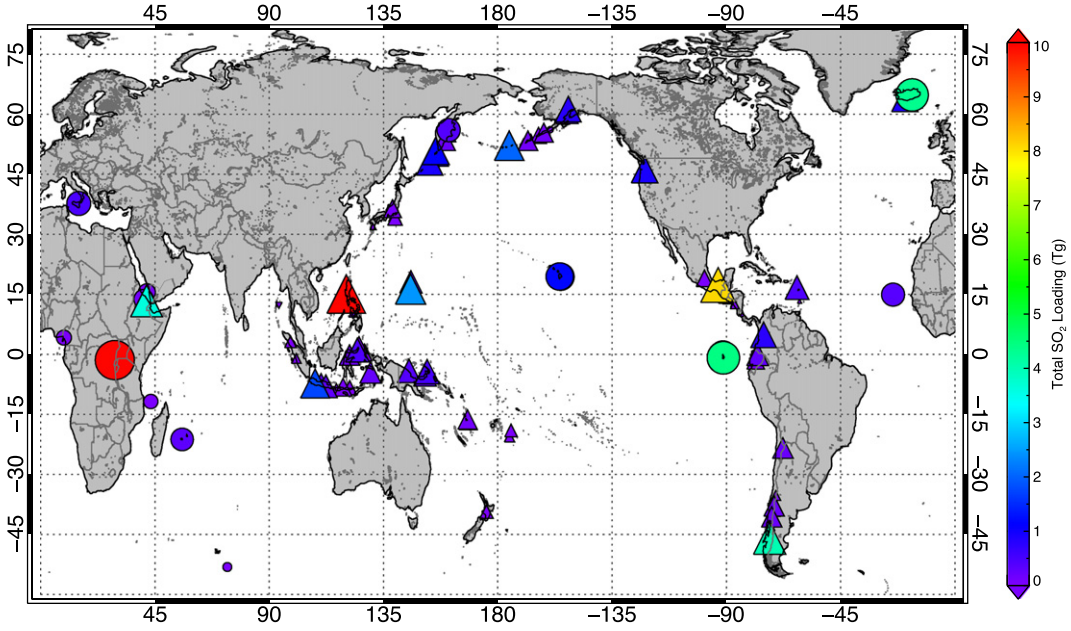

Fig. 12. Global map of sources of eruptive SO_2 emissions detected from space in 1978–2014. Symbol size is proportional to total SO_2 emissions measured for each volcano (Table 6), which is also indicated by the symbol color scale. *Triangles* indicate explosive eruptions and *circles* indicate effusive eruptions.

Table 6
Sources of eruptive volcanic SO_2 emissions (>10 kt), 1978–2014.

Volcano	Total SO_2 emission (Tg)	Eruptions	Degassing style*
Nyamuragira	25.149	17	1
Pinatubo	20.194	1	0
El Chichon	8.090	1	0
Sierra Negra	4.452	2	0
Holuhraun[a]	4.305	1	0
Hudson	4.001	2	0
Nabro	3.65	1	0
Anatahan	2.818	2	1
Kasatochi	2.000	1	0
Fernandina	1.821	5	0
Galunggung[b]	1.730	24	0
Cerro Azul	1.229	3	0
Sarychev Peak	1.200	1	0
Mauna Loa	1.197	1	0
Kilauea[b]	1.147	39	3
Alaid	1.110	2	0
Wolf	1.080	1	0
Mt St Helens	0.910	1	1
Hekla	0.883	4	0
Chikurachki	0.830	7	0
Spurr	0.800	3	0
Ruiz	0.762	3	3
Krafla	0.685	3	0
Rabaul	0.531	3	2
Etna	0.505	51	3
Copahue	0.500	1	1
Eyjafjallajökull	0.466	1	0
Soputan	0.455	19	1
Lascar	0.455	3	3
Soufriere Hills[b]	0.450	17	3
Manam	0.420	12	2
Kliuchevskoi	0.403	6	1
Fogo[a]	0.382	1	0
Kelut	0.350	2	0
Grimsvötn	0.350	4	0
Ulawun	0.347	5	2
P. de la Fournaise	0.334	9	0
Pagan	0.320	1	1
Redoubt	0.315	2	1
Merapi	0.310	2	2
Banda Api	0.250	1	0
Zhupanovsky	0.227	1	0
Colo	0.200	1	0
Marchena	0.200	1	0
Cordon Caulle	0.200	1	0
Tolbachik	0.200	1	0
Dalaffilla	0.150	1	0
Okmok	0.150	1	0
Lopevi	0.149	5	3
Pavlof	0.135	4	1
Ambrym	0.122	3	3
Asama	0.101	2	3
Sangeang Api	0.100	1	0
Tungurahua	0.090	5	3
Ruapehu	0.090	2	1
Popocatepetl[b]	0.087	5	3
Reventador	0.084	1	2
Ruang	0.080	1	0
Jebel at Tair	0.080	1	0
Shishaldin	0.063	1	1
Kizimen	0.060	2	0
Manda Hararo	0.060	2	0
Makian	0.050	1	0
Karkar	0.050	1	1
Mayon	0.050	1	3
Cameroon	0.048	2	0
Miyakejima	0.043	1	3
Karthala	0.041	4	0
Llaima	0.040	2	1
Paluweh	0.040	1	1
Bromo	0.031	1	3
Augustine	0.030	2	1
Nyiragongo	0.030	1	3
Bezymianny[b]	0.026	5	1
Home Reef	0.025	1	0
Pacaya	0.025	2	3
Oshima	0.022	1	1
Lokon-Empung	0.020	1	3
Sinabung	0.020	1	1
H. T. Hungaapai	0.014	1	0
Gamalama	0.013	2	1
Sheveluch[b]	0.012	2	3
Santa Ana	0.012	1	3

0: Entirely eruptive degassing. No significant passive SO_2 degassing known or reported.
1: Some passive degassing likely/measured/reported but eruptive degassing dominant.
2. Approximately equal passive/eruptive degassing.
3. Some eruptive degassing likely/measured/reported but passive degassing dominant.
* Qualitative assessment of degassing style:
[a] Preliminary estimate of SO_2 emissions through the end of 2014.
[b] 'Eruptions' listed correspond to discrete eruptive events producing the measured SO_2 (although only a single long-lived eruption may be recorded in the VOTW 4.3 database).

2010 events at SHV; Figs. 4, 7, 13; Prata et al., 2007; Carn and Prata, 2010).

Smaller eruptive SO_2 emissions may be a consequence of shorter inter-eruptive repose times, precluding accumulation of a magmatic gas phase, and/or persistent degassing between eruptions that may bleed off accumulating gases (Table 6). In general, volcanoes exhibiting higher levels of passive degassing appear less prone to large explosive eruptions, although even Etna (one of the strongest sources of passive volcanic SO_2 emissions; Section 4.2) has a significant eruptive SO_2 flux (Table 6). Emissions from frequent, moderate-sized eruptions dominate the short-term eruptive volcanic SO_2 flux and in the tropics they have a higher climate impact than larger eruptions on a time-averaged basis due to their higher frequency (e.g., Miles et al., 2004). In the tropics, small eruptions can have disproportionate impacts on the UTLS due to vertical transport of SO_2 assisted by deep convection (e.g., Tupper et al., 2009; Tupper and Wunderman, 2009). Several of these modest tropical eruptions (e.g., 2002 Ruang, 2005 Manam, 2006 Soufriere Hills, 2006 Rabaul) have been responsible for small SAOD perturbations since 2000 (e.g., Figs. 9, 13), maintaining the stratospheric aerosol layer above background (non-volcanic) levels and likely playing a role in the global warming 'hiatus' observed since 1998 (e.g., Solomon et al., 2011; Vernier et al., 2011; Neely et al., 2013; Ridley et al., 2014; Santer et al., 2014, 2015; Carn et al., 2015).

A detailed examination of recent trends in SAOD (Figs. 9, 13) confirms the dominant influence of volcanic eruptions, but also shows that no major SO_2 emissions have eluded detection by satellite instruments. All major perturbations to SAOD since 1979 can be attributed to a known volcanic eruption, and the more comprehensive record of volcanic SO_2 emissions presented here also elucidates some of the more subtle SAOD variations apparent in Figs. 9 and 13. For example, the September 1994 eruption of Rabaul appears responsible for a small increase in SAOD above the post-Pinatubo background (Figs. 9, 13), and this and other eruptions (e.g., Manam in December 1996) may have prolonged the decay of the Pinatubo aerosol to background levels. It has been shown that the overall increase in SAOD observed since 2002 (Figs. 9, 13) is not due to increased anthropogenic SO_2 emissions, as had previously been suggested (Hofmann et al., 2009), but to moderate-sized volcanic eruptions (Neely et al., 2013). The frequency of UTLS SO_2 injections since 2002 has been sufficient to prevent the return of tropical SAOD to background conditions, although a slight decline in SAOD is apparent from 2012 to 2014 (Figs. 9, 13) due to reduced levels of volcanic activity (at the time of writing, more recent SAOD data were not available to gauge the atmospheric impact of the large eruptions of Kelut in February 2014 and Calbuco in April 2015). We note, however, that there are still discrepancies between SAOD observations and climate model simulations of stratospheric aerosol, even when the latter include forcing by the larger eruptions since 2002 (Neely

et al., 2013). This appears to be due to a combination of incomplete records of volcanic SO_2 forcing used to initialize model simulations, an over-emphasis on VEI as an indication of potential climate impact, and incorrect date assignments for some eruptions. For example, both Neely et al. (2013) and Santer et al. (2014) list a VEI 3 eruption of Anatahan on April 12, 2004. Although this is the date given for the onset of the 2004–2005 Anatahan eruption by the Smithsonian GVP, it actually represents the beginning of an extended phase of activity, which peaked in April–August 2005 with several VEI 3 eruptive events and UTLS SO_2 injections (Figs. 4, 5). Similarly, Vernier et al. (2011) ascribe minor stratospheric impact to an eruption of Shiveluch in May 2001 (based on its VEI of 4), but this produced no detectable SO_2 emissions and we therefore contend that a smaller (VEI 3) eruption of Ulawun on April 30, 2001 (which injected at least ~30 kt SO_2 into the tropical UTLS) was more significant. Thus in these cases the satellite measurements provide the key information on the timing and location of SO_2 emissions required for accurate climate model simulations. We expect that use of our comprehensive volcanic SO_2 emissions database will likely resolve some of the remaining discrepancies between model simulations and observations, and also assist efforts to identify periods when the stratosphere was truly free of any volcanic influence.

4.1.5. Lifetimes of SO_2 in the UTLS

The lifetime of SO_2 in UTLS volcanic plumes (typically represented by an e-folding time; i.e., the time for SO_2 mass reduction by a factor of e^{-1}) is one of the key factors determining the climate impact of an eruption (along with SO_2 amount, injection altitude and latitude; Robock, 2000). Observations of SO_2 lifetime can also be used to test climate model simulations of volcanic plumes and improve the chemical schemes embedded in such models. With growing numbers of volcanic eruptions observed from space, we have increasingly accurate constraints on SO_2 lifetimes in volcanic plumes at a range of altitudes and latitudes, and in all seasons. Fig. 14 shows a representative set of e-folding times for SO_2 removal from volcanic plumes, based on IASI measurements for recent eruptions (since 2007) and values from the literature for older events and lower tropospheric SO_2 plumes. Note that the e-folding times shown in Fig. 14 characterize SO_2 removal (e.g., via gas- or aqueous-phase oxidation, cloud processing or wet/dry deposition) and not sulfate aerosol removal from the UTLS, which also influences climate impact.

The data in Fig. 14 confirm the strong correlation between SO_2 altitude and lifetime, with increasing variability apparent for lower tropospheric plumes. However, it is not absolute altitude but rather altitude relative to the local tropopause that is the main determinant of e-folding time, as evinced by the high-latitude eruptions of Sarychev Peak, Kasatochi, Cordon Caulle and Grimsvötn, among others (Fig. 14). These eruptions exhibit comparatively large e-folding times relative to the main trend defined by tropical eruptions, which is presumably due to the lower tropopause altitude at mid- to high-latitudes. Lower solar insolation at higher latitudes may also extend SO_2 lifetimes by reducing the rate of some photochemical reactions (e.g., the production of OH^-). The 1991 Cerro Hudson eruption, which is also mid-latitude, is somewhat of an anomaly (Fig. 14), but a shorter than expected SO_2 lifetime in this case may be due to the timing of the eruption in the late southern hemisphere winter. With the exception of Cordon Caulle (which also has a slightly lower e-folding time; Fig. 14) the more recent high latitude eruptions all occurred in the spring or summer. There is thus evidence for both altitude and seasonal impacts on the SO_2 lifetime in volcanic plumes, which may be further elucidated as more eruptions are analyzed. The present dataset is too limited (and recent eruptions too small) to draw any conclusions regarding the effects of SO_2 loading alone on SO_2 lifetime, for example, if excessive stratospheric SO_2 loading could sufficiently deplete OH levels to promote extended SO_2 lifetimes (e.g., Bekki, 1995).

4.1.6. Volcanic HCl emissions into the UTLS

A striking feature of Fig. 4 that we highlight here is that MLS has detected injection of HCl into the UTLS by several explosive eruptions

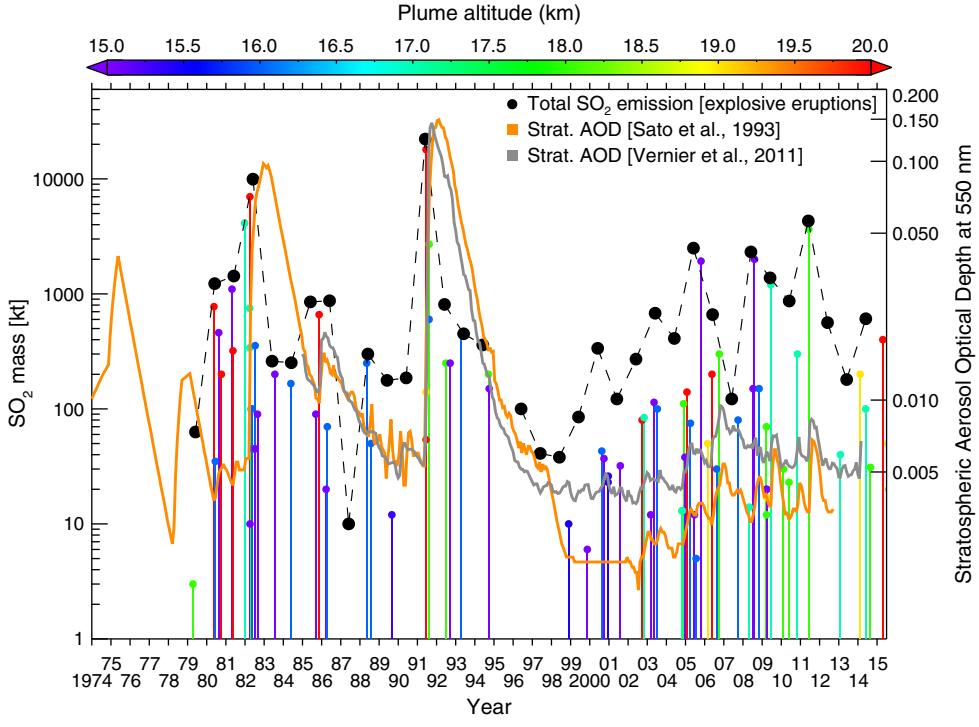

Fig. 13. Time-series of SO_2 mass loading similar to Fig. 1, but with only eruptions reaching altitudes of ≥15 km shown. The time axis is extended to include the 1974–1978 period prior to the satellite remote sensing era. *Orange line* shows stratospheric aerosol optical depth (SAOD) at 550 nm from Sato et al. (1993) and recent updates through December 2012 (http://data.giss.nasa.gov/modelforce/strataer/); *gray line* shows the tropical (30°S–30°N) SAOD at 525 nm data of Vernier et al. (2011; with recent updates) for 1985–2014 based on SAGE II, GOMOS and CALIPSO observations of aerosol between 15 and 40 km altitude. Differences between the SAOD datasets are explained in Fig. 9.

since 2004. We do not provide a detailed analysis of the MLS HCl data here, but rather point out the value of the MLS measurements (also including SO_2 and potentially other halogen species such as CH_3Cl; Table 1), which have not been widely used by the volcanological community (see also Pumphrey et al., 2015). HCl is an important halogen compound in the stratosphere. It is the dominant chlorine reservoir species and although it does not react directly with ozone, it is nevertheless a potential source of reactive halogen species (such as ClO) that destroy ozone, and hence any volcanic input of HCl into the stratosphere could be significant. Also notable in Fig. 4 is an inverted 'tape-recorder'-like signal in the MLS HCl data (absent in the SO_2 data), with higher HCl mixing ratios transported to lower altitudes in the northern hemisphere winter. Since the major source of stratospheric HCl is the UV photolysis of chlorine-containing compounds (e.g., CFCs) in the upper stratosphere (note that Fig. 4 only extends to 47 hPa pressure), we assume that this pattern is due to tropical upwelling of HCl-poor air during the northern hemisphere summer, HCl production at higher altitudes, followed by HCl redistribution by the Brewer-Dobson circulation. The MLS HCl data at 147 hPa are noisy and although MLS HCl retrievals at pressures above 100 hPa are not recommended for scientific use (Livesey et al., 2011), the volcanic HCl signal in large eruption clouds is clearly strong enough to be detected at this level (Fig. 4).

Over the past few decades, opinions have varied on the potential for volcanic injection of HCl (and other halogens) into the stratosphere. Symonds et al. (1988) estimated an annual global volcanic HCl flux of 0.4–11 Tg and suggested that <10% of these emissions originated from large explosive eruptions that would transmit them efficiently to the stratosphere. However, direct measurements of stratospheric HCl after major eruptions found relatively modest (1982 El Chichón) or barely detectable (1991 Pinatubo) increases in HCl loadings above the stratospheric background (Mankin and Coffey, 1984; Mankin et al., 1992; Wallace and Livingston, 1992), although the observations were made weeks or months after the eruptions (and both eruptions produced measurable ozone depletion). Subsequent modeling work by Tabazadeh and Turco (1993) suggested that scavenging of volcanic HCl by condensed supercooled water in Plinian eruption columns could effectively remove more than 99% of emitted chlorine, precluding stratospheric HCl injection, whilst having minimal impact on less soluble SO_2. However, Textor et al. (2003) pointed out flaws in the Tabazadeh and Turco (1993) study, namely that they used a relatively simple treatment of the dynamics, omitted some detailed cloud microphysical processes, and assumed that all hydrometeors were liquid (ice was later discovered to be dominant in some volcanic clouds; e.g., Rose et al., 1995). Accounting for the effects of ice particles, Textor et al. (2003) concluded that ice could scavenge 50–90% of HCl and 10–30% of SO_2 in eruption columns, and predicted that >25% and 80% of emitted HCl and SO_2, respectively, could potentially reach the stratosphere during explosive eruptions.

Recent satellite observations seem to confirm the predictions of Textor et al. (2003), and suggest that explosive eruptions frequently inject detectable HCl into the stratosphere (Fig. 4; e.g., Prata et al., 2007; Theys et al., 2014). Note that daily maximum SO_2 and HCl mixing ratios retrieved by MLS are shown in Fig. 4, and some weaker volcanic signals may be omitted, although the larger eruptions clearly stand out. Furthermore, due to the limited spatial sampling of MLS (Section 3.5) some smaller eruptions may not be detected, or the regions of highest SO_2 and HCl concentrations in volcanic clouds may not be sampled. Table 7 lists some HCl and SO_2 mixing ratios measured by MLS in volcanic clouds since 2004, along with estimated HCl/SO_2 mass ratios calculated from collocated SO_2 and HCl vertical profiles. Actual volcanic SO_2 and HCl concentrations are likely to be underestimated by MLS since the vertical extent of volcanic plumes is typically much smaller than the MLS vertical resolution of ~3 km (Livesey et al., 2011; Theys et al., 2014). Furthermore, since SO_2 and HCl are retrieved using data from separate MLS radiometers with different fields of view, the averaging effects differ for the two gases: the vertical × horizontal (cross-track) × along-track resolution of MLS SO_2 and HCl retrievals in the lower stratosphere is ~3 × 6 × 180 km and ~3 × 3 × 300–400 km, respectively (Livesey et al., 2011). Thus, since MLS averages volcanic SO_2 and HCl concentrations over different atmospheric volumes, coupled with limited spatial sampling, we treat the HCl/SO_2 ratios in Table 7 with caution. Nevertheless, some broad conclusions can be drawn. The HCl/SO_2 ratios observed in volcanic eruption clouds (~0.01–0.03; Table 7) are around an order of magnitude lower than values (~0.1–0.3) estimated for other eruptions based on petrological data or in-situ measurements (e.g., Westrich and Gerlach, 1992; Gerlach et al., 1996; Rose et al., 2006). This may partly reflect uncertainties on the MLS-derived ratios, but would also be consistent with greater scavenging of HCl relative to SO_2 in eruption plumes (Textor et al., 2003). Observed variations in HCl/SO_2 ratios between eruptions may be a consequence of variable HCl/SO_2 ratios in the source emissions (related to depth of degassing) or may reflect variable plume liquid water or total water content. Fig. 4 shows a notable contrast in HCl signal between the 2008 Kasatochi and 2009 Sarychev Peak eruptions, which were similar in magnitude. Sampling issues notwithstanding, a possible explanation for the difference is that liquid water was more abundant in the Kasatochi eruption plume, since it erupted through a pre-existing crater lake (Waythomas et al., 2010), resulting in more effective scrubbing of HCl in the emissions. The 2011 Nabro eruption also produced a surprisingly strong UTLS HCl signal (Figs. 4, 10), given its non-subduction tectonic setting (northeast Afar, Eritrea) where Cl enrichment from subducted seawater is absent. However, in this case the MLS-derived HCl/SO_2 ratio of 0.03 is roughly commensurate with ratios measured in tropospheric plumes at other East African Rift volcanoes (~0.04 at Erta 'Ale and ~0.03 at Nyiragongo; Sawyer et al., 2008a, 2008b), perhaps suggesting minimal scavenging of HCl in the Nabro plume (or similar scavenging efficiencies of SO_2 and HCl).

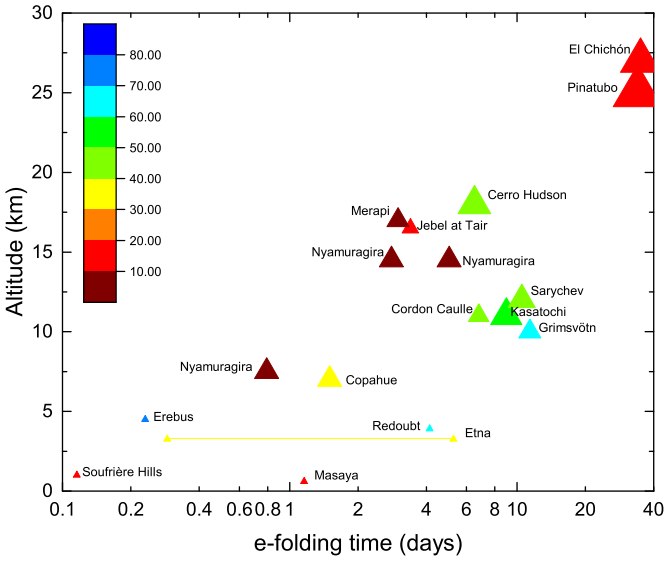

Fig. 14. Altitude of SO_2 injection against e-folding time for SO_2 removal for selected volcanic eruptions and emissions since 1980, with e-folding times derived from the literature (pre-2007) and from IASI SO_2 measurements (2007–2014). Symbol size is proportional to total SO_2 emission, and symbol color indicates volcano latitude. The SO_2 emissions represented are from: Erebus 1980 (Radke, 1982), Nyamuragira 1981 (Krueger et al., 1996; Bluth and Carn, 2008), Nyamuragira 1980–2004 (Bluth and Carn, 2008), El Chichón 1982 (Bluth et al., 1997), Pinatubo 1991 (Bluth et al., 1997), Etna 1983 (Martin et al., 1986), Redoubt 1990 (Hobbs et al., 1991), Cerro Hudson 1991 (Constantine et al., 2000), Soufrière Hills 1996 (Oppenheimer et al., 1998), Masaya 2003 (McGonigle et al., 2004b), Soufrière Hills 2004 (Rodríguez et al., 2008), Jebel at Tair 2007 (Clarisse et al., 2008), Kasatochi 2008 (Krotkov et al., 2010), Sarychev Peak 2009 (Haywood et al., 2010), Cordon Caulle 2011 (Theys et al., 2013), Merapi 2010 (IASI derived), Grimsvötn 2011 (IASI derived), and Copahue 2012 (IASI derived). Several e-folding times below 0.1 days were reported by Oppenheimer et al. (1998) for lower tropospheric SO_2 plumes but are not shown here.

4.2. Passive volcanic SO_2 degassing

We have shown above that the flux of SO_2 from volcanic eruptions is well constrained, with the exception of lower magnitude events (VEI ≤2). However, there is more uncertainty on the global flux of SO_2 emitted by passive (i.e., non-eruptive) degassing (e.g., Oppenheimer et al., 2011; Shinohara, 2013), which also propagates into estimates of volcanic fluxes of other gases, such as CO_2 (e.g., Burton et al., 2013). The ground-based perspective on global volcanic degassing must be aggregated from diverse sources, including journal publications, volcano observatories, instrument networks (e.g., Galle et al., 2010), and Smithsonian GVP reports, and consequently takes considerable time to generate and update. Satellite measurements offer the significant advantage of providing a daily, global snapshot of volcanic SO_2 emissions, collected by a single instrument using the same retrieval technique, and thus provide more timely and consistent assessments of the dominant volcanic SO_2 sources at a given time.

Currently, OMI, GOME-2 and OMPS can provide daily observations of tropospheric volcanic SO_2 plumes from space (e.g., Carn et al., 2007, 2008b, 2013; McCormick et al., 2012, 2013; Yang et al., 2013), and the quality of measurements will improve with future sensors such as the Tropospheric Monitoring Instrument (TROPOMI; http://www.tropomi.eu). Measurement noise and variable spatial resolution limits the SO_2 sources that can be detected in a single, daily satellite measurement to the strongest emitters (OMI has greater sensitivity than GOME-2 or OMPS, due to higher spatial resolution), but spatial and temporal data averaging techniques can also be used to detect weaker SO_2 sources (e.g., Fioletov et al., 2011, 2013). The latter are less useful for volcano monitoring purposes, where timeliness is critical, but can be used to generate accurate, annual SO_2 emissions inventories based on satellite observations. Here, we have used the technique described in Section 3.4 to identify the most persistent volcanic SO_2 sources detected by OMI in the 2004–2014 period (Fig. 15).

Results of the daily OMI SO_2 data analysis are shown in Fig. 15. In these plots higher average values of the OSI generally indicate stronger SO_2 emissions; hence the observations of Anatahan and Nevado del Ruiz, for example, indicate shorter periods of strong SO_2 degassing in 2004–2013. The SO_2 emissions from four volcanoes (Ambrym, Kilauea, Popocatepetl and Nyiragongo-Nyamulagira) have been notably more persistent than others in the ~10 years of satellite data, and SO_2 emissions from Ambrym and Nyiragongo were also detected prior to 2004 in TOMS SO_2 data (e.g., Carn, 2004). Three of these persistent SO_2 sources host at least one active lava lake (Ambrym, Kilauea, and Nyiragongo-Nyamulagira), reflecting efficient and persistent SO_2 outgassing from low-viscosity, basaltic magmas. Although many of the detected sources (e.g., Etna, Bagana, Nevado del Ruiz) figure prominently in previous volcanic SO_2 emissions inventories (e.g., Andres and Kasgnoc, 1998), the global OMI measurements permit identification of sources in poorly monitored regions such as Papua New Guinea, Indonesia, Vanuatu and Kamchatka, and also provide unique insight into the interannual variability of SO_2 emissions (Fig. 15). For example, Sabancaya (Peru) and Sinabung (Indonesia) do not appear as strong SO_2 sources based on OMI measurements in 2004–2013 (Fig. 15A), but are prominent in 2014 due to recently increased activity (Fig. 15B; Global Volcanism Program, 2014).

Although we do not convert the OMI SO_2 measurements into SO_2 emission rates here (techniques for doing this are under development; e.g., Carn et al., 2013), recent compilations of ground-based SO_2 measurements confirm high SO_2 fluxes (exceeding ~10 kt/day at times) at Ambrym, Kilauea, Popocatepetl, Nyiragongo, Etna and Bagana, among others (e.g., Oppenheimer et al., 2011; Elias and Sutton, 2012; Shinohara, 2013). We also note that several of these volcanoes (Nyiragongo, Popocatepetl, Ambrym, Etna) are regarded to be dominant sources of volcanic CO_2 emissions (Burton et al., 2013). However, other sources with previously reported high SO_2 emission rates, such as Láscar (N. Chile; 2.4 kt/day; Mather et al., 2004) are conspicuously absent from Fig. 15, and this appears to be corroborated by more recent (post-2004) ground-based SO_2 measurements indicating substantially reduced SO_2 emissions from Láscar (~0.1–0.6 kt/day; Henney et al., 2012; Tamburello et al., 2014; Lopez et al., 2015). We therefore contend that UV satellite measurements of tropospheric SO_2 plumes provide arguably the timeliest information on the status of global volcanic SO_2 sources, especially considering that it is crucial to constrain the strongest sources in order to estimate global or regional SO_2 fluxes (e.g., Mori et al., 2013). We are not aware of any volcano with a reported SO_2 emission rate of 1 kt/day or more since 2004 that has not been detected at some point in OMI SO_2 measurements. As SO_2 fluxes from an increasing number of weaker volcanic SO_2 sources are being measured using sensitive ground-based or airborne techniques (e.g., McGonigle et al., 2004a; Mori et al., 2006; Bani et al., 2013; Lopez et al., 2013b; Tamburello et al., 2014; Saing et al., 2014; Lopez et al., 2015; Smekens et al., 2015; Stebel et al., 2015), combining these new data with satellite observations will result in more accurate volcanic SO_2 emissions inventories, encompassing a wider range of sources.

Whilst the tropospheric SO_2 plume detection method employed here (Section 3.4) aims to omit major eruptive emissions (since eruptive SO_2 clouds typically drift rapidly away from the source, beyond the 50 km search radius), SO_2 plumes associated with continuous eruptive activity may still be captured. It is either known or likely that much of the SO_2 detected at Dukono, Anatahan, Kliuchevskoi, Zhupanovsky, Soufriere Hills, Sakura-jima and perhaps others is associated with continuous eruptions, i.e., the emissions are not passive in the strict sense (involving no coeval eruption of magma). Both Kilauea's and Bagana's SO_2 emissions are also associated with ongoing, long-term effusive eruptions (Elias and Sutton, 2012; McCormick et al., 2012) and hence could be regarded as eruptive discharges. Satellite observations of volcanic ash could potentially be used to distinguish plumes emitted by continuous eruptions, but ash measurements are typically less sensitive and noisier than SO_2 measurements. Although of minor importance when attempting to estimate total volcanic SO_2 fluxes to the atmosphere, the distinction between passive and eruptive degassing becomes important when assessing volcanic hazards or calculating volumes of degassed magma stored in the crust based on observed SO_2 emissions.

To visualize the geographical distribution and temporal variation of the major tropospheric volcanic SO_2 sources, the latitudes of the tropospheric SO_2 plumes detected by OMI in 2004–2014 are shown in Fig. 16 (note that some eruptive degassing is also apparent). Persistent volcanic SO_2 sources are manifested as continuous horizontal 'bands' on this plot (Fig. 16): prominent near-continuous bands occur at ~20°N (Kilauea and Popocatepetl; with increased SO_2 degassing apparent in March 2008 associated with the summit eruption at Kilauea; Elias and Sutton, 2012); ~1–2°S (Nyiragongo and Nyamuragira); ~4–9°S (volcanoes of Indonesia and Papua New Guinea); and ~16°S (Ambrym and

Table 7
HCl and SO_2 mixing ratios measured by Aura/MLS in volcanic clouds.

Volcano	Eruption Date	HCl (ppbv)	SO_2 (ppbv)	Pressure (hPa)	HCl/SO_2
Manam	Jan 27, 2005	4–6	279	68–100	0.01
Anatahan	Apr 6, 2005	3.5	133	100	0.02
Soufriere Hills	May 20, 2006	3	200	68	0.01
Chaitén	May 6, 2008	1.6	28	147	0.03
Okmok	Jul 12, 2008	5	212	147	0.01–0.02
Kasatochi	Aug 7, 2008	5–6	392	68–215	0.01–0.014
Redoubt	Mar 26, 2009	4–5	175	100–215	0.02
Sarychev Peak	Jun 15, 2009	7–9	529	32–215	0.03
Merapi	Nov 5, 2010	6–7	172	100–215	0.03
Cordón Caulle[1]	Jun 4, 2011	2–3	77	147–215	0.03
Nabro	Jun 15, 2011	9	306	46–215	0.03
Paluweh	Feb 2, 2013	2.2	129	100–215	0.01
Kelut	Feb 14, 2014	7	398	32–147	0.01
Sangeang Api	May 31, 2014	2–3	53	146	0.03

1. Data from Theys et al. (2014).

other Vanuatuan volcanoes such as Aoba and Gaua). Other notable features of Fig. 16 include elevated SO_2 emissions from Anatahan (~16°N) in 2005–2008 with a subsequent decline in 2009–2014 (McCormick et al., 2015), increased SO_2 emissions from Nevado del Ruiz (~5°N) in early 2012 (Global Volcanism Program, 2012), and at Turrialba (~10°N) in 2009–2010 (Campion et al., 2012). There is also a striking contrast between the tropics and high latitudes (Fig. 16). This partly reflects the distribution of SO_2 sources (most of the dominant volcanic SO_2 sources are in the tropics) but is also a result of seasonal variations in the availability and sensitivity of UV measurements at high latitudes, and higher wind speeds at extratropical latitudes (which dilute SO_2 column amounts in tropospheric plumes). Detection of degassing from Etna (~37°N), Kamchatkan volcanoes (~50–60°N) and southern Chilean volcanoes (~35–40°S) shows a clear seasonal dependence with wintertime observational gaps. However, the absence of a persistent SO_2 degassing signal in Iceland (~63–66°N) is probably genuine, due to a lack of intereruptive SO_2 emissions from Icelandic volcanoes.

One conclusion that can be drawn from this analysis is that more ground-based measurements of SO_2 emissions from high-latitude volcanoes (e.g., in Kamchatka, the Kurile Islands and the Aleutian Islands), especially in winter, are required to improve volcanic gas emissions budgets. However, ground-based UV remote sensing techniques are also likely to be challenging in the relative darkness and adverse weather conditions of high-latitude winter, although IR spectroscopy and camera techniques have potential as they are not dependent on UV radiation (e.g., Lopez et al., 2013b; Prata and Bernardo, 2014; Lopez et al., 2015). Moderate- to high-resolution IR satellite retrievals of lower tropospheric SO_2 (e.g., MODIS, ASTER) may also be possible for some plumes but routine detection of passive SO_2 degassing is likely to be restricted by thermal contrast and sensitivity issues.

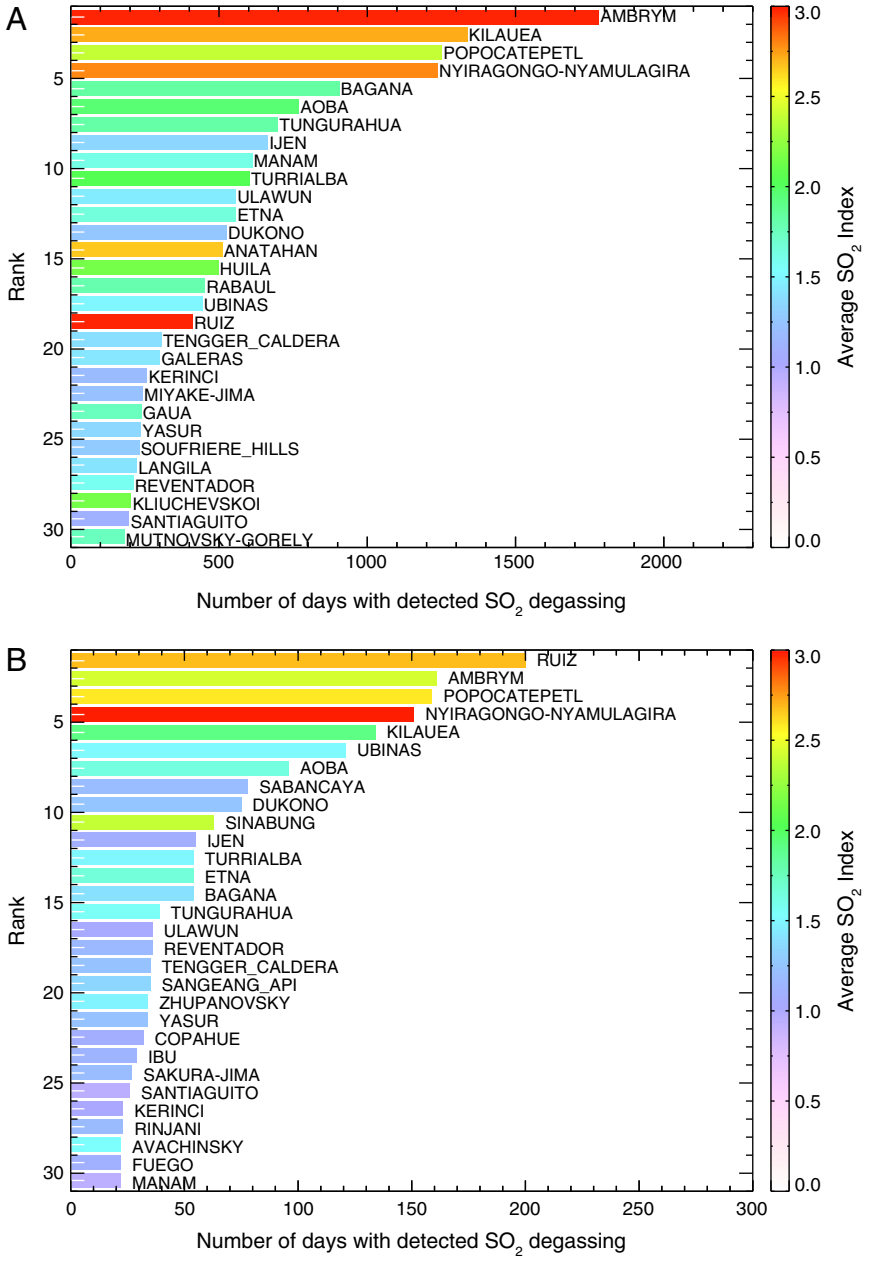

Fig. 15. Sources of passive volcanic SO_2 emissions detected by OMI: (A) Most persistent sources (in rank order) detected in OMI data collected between September 2004 and December 2013; (B) Most persistent sources detected by OMI in 2014. Colors correspond to the average value of the OSI for each volcano. Note that for some volcanoes in close proximity, the source of observed SO_2 emissions can be ambiguous (e.g., Nyiragongo-Nyamulagira, DR Congo; Mutnovsky–Gorely, Kamchatka).

5. Discussion

With at least 16 satellite instruments capable of measuring volcanic SO_2 emissions currently in orbit (Table 1), the flow of SO_2 observations from space has never been more profuse. This availability of remote sensing assets for detecting volcanic SO_2 is set to continue for at least the next decade, as degrading instruments or those nearing the end of their operational lifetimes are supplanted by sensors such as TROPOMI, ensuring that the SO_2 flux from volcanic eruptions will remain well constrained for the foreseeable future. Furthermore, should another Pinatubo-scale or larger eruption occur in the near future, current satellite measurements are capable of providing much higher quality data than they were in 1991. A Pinatubo-scale SO_2 emission could potentially be tracked for weeks or months with the improved sensitivity of existing sensors relative to TOMS. Open questions to consider include whether an even larger SO_2 release would saturate current SO_2 retrieval algorithms during the initial emission, precluding accurate SO_2 mass loading measurements until the cloud began to disperse, and how a persistent, widespread SO_2 and sulfate aerosol veil from such a large event would impact remote sensing measurements during its atmospheric residence.

Although SO_2 emissions are reasonably well constrained, a major unresolved question concerns the magnitude of global volcanic emissions of other sulfur species, most notably H_2S, which have been previously estimated at 1.4–35 Tg/yr. of S (e.g., Halmer et al., 2002; Oppenheimer et al., 2011). Hydrogen sulfide can comprise up to ~40% of total sulfur gases ($SO_2 + H_2S$) in high-temperature volcanic gas samples (Oppenheimer et al., 2011), and petrological evidence suggests that it may be dominant in some eruptions. Luhr et al. (1984) proposed that most of the sulfur gases released by the 1982 El Chichón eruption were in the form of H_2S, and Hobbs et al. (1982) reported significant quantities of H_2S in the May 1980 Mt. St Helens eruption cloud. Although IASI is capable of detecting volcanic H_2S from space (Table 1), the only reported observations to date are for the 2008 Kasatochi and 2011 Grimsvötn eruptions (Clarisse et al., 2011a,b; Sigmarsson et al., 2013). These new observations of eruptive H_2S emissions are valuable, though satellite measurements of H_2S will never be as comprehensive as SO_2 measurements since the IR H_2S absorption lines are weak and hence sensitivity is low (Clarisse et al., 2011b).

There appears to be significant scope for more work on the rates of key reactions involved in H_2S oxidation, but McKeen et al. (1984) suggest that H_2S is oxidized to SO_2 relatively quickly (~3 day chemical lifetime) provided OH is readily available. Hence the degree to which satellite measurements will capture H_2S emissions converted to SO_2 will depend on the relative rates of H_2S oxidation to SO_2 and SO_2 conversion to sulfate, i.e., if H_2S is oxidized relatively quickly, the SO_2 produced will be detected and factored in to the total eruption sulfur budget. However, if OH concentrations were sufficient to promote efficient H_2S oxidation, then it also likely that SO_2 would be simultaneously oxidized. Oxidation of H_2S has been invoked to explain increases in measured SO_2 observed in the days following some explosive eruptions, such as the 1982 El Chichón and 1992 Mount Spurr eruptions (e.g., Bluth et al., 1995; Schneider et al., 1999; Rose et al., 2000, 2001), but such increases could also be reasonably attributed to other causes such as a reduction in volcanic cloud optical depth, reduced ash content, or sequestration of SO_2 by ice in the young volcanic cloud (e.g., Rose et al., 2000, 2001), and are often subject to some ambiguity.

Although some H_2S is likely to be present in all volcanic eruption plumes, it may be safe to assume that SO_2 dominates the sulfur inventory in emissions from volcanoes in subduction zone environments (where most of the major volcanic SO_2 sources are located), where oxidized magmas with high SO_2:H_2S ratios are typical. Magmas in hot-spot and divergent plate contexts may also be relatively oxidized (Oppenheimer et al., 2011). Aiuppa et al. (2005) report a SO_2/H_2S molar ratio of 20 in emissions from Etna in 2003, and H_2S was not detected in emissions from Gorely volcano (Kamchatka) in 2011 (Aiuppa et al., 2012), although Edmonds et al. (2010) found a relatively significant quantities of H_2S in gas emissions from SHV (Montserrat) in July 2008 during an eruptive pause ($SO_2/H_2S = 1.9–3.6$). Emissions of H_2S may be more significant during precursory activity at wet volcanoes, where phreatomagmatic eruptions may precede the main magmatic eruption phase, as was suggested for Kasatochi (Clarisse et al., 2011b). Clearly, however, further work is needed to better constrain volcanic H_2S emissions on a global scale. Global S emissions from volcanic arcs have been estimated to be ~10–11 Tg/year (Hilton et al., 2002; Shinohara, 2013), equivalent to ~20–22 Tg/yr. SO_2. Assuming ~16 Tg/yr. SO_2 emitted by passive degassing in volcanic arcs (Shinohara, 2013) and ~2 Tg/yr. SO_2 emitted by explosive eruptions (Table 3) yields a total of ~18 Tg/yr. SO_2 or 9 Tg/yr. S. Based on an estimated annual emission of 10–11 Tg S, this leaves a 1–2 Tg/yr. S shortfall, which if emitted as H_2S would be ~1.2–2.1 Tg/yr. H_2S.

One approach that could provide further insight into eruptive emissions of H_2S is to identify significant discrepancies between petrological estimates of S in pre-eruptive magmatic gas phases (Scaillet and Pichavant, 2003; Scaillet et al., 2003) and observations of SO_2 emissions. Such disagreement could indicate the discharge of substantial H_2S emissions that were not detected in satellite data (or alternatively, rapid removal of SO_2). One possible example is the April 1979 eruption of Soufriere St Vincent, for which Scaillet et al. (2003) predicted a total S release of ~0.5 Tg from the melt and gas phase (i.e., ~1 Tg SO_2). However, only ~3 kt of SO_2 (0.3% of the predicted SO_2 yield) was detected by TOMS following the eruption, despite adequate measurement conditions (a volcanic ash cloud was detected). Furthermore, the eruption has been linked to a large SAOD anomaly in 1979–80 (Fig. 13; Rosen and Hofmann, 1980), which would not be commensurate with such a low SO_2 release. Taken together, this evidence may suggest that the bulk of the sulfur emitted by Soufriere St Vincent was in the form of H_2S, which may have been oxidized sufficiently slowly to prevent any SO_2 detection by TOMS.

Finally, although we do not discuss them in detail here, UV satellite measurements are also providing unique observations of reactive halogen species such as BrO and OClO in volcanic clouds (e.g., Afe et al., 2004; Theys et al., 2009; Rix et al., 2012; Hörmann et al., 2013; Theys et al., 2014). Such measurements permit assessment of the potential impacts of volcanic eruptions on stratospheric ozone (e.g., Kutterolf et al., 2013). The HCl and SO_2 profile measurements from MLS are also advantageous, since the impact of a volcanic eruption on the stratospheric ozone layer will depend primarily on the altitude of the volcanic emissions relative to the peak in the ozone concentration. Theys et al. (2014) found significant differences in the quality of volcanic BrO and OClO retrievals from available UV satellite instruments (SCIAMACHY, OMI and GOME-2), with certain sensors optimized for particular volatile species, highlighting the fact that multiple instruments are required to ensure accurate measurements of all volcanic emissions. Another potentially interesting but as yet unexplored aspect of satellite measurements of reactive halogens in volcanic clouds is the different overpass times of the sensors. For example, we might expect systematic differences between BrO measurements by GOME-2 (9:30 am overpass) and OMI (1:45 pm overpass) due to photochemical effects on BrO production in volcanic plumes (e.g., von Glasow et al., 2009), although other factors such as spatial resolution and plume aerosol loading will also play a role.

6. Conclusions

In this contribution we have reviewed ~36 years of satellite measurements of volcanic SO_2 emissions from 1978 to 2014. During this period, SO_2 emissions from every significant volcanic eruption (VEI ≥ 4) have been detected and quantified, providing accurate constraints on the mean volcanic SO_2 flux to the UTLS (~1–2 Tg/yr) and allowing robust interpretation of trends in SAOD. Measurements from multiple UV and IR satellite instruments are required to achieve optimum

coverage, to ensure detection of eruptions at all latitudes and at night, and to reduce uncertainty on measured SO_2 loadings for individual eruptions. Microwave sensors such as MLS can provide crucial complementary information on the altitude of volcanic SO_2 and HCl injections. Although there is greater uncertainty on SO_2 emissions from smaller eruptions (VEI 0–3), this SO_2 is not expected to be significant for climate. New techniques being adopted for ground-based measurements of volcanic SO_2 (e.g., UV and IR imaging cameras) will likely improve constraints on SO_2 fluxes from small eruptions, which may be an important component of the tropospheric volcanic SO_2 budget in years with low total SO_2 emissions or no large eruptions. Furthermore, CO_2 emissions from such activity may be more significant due to the longer atmospheric residence time of CO_2 relative to SO_2.

Reanalysis of the relationship between VEI and SO_2 emissions with the inclusion of recent satellite measurements confirms a first-order relationship between eruption magnitude and SO_2 loading. However, due to significant variability in SO_2 loading for individual VEI classes (coupled with the inherent challenges in assigning accurate VEIs), the use of VEI to assess the potential climate impact of eruptions in the remote sensing era is discouraged. Current satellite measurements can provide accurate and timely estimates of both SO_2 loading and altitude, with this capability expected to continue in the next decade, obviating the need for any proxy for climate impact (but the VEI certainly remains a useful indicator of the overall significance of an eruption). Specification of eruption altitude is crucial for climate modeling (e.g., Robock, 2000; Arfeuille et al., 2014), and one of the weaknesses of our current volcanic SO_2 emissions database is that eruptions are characterized by a single altitude, whereas in reality the vertical profile of an explosive eruption column can be complex and variable. The assumption of a single SO_2 injection altitude can result in significant errors in the UTLS SO_2 budget, especially for complex, continuous eruptions (e.g., the 2010 Eyjafjallajökull, 2011 Nabro and 2014–15 Holuhraun eruptions), which will propagate into estimates of climate impacts. In this regard, the application of inverse modeling techniques to estimate the syn-eruptive vertical profile of SO_2 emissions appears particularly powerful, and is facilitated by the availability of multiple UV and IR satellite measurements of volcanic SO_2 emissions. Such techniques could be used to determine the peak injection altitude or multiple injection altitudes.

For the past decade, satellite instruments have also provided new constraints on passive volcanic degassing of SO_2. A synthesis of ~10 years of OMI SO_2 measurements reveals the most persistent volcanic SO_2 sources detected from space, several of which have minimal or no ground-based monitoring currently in place. Our analysis demonstrates the key role of satellite observations in identifying the major volcanic SO_2 sources at any given time. It has been postulated that a few dominant SO_2 sources exert a major control over regional and global volcanic SO_2 fluxes (e.g., Mori et al., 2013; Shinohara, 2013), and hence a combination of satellite SO_2 measurements of the major SO_2 emitters with the increasingly comprehensive ground-based SO_2 data for volcanoes with lower SO_2 emission rates will lead to vastly improved SO_2 emissions budgets. However, observations of SO_2 emissions from high-latitude volcanoes (e.g., in Kamchatka, the Kurile Islands and the Aleutian Islands) remain challenging, especially in winter.

Collation of a multi-decadal record of volcanic SO_2 emissions allows us to draw some broad conclusions from the patterns that emerge. Volcanoes that exhibit minimal levels of passive or inter-eruptive SO_2 degassing are responsible for sporadic ($\geq 10^2$ years), large (≥ 1 Tg) SO_2 emissions with potentially significant impacts on climate or SAOD (e.g., Pinatubo, El Chichón, Kasatochi, Nabro); it is highly likely that the next, major SO_2-producing eruption will occur at a volcano that has not erupted for centuries or more, where accumulation of a stored vapor phase may be occurring. We also note that such volcanoes may emit substantial amounts of CO_2 in apparently quiescent periods, and more widespread ground-based or airborne CO_2 flux measurements would be desirable; the challenge is to select appropriate targets from the many currently dormant volcanoes (active ground deformation may be one useful criterion). Perhaps more significant for climate on shorter timescales are the restless, volatile-rich systems exhibiting both passive and eruptive SO_2 degassing (e.g., Rabaul, Manam, SHV, Ulawun) that produce smaller (VEI ≤ 4) but frequent UTLS eruptions, which may have significant cumulative impacts on climate. For such systems, the magnitude of SO_2 release is likely limited (≤1 Tg is typical) by near-continuous activity and bleeding of volatiles from resident magma at depth. This effect is even stronger for other systems where passive SO_2 degassing dominates the total SO_2 discharge and large eruptive SO_2 emissions appear unlikely unless passive degassing is curtailed (e.g., Popocatepetl, Tungurahua).

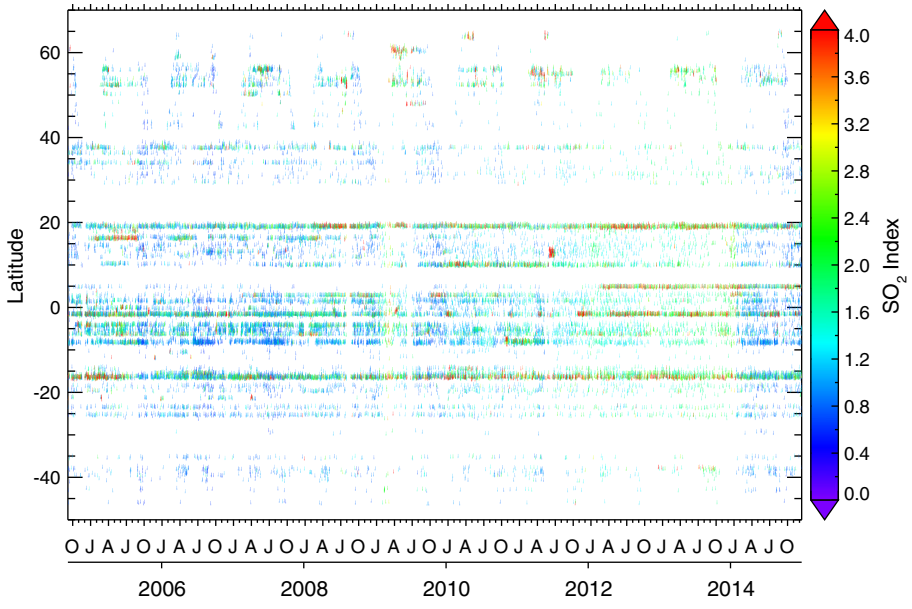

Fig. 16. Latitude and strength of persistent volcanic SO_2 sources against time based on OMI SO_2 measurements from September 2004 to December 2014. For each day, the latitudes of all OMI pixels that show the highest daily values of the OMI SO_2 Index (OSI; see Section 3.4 for definition) and are located within 50 km of an active volcano are plotted. Persistent SO_2 sources thus appear as horizontal bands on this plot. Although most eruptive SO_2 emissions are excluded from this plot (see Section 3.4), short discontinuities in the data are due to large SO_2-rich eruptions temporarily overwhelming the OSI measurements (e.g., the Kasatochi eruption in August 2008, the Sarychev Peak eruption in June 2009, and the Nabro eruption in June 2011).

Although the SO_2 data products from both UV and IR satellite instruments enjoy a long heritage and can be deemed relatively mature, some outstanding questions remain. Unraveling the causes of differences between UV and IR SO_2 retrievals, or between IR retrievals in different spectral bands, found for some eruptions (e.g., Table 2) is needed to reduce the uncertainties on some eruption SO_2 loadings. Such differences are most likely to originate from a complex combination of effects of SO_2 altitude or vertical profile, overpass timing, plume aerosol loading (e.g., ash, sulfate, hydrometeors), sensor spatial and spectral resolution, atmospheric water vapor, and total column ozone, and may be very challenging to untangle. Efforts should be made to determine the 'optimum' satellite SO_2 retrieval for each eruption. Validation of satellite SO_2 measurements remains a challenge, particularly for the largest volcanic clouds, but may become more achievable using unmanned aerial vehicles (UAVs) or other rapidly-deployable in-situ measurement techniques. Finally, volcanic H_2S emissions remain poorly constrained on a global scale and may be a significant fraction of the total S budget for some eruptions.

Although much can be achieved using satellite instruments deployed on multiple polar-orbiting platforms (and such observations are crucial for high latitude volcanoes), monitoring of volcanic SO_2 emissions from space would greatly benefit from a global, geostationary capability, particularly in the UV. Currently, only the European SEVIRI and Japanese Advanced Himawari Imager (AHI) sensors have IR channels capable of detecting SO_2 emissions from geostationary orbit (Table 1). However, prospects for high temporal resolution UV monitoring of SO_2 from geostationary or alternative orbits are improving. The recently deployed EPIC instrument on the DSCOVR satellite at the L_1 Earth-Sun. Lagrange point will soon provide multiple daily UV SO_2 retrievals for the sunlit Earth disk (including some coverage of high latitudes during the summer months). The SO_2 sensitivity of EPIC will likely be intermediate between TOMS and OMI, permitting detection of large eruptions and strong passive SO_2 degassing. Later in the decade (around 2017), the Tropospheric Emissions: Monitoring of Pollution (TEMPO) instrument will be launched on a geostationary satellite, providing UV observations of North America (including Mexico). Since SO_2 is a criteria pollutant affecting air quality, volcanic SO_2 surveillance will indirectly benefit from efforts (such as the TEMPO mission) to measure anthropogenic SO_2 emissions more frequently and track intercontinental transport of air pollution. TEMPO will form part of a global geostationary constellation for pollution monitoring, including UV instruments from Europe (Sentinel 4) and Asia (the Geostationary Environment Monitoring Spectrometer [GEMS] being developed in Korea). We are therefore on the cusp of another major advance in our ability to measure volcanic SO_2 emissions from space.

Acknowledgments

We acknowledge editors Tim Horscroft and Alessandro Aiuppa for inviting this review article. NASA has provided generous support of satellite-based volcanic SO_2 measurements to S.A.C, including recent grants NNX10AG60G (A Combined EOS Data and GEOS-Chem Modeling Study of the Direct Radiative Forcing of Volcanic Sulfate Aerosols; PI: J. Wang), NNX11AK95G (Continuation of Long-Term Sulfur Dioxide EDR with the SNPP/OMPS Nadir Mapper; PI: K. Yang) and NNX13AF50G (Multi-Decadal Sulfur Dioxide Climatology from Satellite Instruments; PI: N.A. Krotkov). L.C. is a research associate supported by the Belgian Fonds de la Recherche Scientifique (F.R.S-FNRS). We thank Jean-Paul Vernier (NASA Langley) for providing recent stratospheric aerosol data and Mauro Tomasi (ULB) for collating the data used to produce an earlier version of Fig. 14. David Pyle and an anonymous reviewer provided thorough and constructive reviews of the paper. The article was written whilst the first author was on sabbatical at the Department of Mineral Sciences (DMS), National Museum of Natural History, Smithsonian Institution, and SAC acknowledges the Smithsonian for a visiting fellowship and the DMS staff for their hospitality. The volcanic SO_2 emissions database described in this paper is available from the NASA Goddard Earth Sciences (GES) Data and Information Services Center (DISK) as a level 4 MEaSUREs (Making Earth System Data Records for Use in Research Environments) data product (Carn, 2015c).

Appendix A. Supplementary data

Supplementary data to this article can be found online at http://dx.doi.org/10.1016/j.jvolgeores.2016.01.002.

References

Afe, O.T., Richter, A., Sierk, B., Wittrock, F., Burrows, J.P., 2004. BrO emission from volcanoes — a survey using GOME and SCIAMACHY measurements. Geophys. Res. Lett. 31, L24113. http://dx.doi.org/10.1029/2004GL020994.

Aiuppa, A., Inguaggiato, S., McGonigle, A.J.S., O'Dwyer, M., Op-penheimer, C., Padgett, M.J., Rouwet, D., Valenza, M., 2005. H_2S fluxes from Mt. Etna, Stromboli, and Vulcano (Italy) and implications for the sulfur budget at volcanoes. Geochim. Cosmochim. Acta 69, 1861–1871.

Aiuppa, A., Giudice, G., Liuzzo, M., Tamburello, G., Allard, P., Calabrese, S., Chaplygin, I., McGonigle, A.J.S., Taran, Y., 2012. First volatile inventory for gorely volcano, Kamchatka. Geophys. Res. Lett. 39, L06307. http://dx.doi.org/10.1029/2012GL051177.

Andres, R.J., Kasgnoc, A.D., 1998. A time-averaged inventory of subaerial volcanic sulfur emissions. J. Geophys. Res. 103, 25251–25261.

Arfeuille, F., Weisenstein, D., Mack, H., Rozanov, E., Peter, T., Brönnimann, S., 2014. Volcanic forcing for climate modeling: a new microphysics-based data set covering years 1600–present. Clim. Past 10, 359–375. http://dx.doi.org/10.5194/cp-10-359-2014.

Bani, P., Oppenheimer, C., Tsanev, V.I., Carn, S.A., Cronin, S.J., Crimp, R., Calkins, J.A., Charley, D., Lardy, M., Roberts, T.R., 2009. Surge in sulfur and halogen degassing from Ambrym volcano, Vanuatu. Bull. Volcanol. 71 (10), 1159–1168. http://dx.doi.org/10.1007/s00445-009-0293-7.

Bani, P., Oppenheimer, C., Allard, P., Shinohara, H., Tsanev, V., Carn, S., Lardy, M., Garaebeti, E., 2012. First arc-scale volcanic SO_2 budget for the Vanuatu archipelago. J. Volcanol. Geotherm. Res. 211-212, 36–46. http://dx.doi.org/10.1016/j.jvolgeores.2011.10.005.

Bani, P., Surono, Hendrasto, M., Gunawan, H., Primulyana, S., 2013. Sulfur dioxide emissions from Papandayan and Bromo, two Indonesian volcanoes. Nat. Hazards Earth Syst. Sci. 13, 2399–2407. http://dx.doi.org/10.5194/nhess-13-2399-2013.

Barnie, T., Keir, D., Hamling, I., Hofmann, B., Belachew, M., Carn, S.A., Eastwell, D., Hammond, J.O.S., Ayele, A., Oppenheimer, C., Wright, T., 2015. A multidisciplinary study of the final episode of the Manda Hararo dyke sequence, Ethiopia, and implications for trends in volcanism during the rifting cycle. In: Wright, T.J., Ayele, A., Ferguson, D.J., Kidane, T., Vye-Brown, C. (Eds.), Magmatic Rifting and Active Volcanism. Geol. Soc. Lon, Special Publications 420 (in press).

Bauduin, S., Clarisse, L., Clerbaux, C., Hurtmans, D., Coheur, P.-F., 2014. IASI observations of sulfur dioxide (SO_2) in the boundary layer of Norilsk. J. Geophys. Res. Atmos. 119, 4253–4263. http://dx.doi.org/10.1002/2013JD021405.

Bekki, S., 1995. Oxidation of volcanic SO_2: a sink for stratospheric OH and H_2O. Geophys. Res. Lett. 22 (8), 913–916.

Berresheim, H., Jaeschke, W., 1983. The contribution of volcanoes to the global atmospheric sulfur budget. J. Geophys. Res. 88, 3732–3740.

Bhartia, P.K., Wellemeyer, C.W., 2002. TOMS-V8 Total O_3 Algorithm, Version 2.0, ATBD-OMI-02. NASA Goddard Space Flight Cent., Greenbelt, Md. (Available at http://eospso.gsfc.nasa.gov/eos_homepage/for_scientists/atbd/docs/OMI/ATBD-OMI-02.pdf).

Blake, S., 2003. Correlations between eruption magnitude, SO_2 yield, and surface cooling. In: Oppenheimer, C., Pyle, D.M., Barclay, J. (Eds.), Volcanic Degassing. Geological Society, London, Special Publications 213, pp. 371–380.

Bluth, G.J.S., Carn, S.A., 2008. Exceptional sulfur degassing from Nyamuragira volcano, 1979–2005. Int. J. Remote Sens. 29 (22), 6667–6685.

Bluth, G.J.S., Doiron, S.D., Schnetzler, S.C., Krueger, A.J., Walter, L.S., 1992. Global tracking of the SO_2 clouds from the June, 1991 Mount Pinatubo eruptions. Geophys. Res. Lett. 19, 151–154. http://dx.doi.org/10.1029/91GL02792.

Bluth, G.J.S., Schnetzler, C.C., Krueger, A.J., Walter, L.S., 1993. The contribution of explosive volcanism to global atmospheric sulfur dioxide concentrations. Nature 366, 327–329.

Bluth, G.J.S., Casadevall, T.J., Schnetzler, C.C., Doiron, S.D., Walter, L.S., Krueger, A.J., Badruddin, M., 1994. Evaluation of sulfur dioxide emissions from explosive volcanism: the 1982–83 eruptions of Galunggung, Java, Indonesia. J. Volcanol. Geotherm. Res. 63, 243–256.

Bluth, G.J.S., Scott, C.J., Sprod, I.E., Schnetzler, C.C., Krueger, A.J., Walter, L.S., 1995. Explosive emissions of sulfur dioxide from the 1992 Crater Peak eruptions, Mount Spurr volcano, Alaska. In: Keith, T.E.C. (Ed.), The 1992 Eruptions of Crater Peak Vent, Mount Spurr Volcano, AlaskaU.S. Geol. Surv. Bull. 2139. US Government Printing Office, Washington, D.C., pp. 37–45.

Bluth, G.J.S., Rose, W.I., Sprod, I.E., Krueger, A.J., 1997. Stratospheric loading of sulfur from explosive volcanic eruptions. J. Geol. 105, 671–683.

Boichu, M., Menut, L., Khvorostyanov, D., Clarisse, L., Clerbaux, C., Turquety, S., Coheur, P.-F., 2013. Inverting for volcanic SO_2 flux at high temporal resolution using spaceborne plume imagery and chemistry-transport modelling: the 2010 Eyjafjallajökull eruption case study. Atmos. Chem. Phys. 13, 8569–8584. http://dx.doi.org/10.5194/acp-13-8569-2013.

Bonny, E., Carn, S.A., Donnadieu, F., Coltelli, M., 2015. Paroxysmal degassing at Mt. Etna in 2011-12. Earth Planet. Sci. Lett. (in preparation).

Bourassa, A.E., Degenstein, D.A., Elash, B.J., Llewellyn, E.J., 2010. Evolution of the stratospheric aerosol enhancement following the eruptions of Okmok and Kasatochi: Odin-OSIRIS measurements. J. Geophys. Res. 115, D00L03. http://dx.doi.org/10.1029/2009JD013274.

Bourassa, A.E., Robock, A., Randel, W.J., Deshler, T., Rieger, L.A., Lloyd, N.D., Llewellyn, E.J., Degenstein, D.A., 2012. Large volcanic aerosol load in the stratosphere linked to Asian monsoon transport. Science 337 (6090), 78–81. http://dx.doi.org/10.1126/science.1219371.

Bourassa, A.E., Robock, A., Randel, W.J., Deshler, T., Rieger, L.A., Lloyd, N.D., Llewellyn, E.J., Degenstein, D.A., 2013. Response to comments on "Large volcanic aerosol load in the stratosphere linked to Asian monsoon transport". Science 339 (6120), 647. http://dx.doi.org/10.1126/science.1227961.

Bovensmann, H., et al., 1999. SCIAMACHY - mission objectives and measurement modes. J. Atmos. Sci. 56 (2), 127–150.

Boynard, A., et al., 2014. First simultaneous space measurements of atmospheric pollutants in the boundary layer from IASI: a case study in the North China Plain. Geophys. Res. Lett. 41, 645–651. http://dx.doi.org/10.1002/2013GL058333.

Brenot, H., Theys, N., Clarisse, L., van Geffen, J., van Gent, J., Van Roozendael, M., A.R., v.d., Hurtmans, D., Coheur, P.-F., Clerbaux, C., Valks, P., Hedelt, P., Prata, F., Rasson, O., Sievers, K., Zehner, C., 2014. Support to Aviation Control Service (SACS): an online service for near-real-time satellite monitoring of volcanic plumes. Nat. Hazards Earth Syst. Sci. 14, 1099–1123. http://dx.doi.org/10.5194/nhess-14-1099-2014.

Brühl, C., Lelieveld, J., Tost, H., Höpfner, M., Glatthor, N., 2015. Stratospheric sulfur and its implications for radiative forcing simulated by the chemistry climate model EMAC. J. Geophys. Res. Atmos. 120, 2103–2118. http://dx.doi.org/10.1002/2014JD022430.

Burrows, J.P., et al., 1999. The Global Ozone Monitoring Experiment (GOME): mission concept and first scientific results. J. Atmos. Sci. 56, 151–175.

Burton, M.R., Sawyer, G.M., Granieri, D., 2013. Deep carbon emissions from volcanoes. Rev. Mineral. Geochem. 75, 323–354. http://dx.doi.org/10.2138/rmg.2013.75.11.

Cadle, R.D., 1975. Volcanic emissions of halides and sulfur compounds to the troposphere and stratosphere. J. Geophys. Res. 88, 1650–1652.

Campbell, J.R., Welton, E.J., Krotkov, N.A., Yang, K., Stewart, S.A., Fromm, M.D., 2012. Likely seeding of cirrus clouds by stratospheric Kasatochi volcanic aerosol particles near a mid-latitude tropopause fold. Atmos. Environ. 46, 441–448.

Campion, R., Salerno, G.G., Coheur, P.-F., Hurtmans, D., Clarisse, L., Kazahaya, K., Burton, M., Caltabiano, T., Clerbaux, C., Bernard, A., 2010. Measuring volcanic degassing of SO_2 in the lower troposphere with ASTER band ratios. J. Volcanol. Geotherm. Res. 194, 42–54.

Campion, R., Martinez-Cruz, M., Lecoq, T., Caudron, C., Pacheco, J., Pinardi, G., Hermans, C., Carn, S.A., Bernard, A., 2012. Space- and ground-based measurements of sulfur dioxide emissions from Turrialba volcano (Costa Rica). Bull. Volcanol. 74 (7), 1757–1770. http://dx.doi.org/10.1007/s00445-012-0631-z.

Carboni, E., Grainger, R., Walker, J., Dudhia, A., Siddans, R., 2012. A new scheme for Sulphur dioxide retrieval from IASI measurements: application to the Eyjafjallajökull eruption of April and May 2010. Atmos. Chem. Phys. 12, 11417–11434. http://dx.doi.org/10.5194/acp-12-11417-2012.

Carn, S.A., 2004. Eruptive and passive degassing of sulfur dioxide at Nyiragongo volcano (D.R. Congo): the 17 January 2002 eruption and its aftermath. Acta Vulcanol. 14-15, 75–86.

Carn, S.A., 2015a. Gas, Plume, and Thermal Monitoring. In: Sigurdsson, H., Houghton, B., Rymer, H., Stix, J., McNutt, S. (Eds.), The Encyclopedia of Volcanoes, second ed. Elsevier, pp. 1125–1149.

Carn, S.A., 2015b. On the detection and monitoring of effusive eruptions using satellite SO_2 measurements. In: Harris, A.J.L.,, de Groeve, T., Garel, F., Carn, S.A. (Eds.), Detecting, Modeling and Responding to Effusive Eruptions. Geological Society of London, Special Publications 426 (in press).

Carn, S.A., 2015c. Multi-Satellite Volcanic Sulfur Dioxide (SO_2) Database Long-Term L4 Global, Version 1. Goddard Earth Science Data and Information Services Center (GES DISC), Greenbelt, MD, USA Accessed Dec 22, 2015 at http://dx.doi.org/10.5067/MEASURES/SO2/DATA401 (or http://disc.sci.gsfc.nasa.gov/datacollection/MSVOLSO2L4_V1.html).

Carn, S.A., Bluth, G.J.S., 2003. Prodigious sulfur dioxide emissions from Nyamuragira volcano, D.R. Congo. Geophys. Res. Lett. 30 (23), 2211. http://dx.doi.org/10.1029/2003GL018465.

Carn, S.A., Lopez, T.M., 2011. Opportunistic validation of sulfur dioxide in the Sarychev Peak volcanic eruption cloud. Atmos. Meas. Tech. 4, 1705–1712. http://dx.doi.org/10.5194/amt-4-1705-2011.

Carn, S.A., Prata, F.J., 2010. Satellite-based constraints on explosive SO_2 release from Soufrière Hills Volcano, Montserrat. Geophys. Res. Lett. 37, L00E22. http://dx.doi.org/10.1029/2010GL044971.

Carn, S.A., Krueger, A.J., Bluth, G.J.S., Schaefer, S.J., Krotkov, N.A., Watson, I.M., Datta, S., 2003. Volcanic eruption detection by the Total Ozone Mapping Spectrometer (TOMS) instruments: a 22-year record of sulfur dioxide and ash emissions. In: Oppenheimer, C., Pyle, D.M., Barclay, J. (Eds.), Volcanic Degassing. Geological Society, London, Special Publications 213, pp. 177–202.

Carn, S.A., Krueger, A.J., Krotkov, N.A., Gray, M.A., 2004. Fire at Iraqi sulfur plant emits SO_2 clouds detected by earth probe TOMS. Geophys. Res. Lett. 31 (19), L19105. http://dx.doi.org/10.1029/2004GL020719.

Carn, S.A., Strow, L.L., de Souza-Machado, S., Edmonds, Y., Hannon, S., 2005. Quantifying tropospheric volcanic emissions with AIRS: the 2002 eruption of Mt. Etna (Italy). Geophys. Res. Lett. 32, L02301. http://dx.doi.org/10.1029/2004GL021034.

Carn, S.A., Krotkov, N.A., Krueger, A.J., Yang, K., Levelt, P.F., 2007. Sulfur dioxide emissions from Peruvian copper smelters detected by the ozone monitoring instrument. Geophys. Res. Lett. 34, L09801. http://dx.doi.org/10.1029/2006GL029020.

Carn, S.A., Prata, A.J., Karlsdóttir, S., 2008a. Circumpolar transport of a volcanic cloud from Hekla (Iceland). J. Geophys. Res. 113, D14311. http://dx.doi.org/10.1029/2008JD009878.

Carn, S.A., Krueger, A.J., Krotkov, N.A., Arellano, S., Yang, K., 2008b. Daily monitoring of Ecuadorian volcanic degassing from space. J. Volcanol. Geotherm. Res. 176 (1), 141–150. http://dx.doi.org/10.1016/j.jvolgeores.2008.01.029.

Carn, S.A., Krueger, A.J., Krotkov, N.A., Yang, K., Evans, K., 2009a. Tracking volcanic sulfur dioxide clouds for aviation hazard mitigation. Nat. Hazards 51 (2), 325–343.

Carn, S.A., Pallister, J.S., Lara, L., Ewert, J.W., Watt, S., Prata, A.J., Thomas, R.J., Villarosa, G., 2009b. The unexpected awakening of Chaitén volcano, Chile. EOS Trans. AGU 90 (24), 205–206.

Carn, S.A., Froyd, K., Anderson, B.E., Wennberg, P., Crounse, J., Spencer, K., Dibb, J., Krotkov, N.A., Browell, E.V., Hair, J.W., Diskin, G., Sachse, G., Vay, S., 2011. In-situ measurements of tropospheric volcanic plumes in Ecuador and Colombia during TC^4. J. Geophys. Res. 116, D00J24. http://dx.doi.org/10.1029/2010JD014718.

Carn, S.A., Krotkov, N.A., Yang, K., Krueger, A.J., Biggs, J., 2013. Measuring global volcanic degassing with the Ozone Monitoring Instrument (OMI). In: Pyle, D.M., Mather, T.A. (Eds.), Remote Sensing of Volcanoes and Volcanic Processes: Integrating Observation and Modeling. Geol. Soc. Lon, Special Publications 380. http://dx.doi.org/10.1144/SP380.12.

Carn, S.A., Yang, K., Prata, A.J., Krotkov, N.A., 2015. Extending the long-term record of volcanic SO_2 emissions with the Ozone Mapping and Profiler Suite (OMPS) Nadir Mapper. Geophys. Res. Lett. 42. http://dx.doi.org/10.1002/2014GL062437.

Chahine, M.T., et al., 2006. AIRS: improving weather forecasting and providing new data on greenhouse gases. Bull. Am. Meteorol. Soc. 87 (7), 911–926. http://dx.doi.org/10.1175/BAMS-87-7-911.

Chin, M., Jacob, D.J., 1996. Anthropogenic and natural contributions to tropospheric sulfate: a global model analysis. J. Geophys. Res. 101 (D13), 18,691–18,699. http://dx.doi.org/10.1029/96JD01222.

Christenson, B.W., 2000. Geochemistry of fluids associated with the 1995–1996 eruption of Mt. Ruapehu, New Zealand: signatures and processes in the magmatic-hydrothermal system. J. Volcanol. Geotherm. Res. 97, 1–30.

Christopher, T., Edmonds, M., Humphreys, M.C.S., Herd, R.A., 2010. Volcanic gas emissions from Soufrière Hills Volcano, Montserrat 1995–2009, with implications for mafic magma supply and degassing. Geophys. Res. Lett. 37, L00E04. http://dx.doi.org/10.1029/2009GL041325.

Clarisse, L., Coheur, P.F., Prata, A.J., Hurtmans, D., Razavi, A., Phulpin, T., Hadji-Lazaro, J., Clerbaux, C., 2008. Tracking and quantifying volcanic SO_2 with IASI, the September 2007 eruption at Jebel at Tair. Atmos. Chem. Phys. 8, 7723–7734. http://dx.doi.org/10.5194/acp-8-7723-2008.

Clarisse, L., Hurtmans, D., Prata, A.J., Karagulian, F., Clerbaux, C., 2010. Retrieving radius, concentration, optical depth, and mass of different types of aerosols from high-resolution infrared nadir spectra. Appl. Opt. 49 (19), 3713–3722.

Clarisse, L., R'Honi, Y., Coheur, P.-F., Hurtmans, D., Clerbaux, C., 2011a. Thermal infrared nadir observations of 24 atmospheric gases. Geophys. Res. Lett. 38, L10802. http://dx.doi.org/10.1029/2011GL047271.

Clarisse, L., Coheur, P.-F., Chefdeville, S., Lacour, J.-L., Hurtmans, D., Clerbaux, C., 2011b. Infrared satellite observations of hydrogen sulfide in the volcanic plume of the August 2008 Kasatochi eruption. Geophys. Res. Lett. 38, L10804. http://dx.doi.org/10.1029/2011GL047402.

Clarisse, L., Hurtmans, D., Clerbaux, C., Hadji-Lazaro, J., Ngadi, Y., Coheur, P.-F., 2012. Retrieval of sulphur dioxide from the infrared atmospheric sounding interferometer (IASI). Atmos. Meas. Tech. 5, 581–594. http://dx.doi.org/10.5194/amt-5-581-2012.

Clarisse, L., Coheur, P.-F., Theys, N., Hurtmans, D., Clerbaux, C., 2014. The 2011 Nabro eruption, a SO_2 plume height analysis using IASI measurements. Atmos. Chem. Phys. 14, 3095–3111. http://dx.doi.org/10.5194/acp-14-3095-2014.

Clerbaux, C., Hadji-Lazaro, J., Turquety, S., George, M., Coheur, P.-F., Hurtmans, D., Wespes, C., Herbin, H., Blumstein, D., Tournier, B., Phulpin, T., 2007. The IASI/MetOp I Mission: First observations and highlights of its potential contribution to GMES. Space Res. Today 168, 19–24. http://dx.doi.org/10.1016/S0045-8732(07)80046-5.

Clerbaux, C., Coheur, P.-F., Clarisse, L., Hadji-Lazaro, J., Hurtmans, D., Turquety, S., Bowman, K., Worden, H., Carn, S.A., 2008. Measurements of SO_2 profiles in volcanic plumes from the NASA Tropospheric Emission Spectrometer (TES). Geophys. Res. Lett. 35, L22807. http://dx.doi.org/10.1029/2008GL035566.

Constantine, E.K., Bluth, G.J.S., Rose, W.I., 2000. TOMS and AVHRR observations of drifting volcanic clouds from the August 1991 eruptions of Cerro Hudson. In: Mouginis-Mark, P.J., Crisp, J.A., Fink, J.H. (Eds.), Remote Sensing of Active VolcanismGeophysical Monograph 116. AGU, Washington, DC, pp. 45–64.

Corradini, S., Merucci, L., Prata, A.J., 2009. Retrieval of SO_2 from thermal infrared satellite measurements: correction procedures for the effects of volcanic ash. Atmos. Meas. Tech. 2, 177–191. http://dx.doi.org/10.5194/amt-2-177-2009.

Corradini, S., Merucci, L., Prata, A.J., Piscini, A., 2010. Volcanic ash and SO_2 in the 2008 Kasatochi eruption: retrievals comparison from different IR satellite sensors. J. Geophys. Res. 115, D00L21. http://dx.doi.org/10.1029/2009JD013634.

Crutzen, P., 2006. Albedo enhancement by stratospheric sulfur injections: a contribution to resolve a policy dilemma? Clim. Chang. 77, 211–219.

Deshler, T., Anderson-Sprecher, R., Jäger, H., Barnes, J., Hofmann, D.J., Clemesha, B., Simonich, D., Osborn, M., Grainger, R.G., Godin-Beekmann, S., 2006. Trends in the nonvolcanic component of stratospheric aerosol over the period 1971–2004. J. Geophys. Res. 111, D01201. http://dx.doi.org/10.1029/2005JD006089.

Diehl, T., Heil, A., Chin, M., Pan, X., Streets, D., Schultz, M., Kinne, S., 2012. Anthropogenic, biomass burning, and volcanic emissions of black carbon, organic carbon, and SO_2 from 1980 to 2010 for hindcast model experiments. Atmos. Chem. Phys. Discuss. 12, 24895–24954. http://dx.doi.org/10.5194/acpd-12-24895-2012.

Doeringer, D., Eldering, A., Boone, C.D., González Abad, G., Bernath, P.F., 2012. Observation of sulfate aerosols and SO_2 from the Sarychev volcanic eruption using data from the Atmospheric Chemistry Experiment (ACE). J. Geophys. Res. 117, D03203. http://dx.doi.org/10.1029/2011JD016556.

Doiron, S.D., Bluth, G.J.S., Schnetzler, C.C., Krueger, A.J., Walter, L.S., 1991. Transport of Cerro Hudson SO_2 clouds. EOS Trans. AGU 72 (45), 489–498. http://dx.doi.org/10.1029/90EO00354.

Eckhardt, S., Prata, A.J., Seibert, P., Stebel, K., Stohl, A., 2008. Estimation of the vertical profile of sulfur dioxide injection into the atmosphere by a volcanic eruption using satellite column measurements and inverse transport modeling. Atmos. Chem. Phys. 8, 3881–3897. http://dx.doi.org/10.5194/acpd-8-3881-2008.

Edmonds, M., Aiuppa, A., Humphreys, M., Moretti, R., Giudice, G., Martin, R.S., Herd, R.A., Christopher, T., 2010. Excess volatiles supplied by mingling of mafic magma at an andesite arc volcano. Geochem. Geophys. Geosyst. 11, Q04005. http://dx.doi.org/10.1029/2009GC002781.

Eisinger, M., Burrows, J.P., 1998. Tropospheric sulfur dioxide observed by the ERS-2 GOME instrument. Geophys. Res. Lett. 25, 4177–4180.

Elias, T., Sutton, A.J., 2012. Sulfur dioxide emission rates from Kīlauea Volcano, Hawaii, 2007–2010. U.S. Geological Survey Open-File Report 2012–1107 (25 pp., available at: http://pubs.usgs.gov/of/2012/1107/).

Fairlie, T.D., Vernier, J.-P., Natarajan, M., Bedka, K.M., 2014. Dispersion of the Nabro volcanic plume and its relation to the Asian summer monsoon. Atmos. Chem. Phys. 14, 7045–7057. http://dx.doi.org/10.5194/acp-14-7045-2014.

Fee, D., Matoza, R.S., Gee, K.L., Neilsen, T.B., Ogden, D.E., 2013. Infrasonic crackle and supersonic jet noise from the eruption of Nabro Volcano, Eritrea. Geophys. Res. Lett. 40, 4199–4203. http://dx.doi.org/10.1002/grl.50827.

Ferguson, D.J., Barnie, T.D., Pyle, D.M., Oppenheimer, C., Yirgu, G., Lewi, E., Kidane, T., Carn, S.A., Hamling, I., 2010. Recent rift-related volcanism in Afar, Ethiopia. Earth Planet. Sci. Lett. 292 (3–4), 409–418. http://dx.doi.org/10.1016/j.epsl.2010.02.010.

Fioletov, V.E., Griffioen, E., Kerr, J., Wardle, D., Uchino, O., 1998. Influence of volcanic sulfur dioxide on spectral UV irradiance as measured by Brewer spectrophotometers. Geophys. Res. Lett. 25, 1665–1668.

Fioletov, V.E., McLinden, C.A., Krotkov, N., Moran, M.D., Yang, K., 2011. Estimation of SO_2 emissions using OMI retrievals. Geophys. Res. Lett. 38, L21811. http://dx.doi.org/10.1029/2011GL049402.

Fioletov, V.E., et al., 2013. Application of OMI, SCIAMACHY, and GOME-2 satellite SO_2 retrievals for detection of large emission sources. J. Geophys. Res. Atmos. 118. http://dx.doi.org/10.1002/jgrd.50826.

Froidevaux, L., et al., 2008. Validation of Aura Microwave Limb Sounder HCl measurements. J. Geophys. Res. 113, D15S25. http://dx.doi.org/10.1029/2007JD009025.

Fromm, M., Nedoluha, G., Charvát, Z., 2013. Comment on "Large volcanic aerosol load in the stratosphere linked to Asian monsoon transport". Science 339, 647. http://dx.doi.org/10.1126/science.1228605.

Fromm, M., Kablick III, G., Nedoluha, G., Carboni, E., Grainger, R., Campbell, J., Lewis, J., 2014. Correcting the record of volcanic stratospheric aerosol impact: Nabro and Sarychev Peak. J. Geophys. Res. Atmos. 119, 10,343–10,364. http://dx.doi.org/10.1002/2014JD021507.

Galle, B., Johansson, M., Rivera, C., Zhang, Y., Kihlman, M., Kern, C., Lehmann, T., Platt, U., Arellano, S., Hidalgo, S., 2010. Network for observation of volcanic and atmospheric change (NOVAC)—a global network for volcanic gas monitoring: network layout and instrument description. J. Geophys. Res. 115, D05304. http://dx.doi.org/10.1029/2009JD011823.

Gambacorta, A., Barnet, C.D., 2013. Methodology and information content of the NOAA NESDIS operational channel selection for the cross-track infrared sounder (CrIS). IEEE Trans. Geosci. Remote Sens. 51 (6), 3207–3216. http://dx.doi.org/10.1109/TGRS.2012.2220369.

Gerlach, T.M., 2011. Volcanic versus anthropogenic carbon dioxide. EOS Trans. AGU 92 (24), 201–208.

Gerlach, T.M., Westrich, H.R., Symonds, R.B., 1996. Preeruption vapor in magma of the climactic Mount Pinatubo eruption: source of the giant stratospheric sulfur dioxide cloud. In: Newhall, C.G., Punongbayan, R.S. (Eds.), Fire and Mud: Eruptions and Lahars of Mount Pinatubo, Philippines. University of Washington Press, Seattle, USA, pp. 415–434.

Global Volcanism Program, 2008. Report on Kasatochi (United States). In: Wunderman, R. (Ed.)Bulletin of the Global Volcanism Network 33. Smithsonian Institution, p. 7. http://dx.doi.org/10.5479/si.GVP.BGVN200807-311130.

Global Volcanism Program, 2012. Report on Nevado del Ruiz (Colombia). In: Wunderman, R. (Ed.)Bulletin of the Global Volcanism Network 37. Smithsonian Institution, p. 8. http://dx.doi.org/10.5479/si.GVP.BGVN201208-351020.

Global Volcanism Program, 2013. In: Venzke, E. (Ed.), Volcanoes of the World, v. 4.3.0. Smithsonian Institution, Washington, DC http://dx.doi.org/10.5479/si.GVP.VOTW4-2013 (Downloaded 19 Sept 2014).

Global Volcanism Program, 2014. Report on Sabancaya (Peru). In: Sennert, S.K. (Ed.), Weekly Volcanic Activity Report, 9 July-15 July 2014. Smithsonian Institution and US Geological Survey.

Goitom, B., et al., 2015. First recorded eruption of Nabro volcano, Eritrea, 2011. Bull. Volcanol. (in press).

Graf, H.-F., Feichter, J., Langmann, B., 1997. Volcanic sulfur emissions: estimates of source strength and its contribution to the global sulfate distribution. J. Geophys. Res. 102, 10727–10738.

Guo, S., Bluth, G.J.S., Rose, W.I., Watson, I.M., Prata, A.J., 2004. Re-evaluation of SO_2 release of the 15 June 1991 Pinatubo eruption using ultraviolet and infrared satellite sensors. Geochem. Geophys. Geosyst. 5, Q04001. http://dx.doi.org/10.1029/2003GC000654.

Gurevich, G.S., Krueger, A.J., 1997. Optimization of TOMS wavelength channels for ozone and sulfur dioxide retrievals. Geophys. Res. Lett. 24 (17), 2187–2190.

Halmer, M.M., Schmincke, H.-F., Graf, H.-F., 2002. The annual volcanic gas input into the atmosphere, in particular into the stratosphere: a global data set for the past 100 years. J. Volcanol. Geotherm. Res. 115, 511–528.

Hammer, C.U., 1977. Past volcanism revealed by Greenland ice sheet impurities. Nature 270, 482–486.

Hammer, C.U., Clausen, H.B., Dansgaard, W., 1980. Greenland ice sheet evidence of post-glacial volcanism and its climatic impact. Nature 288, 230–235.

Haywood, J.M., Jones, A., Clarisse, L., Bourassa, A., Barnes, J., Telford, P., Bellouin, N., Boucher, O., Agnew, P., Clerbaux, C., Coheur, P., Degenstein, D., Braesicke, P., 2010. Observations of the eruption of the Sarychev volcano and simulations using the HadGEM2 climate model. J. Geophys. Res. 115, D21212. http://dx.doi.org/10.1029/2010JD014447.

Head, E.M., 2005. A Remote Sensing Study of the Galapagos Islands Volcanoes Using TOMS and HIRS/2 Satellite Sensors (MS Thesis) Michigan Technological University, Houghton, MI, USA.

Henney, L., Rodríguez, L., Watson, I., 2012. A comparison of SO_2 retrieval techniques using mini-UV spectrometers and ASTER imagery at Láscar volcano, Chile. Bull. Volcanol. 74, 589–594.

Hilton, D.R., Fischer, T.P., Marty, B., 2002. Noble gases and volatile recycling at subduction zones. Rev. Mineral. 47, 319–370.

Hobbs, P.V., Tuell, J.P., Hegg, D.A., Radke, L.F., Eltgroth, M.W., 1982. Particles and gases in the emission from the 1980–1981 volcanic eruption of Mt. St. Helens. J. Geophys. Res. 87 (11), 062–11,086.

Hobbs, P., Radke, L., Lyons, J., Ferek, R., Coffman, D., 1991. Airborne measurements of particle and gas emissions from the 1990 volcanic eruptions of Mount Redoubt. J. Geophys. Res. 96, 18735–18752.

Hofmann, D., Barnes, J., O'Neill, M., Trudeau, M., Neely, R., 2009. Increase in background stratospheric aerosol observed with Lidar at Mauna Loa observatory and boulder, Colorado. Geophys. Res. Lett. 36, L15808. http://dx.doi.org/10.1029/2009GL039008.

Höpfner, M., Glatthor, N., Grabowski, U., Kellmann, S., Kiefer, M., Linden, A., Orphal, J., Stiller, G., von Clarmann, T., Funke, B., Boone, C.D., 2013. Sulfur dioxide (SO_2) as observed by MIPAS/envisat: temporal development and spatial distribution at 15–45 km altitude. Atmos. Chem. Phys. 13, 10405–10423. http://dx.doi.org/10.5194/acp-13-10405-2013.

Höpfner, M., Boone, C.D., Funke, B., Glatthor, N., Grabowski, U., Günther, A., Kellmann, S., Kiefer, M., Linden, A., Lossow, S., Pumphrey, H.C., Read, W.G., Roiger, A., Stiller, G., Schlager, H., von Clarmann, T., Wissmüller, K., 2015. Sulfur dioxide (SO_2) from MIPAS in the upper troposphere and lower stratosphere 2002–2012. Atmos. Chem. Phys. Discuss. 15, 5801–5847. http://dx.doi.org/10.5194/acpd-15-5801-2015.

Hörmann, C., Sihler, H., Bobrowski, N., Beirle, S., Penning de Vries, M., Platt, U., Wagner, T., 2013. Systematic investigation of bromine monoxide in volcanic plumes from space by using the GOME-2 instrument. Atmos. Chem. Phys. 13, 4749–4781. http://dx.doi.org/10.5194/acp-13-4749-2013.

Hughes, E.J., Sparling, L.C., Carn, S.A., Krueger, A.J., 2012. Using horizontal transport characteristics to infer an emission height time series of volcanic SO_2. J. Geophys. Res. 117, D18307. http://dx.doi.org/10.1029/2012JD017957.

Ialongo, I., Hakkarainen, J., Kivi, R., Anttila, P., Krotkov, N.A., Yang, K., Li, C., Tukiainen, S., Hassinen, S., Tamminen, J., 2015. Comparison of SO_2 operational satellite products with ground-based observations in northern Finland during the Icelandic Holuhraun fissure eruption. Atmos. Meas. Tech. 8, 2279–2289. http://dx.doi.org/10.5194/amt-8-2279-2015.

Kahn, R.A., Limbacher, J., 2012. Eyjafjallajökull volcano plume particle-type characterization from space-based multi-angle imaging. Atmos. Chem. Phys. 12, 9459–9477. http://dx.doi.org/10.5194/acp-12-9459-2012.

Kahn, R.A., Li, W.-H., Moroney, C., Diner, D.J., Martonchik, J.V., Fishbein, E., 2007. Aerosol source plume physical characteristics from space-based multiangle imaging. J. Geophys. Res. 112, D11205. http://dx.doi.org/10.1029/2006JD007647.

Karagulian, F., Clarisse, L., Clerbaux, C., Prata, A.J., Hurtmans, D., Coheur, P.F., 2010. Detection of volcanic SO_2, ash, and H_2SO_4 using the Infrared Atmospheric Sounding Interferometer (IASI). J. Geophys. Res. 115, D00L02. http://dx.doi.org/10.1029/2009JD012786.

Karl, T.R., Arguez, A., Huang, B., Lawrimore, J.H., McMahon, J.R., Menne, M.J., Peterson, T.C., Vose, R.S., Zhang, H.M., 2015. Possible artifacts of data biases in the recent global surface warming hiatus. Science http://dx.doi.org/10.1126/science.aaa5632.

Kearney, C.S., Dean, K., Realmuto, V.J., Watson, I.M., Dehn, J., Prata, F., 2008. Observations of SO_2 production and transport from Bezymianny volcano, Kamchatka using the MODerate resolution Infrared Spectroradiometer (MODIS). Int. J. Remote Sens. 29 (22), 6647–6665.

Kearney, C., Watson, I.M., Bluth, G.J.S., Carn, S.A., Realmuto, V., 2009. A comparison of thermal infrared and ultraviolet retrievals of SO_2 in the cloud produced by the 2003 Al-Mishraq state sulfur plant fire. Geophys. Res. Lett. 36, L10807. http://dx.doi.org/10.1029/2009GL038215.

Kellogg, W.W., Cadle, R.D., Allen, E.R., Lazrus, A.L., Martell, E.A., 1972. The sulfur cycle. Science 175, 587–596.

Kerr, J.B., Evans, W.J., 1987. Comparison of ground-based and TOMS measurements of SO_2 from volcanic emissions. In: Krueger, A.J. (Ed.), Scientific and Operational Requirements for TOMS DataNASA Conf. Publ. 2497. NASA, Washington, D.C., pp. 60–69 (http://ntrs.nasa.gov/archive/nasa/casi.ntrs.nasa.gov/19880004392_1988004392.pdf).

Khokhar, M.F., Frankenberg, C., Van Roozendael, M., Beirle, S., Kühl, S., Richter, A., Platt, U., Wagner, T., 2005. Satellite observations of atmospheric SO_2 from volcanic eruptions during the time-period of 1996–2002. Adv. Space Res. 36, 879–887. http://dx.doi.org/10.1016/j.asr.2005.04.114.

Kratzmann, D.J., Carey, S., Scasso, R., Naranjo, J.-A., 2009. Compositional variations and magma mixing in the 1991 eruptions of Hudson volcano, Chile. Bull. Volcanol. 71 (4), 419–439.

Kristiansen, N.I., et al., 2010. Remote sensing and inverse transport modeling of the Kasatochi eruption sulfur dioxide cloud. J. Geophys. Res. 115, D00L16. http://dx.doi.org/10.1029/2009JD013286.

Kristiansen, N., Prata, A.J., Stohl, A., Carn, S.A., 2015. Stratospheric volcanic ash emissions from the 13 February 2014 Kelut eruption. Geophys. Res. Lett. http://dx.doi.org/10.1002/2014GL062307 (in press).

Krotkov, N.A., Carn, S.A., Krueger, A.J., Bhartia, P.K., Yang, K., 2006. Band residual difference algorithm for retrieval of SO_2 from the aura ozone monitoring instrument (OMI). IEEE Trans. Geosci. Remote Sens. 44 (5), 1259–1266. http://dx.doi.org/10.1109/TGRS.2005.861932.

Krotkov, N.A., et al., 2008. Validation of SO_2 retrievals from the ozone monitoring instrument over NE China. J. Geophys. Res. 113, D16S40. http://dx.doi.org/10.1029/2007JD008818.

Krotkov, N.A., Schoeberl, M.R., Morris, G.A., Carn, S., Yang, K., 2010. Dispersion and lifetime of the SO_2 cloud from the August 2008 Kasatochi eruption. J. Geophys. Res. 115, D00L20. http://dx.doi.org/10.1029/2010JD013984.

Krueger, A.J., 1983. Sighting of El Chichón sulfur dioxide clouds with the Nimbus 7 total ozone mapping spectrometer. Science 220, 1377–1379.

Krueger, A.J., Walter, L.S., Schnetzler, C.C., Doiron, S.D., 1990. TOMS measurement of the sulfur dioxide emitted during the 1985 Nevado del Ruiz eruptions. J. Volcanol. Geotherm. Res. 41, 7–15.

Krueger, A.J., Walter, L.S., Bhartia, P.K., Schnetzler, C.C., Krotkov, N.A., Sprod, I., Bluth, G.J.S., 1995. Volcanic sulfur dioxide measurements from the total ozone mapping spectrometer instruments. J. Geophys. Res. D100, 14057–14076.

Krueger, A.J., Schnetzler, C.C., Walter, L.S., 1996. The December 1981 eruption of Nyamuragira volcano (Zaire), and the origin of the "mystery cloud" of early 1982. J. Geophys. Res. D101, 15191–15196.

Krueger, A.J., Schaefer, S.J., Krotkov, N., Bluth, G., Barker, S., 2000. Ultraviolet remote sensing of volcanic emissions. In: Mouginis-Mark, P.J., Crisp, J.A., Fink, J.H. (Eds.), Remote Sensing of Active VolcanismGeophysical Monograph 116. AGU, Washington, DC, pp. 25–43.

Krueger, A.J., Krotkov, N.A., Carn, S.A., 2008. El Chichon: the genesis of volcanic sulfur dioxide monitoring from space. J. Volcanol. Geotherm. Res. 175, 408–414. http://dx.doi.org/10.1016/j.jvolgeores.2008.02.026.

Krueger, A.J., Krotkov, N., Yang, K., Carn, S., Vicente, G., Schroeder, W., 2009. Applications of satellite-based sulfur dioxide monitoring. IEEE JSTARS 2, 293–298.

Kushendratno, J.S.P., Kristianto, F.R., Bina, W., McCausland, S.A., Carn, N., Haerani, J.G., Keeler, R., 2012. Recent explosive eruptions and volcano hazards at Soputan volcano — a basalt stratovolcano in north Sulawesi, Indonesia. Bull. Volcanol. 74 (7), 1581–1609.

Kutterolf, S., Hansteen, T.H., Appel, K., Freundt, A., Krüger, K., Pérez, W., Wehrmann, H., 2013. Combined bromine and chlorine release from large explosive volcanic eruptions: a threat to stratospheric ozone? Geology 41 (6), 707–710. http://dx.doi.org/10.1130/G34044.1.

Le Guern, F., 1982. Les débits de CO_2 et de SO_2 volcaniques dans l'atmosphère. Bull. Volcanol. 45, 197–202.

Lee, C., Richter, A., Weber, M., Burrows, J.P., 2008. SO_2 retrieval from SCIAMACHY using the weighting function DOAS (WFDOAS) technique: comparison with standard DOAS retrieval. Atmos. Chem. Phys. 8, 6137–6145. http://dx.doi.org/10.5194/acp-8-6137-2008.

Lee, C., Martin, R.V., et al., 2009. Retrieval of vertical columns of sulfur dioxide from SCIAMACHY and OMI: air mass factor algorithm development, validation, and error analysis. J. Geophys. Res. 114, D22303. http://dx.doi.org/10.1029/2009JD012123.

Levelt, P.F., van den Oord, G.H.J., Dobber, M.R., Mälkki, A., Visser, H., de Vries, J., Stammes, P., Lundell, J.O.V., Saari, H., 2006. The ozone monitoring instrument. IEEE Trans. Geosci. Remote Sens. 44 (5), 1093–1101. http://dx.doi.org/10.1109/TGRS.2006.872333.

Li, C., Joiner, J., Krotkov, N.A., Bhartia, P.K., 2013. A fast and sensitive new satellite SO_2 retrieval algorithm based on principal component analysis: application to the ozone monitoring instrument. Geophys. Res. Lett. 40. http://dx.doi.org/10.1002/2013GL058134.

Livesey, N.J., et al., 2011. Earth Observing System (EOS) Aura Microwave Limb Sounder (MLS) Version 3.3 and 3.4 Level 2 Data Quality and Description Document. Tech. Rep. JPL D-33509. NASA Jet Propulsion Laboratory, California Institute of Technology, Pasadena, California (91109-8099, available at: http://mls.jpl.nasa.gov/data/datadocs.php).

Lopez, T., Carn, S.A., Werner, C., Fee, D., Kelly, P., Doukas, M., Pfeffer, M., Webley, P., Cahill, C., Schneider, D., 2013a. Evaluation of redoubt volcano's sulfur dioxide emissions by the ozone monitoring instrument. J. Volcanol. Geotherm. Res. 259, 290–307.

Lopez, T., Fee, D., Prata, F., Dehn, J., 2013b. Characterization and interpretation of volcanic activity at Karymsky Volcano, Kamchatka, Russia, using observations of infrasound, volcanic emissions, and thermal imagery. Geochem. Geophys. Geosyst. 14, 5106–5127.

Lopez, T., Thomas, H.E., Prata, A.J., Amigo, A., Fee, D., Moriano, D., 2015. Volcanic plume characteristics determined using an infrared imaging camera. J. Volcanol. Geotherm. Res. 300, 148–166. http://dx.doi.org/10.1016/j.jvolgeores.2014.12.009.

Luhr, J.F., Carmichael, I.S.E., Varekamp, J.C., 1984. The 1982 eruptions of El Chichòn Volcano, Chiapas, Mexico: mineralogy and petrology of the anhydrite-bearing pumices. J. Volcanol. Geotherm. Res. 23, 69–108.

Mankin, W.G., Coffey, M.T., 1984. Increased stratospheric hydrogen-chloride in the El Chichon cloud. Science 226, 170–172. http://dx.doi.org/10.1126/science.226.4671.170.

Mankin, W.G., Coffey, M.T., Goldman, A., 1992. Airborne observations of SO_2, HCl, and O_3 in the stratospheric plume of the Pinatubo volcano in July 1991. Geophys. Res. Lett. 19 (2), 179–182.

Martin, D., Ardouin, B., Bergametti, G., Carbonnelle, J., Faivre-Pierret, R., Lambert, G., Le Cloarec, M.F., Sennequier, G., 1986. Geochemistry of sulfur in Mount Etna plume. J. Geophys. Res. 91, 12249–12254.

Martínez-Alonso, S., Deeter, M.N., Worden, H.M., Clerbaux, C., Mao, D., Gille, J.C., 2012. First satellite identification of volcanic carbon monoxide. Geophys. Res. Lett. 39, L21809. http://dx.doi.org/10.1029/2012GL053275.

Mateshvili, N., Fussen, D., Mateshvili, G., Mateshvili, I., Vanhellemont, F., Kyrölä, E., Tukiainen, S., Kujanpää, J., Bingen, C., Robert, C., Tétard, C., Dekemper, E., 2013. Nabro volcano aerosol in the stratosphere over Georgia, South Caucasus from ground-based spectrometry of twilight sky brightness. Atmos. Meas. Tech. 6, 2563–2576. http://dx.doi.org/10.5194/amt-6-2563-2013.

Mather, T.A., Tsanev, V.I., Pyle, D.M., McGonigle, A.J.S., Oppenheimer, C., Allen, A.G., 2004. Characterization and evolution of tropospheric plumes from Lascar and Villarica volcanoes, Chile. J. Geophys. Res. 109, D21303. http://dx.doi.org/10.1029/2004JD004934.

Matiella Novak, A., Watson, I.M., Delgado-Granados, H., Rose, W.I., Cárdenas-González, L., Realmuto, V.J., 2008. Volcanic emissions from Popocatépetl volcano, Mexico, quantified using moderate resolution imaging spectroradiometer (MODIS) infrared data: a case study of the December 2000–January 2001 emissions. J. Volcanol. Geotherm. Res. 170 (1–2), 76–85.

McCarthy, E.B., Bluth, G.J.S., Watson, I.M., Tupper, A., 2008. Detection and analysis of the volcanic clouds associated with the 18 and 28 August 2000 eruptions of Miyakejima volcano, Japan. Int. J. Remote Sens. 29 (22), 6597–6620. http://dx.doi.org/10.1080/01431160802168400.

McCormick, B.T., Edmonds, M., Mather, T.A., Carn, S.A., 2012. First synoptic analysis of volcanic degassing in Papua New Guinea. Geochem. Geophys. Geosyst. 13, Q03008. http://dx.doi.org/10.1029/2011GC003945.

McCormick, B.T., Edmonds, M., Mather, T., Campion, R., Hayer, C., Thomas, H.E., Carn, S.A., 2013. Volcano monitoring applications of the Ozone Monitoring Instrument (OMI). In: Pyle, D.M., Mather, T.A., Biggs, J. (Eds.), Remote Sensing of Volcanoes and Volcanic Processes: Integrating Observation and Modeling. Geol. Soc. Lon, Special Publications 380. http://dx.doi.org/10.1144/SP380.11.

McCormick, B., Popp, C., Andrews, B., Cottrell, E., 2015. Ten years of satellite observations reveal highly variable sulphur dioxide emissions at Anatahan volcano, Mariana Islands. J. Geophys. Res. Atmos. 120. http://dx.doi.org/10.1002/2014JD022856.

McGonigle, A.J.S., Oppenheimer, C., Tsanev, V.I., Saunders, S., Mulina, K., Tohui, S., Bosco, J., Nahou, J., Kuduon, J., Taranu, F., 2004a. Sulphur dioxide fluxes from Papua New Guinea's volcanoes. Geophys. Res. Lett. 31, L08606. http://dx.doi.org/10.1029/2004GL019568.

McGonigle, A.J.S., Delmelle, P., Oppenheimer, C., Tsanev, V.I., Delfosse, T., Williams-Jones, G., Horton, K., Mather, T.A., 2004b. SO_2 depletion in tropospheric volcanic plumes. Geophys. Res. Lett. 31, L13201.

McKeen, S.A., Liu, S.C., Kiang, C.S., 1984. On the chemistry of stratospheric SO_2 from volcanic eruptions. J. Geophys. Res. 89 (D3), 4873–4881. http://dx.doi.org/10.1029/JD089iD03p04873.

McPeters, R.D., 1993. The atmospheric SO_2 budget for Pinatubo derived from NOAA-11 SBUV/2 spectral data. Geophys. Res. Lett. 20 (18), 1971–1974.

McPeters, R.D., Heath, D.F., Schlesinger, B.M., 1984. Satellite observation of SO_2 from El Chichon: identification and measurement. Geophys. Res. Lett. 11, 1203–1206.

Miles, G.M., Grainger, R.G., Highwood, E.J., 2004. The significance of volcanic eruption strength and frequency for climate. Q. J. R. Meteorol. Soc. 130, 2361–2376.

Mori, T., Kazahaya, K., Oppenheimer, C., McGonigle, A.J.S., Tsanev, V., Olmos, R., Ohwada, M., Shuto, T., 2006. Sulfur dioxide fluxes from the volcanoes of Hokkaido, Japan. J. Volcanol. Geotherm. Res. 158, 235–243.

Mori, T., Shinohara, H., Kazahaya, K., Hirabayashi, J.-I., Matsushima, T., Mori, T., Ohwada, M., Odai, M., Iino, H., Miyashita, M., 2013. Time-averaged SO_2 fluxes of subduction-zone volcanoes: example of a 32-year exhaustive survey for Japanese volcanoes. J. Geophys. Res. Atmos. 118, 8662–8674. http://dx.doi.org/10.1002/jgrd.50591.

Munro, R., Eisinger, M., Anderson, C., Callies, J., Corpaccioli, E., Lang, R., Lefebvre, A., Livschitz, Y., Perez Albinana, A., 2006. GOME-2 on MetOp, Paper Presented at the 2006 EUMETSAT Meteorological Satellite Conference. Eur. Org. for the Exploit of Meteorol. Satell., Helsinki.

Nagai, T., Liley, B., Sakai, T., Shibata, T., Uchino, O., 2010. Post-Pinatubo evolution and subsequent trend of the stratospheric aerosol layer observed by mid-latitude lidars in both hemispheres. SOLA 6, 69–72. http://dx.doi.org/10.2151/sola.2010-018.

Neely, R.R.I.I.I., Toon, O.B., Solomon, S., Vernier, J.-P., Alvarez, C., English, J.M., Rosenlof, K.H., Mills, M.J., Bardeen, C.G., Daniel, J.S., Thayer, J.P., 2013. Recent anthropogenic increases in SO_2 from Asia have minimal impact on stratospheric aerosol. Geophys. Res. Lett. 40. http://dx.doi.org/10.1002/grl.50263.

Newhall, C.G., Self, S., 1982. The volcanic explosivity index (VEI): an estimate of explosivity magnitude for historic volcanism. J. Geophys. Res. 87, 1231–1238.

Noël, S., Buchwitz, M., Bovensmann, H., Hoogen, R., Burrows, J.P., 1999. Atmospheric water vapor amounts retrieved from GOME satellite data. Geophys. Res. Lett. 26, 1841–1844.

Noël, S., Buchwitz, M., Burrows, J.P., 2004. First retrieval of global water vapour column amounts from SCIAMACHY measurements. Atmos. Chem. Phys. 4, 111–125.

Noël, S., Mieruch, S., Bovensmann, H., Burrows, J.P., 2008. Preliminary results of GOME-2 water vapour retrievals and first applications in polar regions. Atmos. Chem. Phys. 8, 1519–1529.

Nowlan, C.R., Liu, X., Chance, K., Cai, Z., Kurosu, T.P., Lee, C., Martin, R.V., 2011. Retrievals of sulfur dioxide from the global ozone monitoring experiment 2 (GOME-2) using an optimal estimation approach: algorithm and initial validation. J. Geophys. Res. 116, D18301. http://dx.doi.org/10.1029/2011JD015808.

Oppenheimer, C., Francis, P., Stix, J., 1998. Depletion rates of sulfur dioxide in tropospheric volcanic plumes. Geophys. Res. Lett. 25, 2671–2674.

Oppenheimer, C., Scaillet, B., Martin, R.S., 2011. Sulfur degassing from volcanoes: source conditions, surveillance, plume chemistry and earth system impacts. Rev. Mineral. Geochem. 73, 363–421. http://dx.doi.org/10.2138/rmg.2011.73.13.

Penning de Vries, M.J.M., Dörner, S., Puķīte, J., Hörmann, C., Fromm, M.D., Wagner, T., 2014. Characterisation of a stratospheric sulfate plume from the Nabro volcano using a combination of passive satellite measurements in nadir and limb geometry. Atmos. Chem. Phys. 14, 8149–8163. http://dx.doi.org/10.5194/acp-14-8149-2014.

Phulpin, T., Blumstein, D., Prel, F., Tournier, B., Prunet, P., Schlüssel, P., 2007. Applications of IASI on MetOp-A: first results and illustration of potential use for meteorology,

climate monitoring, and atmospheric chemistry. Proc. SPIE, 6684 http://dx.doi.org/10.1117/12.736816.
Prata, A.J., Bernardo, C., 2007. Retrieval of volcanic SO_2 column abundance from atmospheric infrared sounder data. J. Geophys. Res. 112, D20204. http://dx.doi.org/10.1029/2006JD007955.
Prata, A.J., Bernardo, C., 2014. Retrieval of sulfur dioxide from a ground-based thermal infrared imaging camera. Atmos. Meas. Tech. 7, 2807–2828. http://dx.doi.org/10.5194/amt-7-2807-2014.
Prata, A.J., Grant, I.F., 2001. Retrieval of microphysical and morphological properties of volcanic ash plumes from satellite data: application to Mt Ruapehu, New Zealand. Q. J. R. Meteorol. Soc. 127, 2153–2179.
Prata, A.J., Kerkmann, J., 2007. Simultaneous retrieval of volcanic ash and SO_2 using MSG-SEVIRI measurements. Geophys. Res. Lett. 34, L05813. http://dx.doi.org/10.1029/2006GL028691.
Prata, A.J., Self, S., Rose, W.I., O'Brien, D.M., 2003. Global, long-term sulphur dioxide measurements from TOVS data: a new tool for studying explosive volcanism and climate. In: Robock, A., Oppenheimer, C. (Eds.), Volcanism and the Earth's AtmosphereGeophys. Monogr. Ser. vol. 139. AGU, Washington, D. C., pp. 75–92.
Prata, A.J., Carn, S.A., Stohl, A., Kerkmann, J., 2007. Long range transport and fate of a stratospheric volcanic cloud from Soufrière Hills volcano, Montserrat. Atmos. Chem. Phys. 7, 5093–5103.
Prata, A.J., Gangale, G., Clarisse, L., Karagulian, F., 2010. Ash and sulfur dioxide in the 2008 eruptions of Okmok and Kasatochi: insights from high spectral resolution satellite measurements. J. Geophys. Res. 115, D00L18. http://dx.doi.org/10.1029/2009JD013556.
Prata, A.T., Siems, S.T., Manton, M.J., 2015. Quantification of volcanic cloud top heights and thicknesses using A-train observations for the 2008 Chaitén eruption. J. Geophys. Res. Atmos. 120, 2928–2950. http://dx.doi.org/10.1002/2014JD022399.
Pugnaghi, S., Gangale, G., Corradini, S., Buongiorno, M.F., 2006. Mt. Etna sulfur dioxide flux monitoring using ASTER-TIR data and atmospheric observations. J. Volcanol. Geotherm. Res. 152, 74–90. http://dx.doi.org/10.1016/j.jvolgeores.2005.10.004.
Pumphrey, H.C., Read, W.G., Livesey, N.J., Yang, K., 2015. Observations of volcanic SO_2 from MLS on aura. Atmos. Meas. Tech. 8, 195–209. http://dx.doi.org/10.5194/amt-8-195-2015.
Pyle, D.M., 1995. Mass and energy budgets of explosive volcanic eruptions. Geophys. Res. Lett. 22 (5), 563–566.
Pyle, D.M., 2015. Sizes of Volcanic Eruptions. In: Sigurdsson, H., Houghton, B., Rymer, H., Stix, J., McNutt, S. (Eds.), The Encyclopedia of Volcanoes, second ed. Elsevier, pp. 257–264.
Pyle, D.M., Beattie, P.D., Bluth, G.J.S., 1996. Sulphur emissions to the stratosphere from explosive volcanic eruptions. Bull. Volcanol. 57, 663–671.
Radke, L.F., 1982. Sulphur and sulphate from Mt Erebus. Nature 299, 710–712.
Read, W.G., Froidevaux, L., Waters, J.W., 1993. Microwave limb sounder (MLS) measurements of SO_2 from Mt. Pinatubo volcano. Geophys. Res. Lett. 20, 1299–1302. http://dx.doi.org/10.1029/93GL00831.
Realmuto, V.J., 2000. The potential use of earth observing system data to monitor the passive emission of sulfur dioxide from volcanoes. In: Mouginis-Mark, P.J., Crisp, J.A., Fink, J.H. (Eds.), Remote Sensing of Active VolcanismGeophysical Monograph 116. AGU, Washington, DC, pp. 101–115.
Realmuto, V.J., Worden, H.M., 2000. The impact of atmospheric water vapor on the thermal infrared remote sensing of volcanic sulfur dioxide emissions: a case study from the Pu'u 'O'o vent of Kilauea Volcano, Hawaii. J. Geophys. Res. 105, 21,497–21,508.
Realmuto, V.J., Abrams, M.J., Buongiornio, M.F., Pieri, D.C., 1994. The use of multispectral thermal infrared image data to estimate the sulfur dioxide flux from volcanoes: a case study from Mount Etna, Sicily, 29 July 1986. J. Geophys. Res. 99, 481–488.
Realmuto, V.J., Sutton, A.J., Elias, T., 1997. Multispectral thermal infrared imaging of sulfur dioxide plumes: a case study from the east rift zone of Kilauea Volcano, Hawaii. J. Geophys. Res. 102, 15057–15072.
Ridley, D.A., et al., 2014. Total volcanic stratospheric aerosol optical depths and implications for global climate change. Geophys. Res. Lett. 41, 7763–7769. http://dx.doi.org/10.1002/2014GL061541.
Rinsland, C.P., Gunson, M.R., Ko, M.K.W., Weisenstein, D.W., Zander, R., Abrams, M.C., Goldman, A., Sze, N.D., Yue, G.K., 1995. H_2SO_4 photolysis: a source of sulfur dioxide in the upper stratosphere. Geophys. Res. Lett. 22, 1109–1112. http://dx.doi.org/10.1029/95GL00917.
Rix, M., Valks, P., et al., 2009. Satellite monitoring of volcanic sulfur dioxide emissions for early warning of volcanic hazards. IEEE J-STARS 2, 196–206.
Rix, M., Valks, P., Hao, N., Loyola, D., Schlager, H., Huntrieser, H., Flemming, J., Koehler, U., Schumann, U., Inness, A., 2012. Volcanic SO_2, BrO and plume height estimations using GOME-2 satellite measurements during the eruption of eyjafjallajökull in May 2010. J. Geophys. Res. 117, D00U19. http://dx.doi.org/10.1029/2011JD016718.
Robock, A., 2000. Volcanic eruptions and climate. Rev. Geophys. 38, 191–219.
Robock, A., Marquardt, A., Kravitz, B., Stenchikov, G., 2009. Benefits, risks, and costs of stratospheric geoengineering. Geophys. Res. Lett. 36, L19703. http://dx.doi.org/10.1029/2009GL039209.
Rodríguez, L.A., Watson, I.M., Edmonds, M., Ryan, G., Hards, V., Oppenheimer, C.M., Bluth, G.J.S., 2008. SO_2 loss rates in the plume emitted by Soufrière Hills volcano, Montserrat. J. Volcanol. Geotherm. Res. 173, 135–147.
Rose, W.I., Delene, D.J., Schneider, D.J., Bluth, G.J.S., Krueger, A.J., Sprod, I., McKee, C., Davies, H.L., Ernst, G.G.J., 1995. Ice in the 1994 Rabaul eruption cloud: implications for volcano hazard and atmospheric effects. Nature 375, 477–479.
Rose, W.I., Bluth, G.J.S., Ernst, G.G.J., 2000. Integrating retrievals of volcanic cloud characteristics from satellite remote sensors—a summary. Philos. Trans. R. Soc. Lond. A Math. Phys. Sci. 358, 1585–1606.
Rose, W.I., Bluth, G.J.S., Schneider, D.J., Ernst, G.G.J., Riley, C.M., Henderson, L.J., McGimsey, R.G., 2001. Observations of volcanic clouds in their first few days of atmospheric residence: the 1992 eruptions of Crater Peak, Mount Spurr Volcano, Alaska. J. Geol. 109, 677–694.
Rose, W.I., Gu, Y., Watson, I.M., Yu, T., Bluth, G.J.S., Prata, A.J., Krueger, A.J., Krotkov, N., Carn, S., Fromm, M.D., Hunton, D.E., Viggiano, A.A., Miller, T.M., Ballentin, J.O., Ernst, G.G.J., Reeves, J.M., Wilson, C., Anderson, B.E., 2003. The February–March 2000 Eruption of Hekla, Iceland from a Satellite Perspective. In: Robock, A., Oppenheimer, C. (Eds.), Volcanism and the Earth's Atmosphere. AGU Geophysical Monograph 139, pp. 107–132.
Rose, W.I., Millard, G.A., Mather, T.A., et al., 2006. The atmospheric chemistry of a 33–34 hour old volcanic cloud from Hekla volcano (Iceland): insights from direct sampling and the application of chemical box modeling. J. Geophys. Res. 111, D20206. http://dx.doi.org/10.1029/2005JD006872.
Rosen, J.M., Hofmann, D.J., 1980. A stratospheric aerosol increase. Geophys. Res. Lett. 7 (9), 669–672.
Saing, U.B., Bani, P., Kristianto, 2014. Ibu volcano, a center of spectacular dacite dome growth and long-term continuous eruptive discharges. J. Volcanol. Geotherm. Res. 282, 36–42.
Santer, B.D., et al., 2014. Volcanic contribution to decadal changes in tropospheric temperature. Nat. Geosci. 7, 185–189. http://dx.doi.org/10.1038/ngeo2098.
Santer, B.D., et al., 2015. Observed multivariable signals of late 20th and early 21st century volcanic activity. Geophys. Res. Lett. 42, 500–509. http://dx.doi.org/10.1002/2014GL062366.
Sato, M., Hansen, J.E., McCormick, M.P., Pollack, J.B., 1993. Stratospheric aerosol optical depth, 1850-1990. J. Geophys. Res. 98, 22987–22994.
Sawamura, P., Vernier, J., Barnes, J., Berkoff, T., Welton, E., Alados-Arboledas, L., Navas-Guzmán, F., Pappalardo, G.A., Mona, L., Madonna, F., Lange, D., Sicard, M., Godin-Beekmann, S., Payen, G., Wang, Z., Hu, S., Tripathi, S., Cordoba-Jabonero, C., Hoff, R., 2012. Stratospheric AOD after the 2011 eruption of nabro volcano measured by lidars over the northern hemisphere. Environ. Res. Lett. 7, 034013. http://dx.doi.org/10.1088/1748-9326/7/3/034013.
Sawyer, G.M., Carn, S.A., Oppenheimer, C., Tsanez, V.I., Burton, M., 2008a. Investigation into magma degassing at nyiragongo volcano, democratic republic of Congo. Geochem. Geophys. Geosyst. 9, Q02017. http://dx.doi.org/10.1029/2007GC001829.
Sawyer, G.M., Oppenheimer, C., Tsanez, V.I., Yirgu, G., 2008b. Magmatic degassing at erta 'ale volcano, Ethiopia. J. Volcanol. Geotherm. Res. 178, 837–846.
Scaillet, B., Luhr, J.F., Carroll, M.C., 2003. Petrological and Volcanological Constraints on Volcanic Sulfur Emissions to the Atmosphere. In: A., R., C., O. (Eds.), Volcanism and the Earth's AtmosphereGeophysical Monograph 139. AGU, Washington, DC, pp. 11–40.
Schmidt, G.A., Shindell, D.T., Tsigaridis, K., 2014. Reconciling warming trends. Nat. Geosci. 7, 158–160.
Schneider, D.J., Rose, W.I., Coke, L.R., Bluth, G.J.S., Sprod, I.E., Krueger, A.J., 1999. Early evolution of a stratospheric volcanic eruption cloud as observed with TOMS and AVHRR. J. Geophys. Res. 104, 4037–4050.
Schnetzler, C.C., Doiron, S.D., Walter, L.S., Krueger, A.J., 1994. Satellite Measurements of Sulfur Dioxide from the Redoubt Eruptions of 1989–1990. In: Miller, T.P., Chouet, B.A. (Eds.), The 1989–1990 Eruptions of Redoubt Volcano, Alaska. J. Volcanol. Geotherm. Res. 62(1-4), pp. 353–357.
Schnetzler, C.C., Krueger, A.J., Bluth, G.S., Sprod, I.E., Walter, L.S., 1995. Comment on the paper "the atmospheric SO_2 budget for Pinatubo derived from NOAA-11 SBUV/2 spectral data" by R. D. McPeters. Geophys. Res. Lett. 22 (3), 315–316.
Schnetzler, C.C., Bluth, G.J.S., Krueger, A.J., Walter, L.S., 1997. A proposed volcanic sulfur dioxide index (VSI). J. Geophys. Res. 102 (B9), 20087–20091.
Schoeberl, M., Doiron, S.D., Lait, L.R., Newman, P.A., Krueger, A.J., 1993. A simulation of the Cerro Hudson SO_2 cloud. J. Geophys. Res. 98, 2949–2955.
Schwandner, F.M., Carn, S.A., 2011. Detecting Volcanic CO_2 from Space: Target Mode Observations with GOSAT, Abstract A33C-0222. Presented at 2011 Fall Meeting, AGU, San Francisco, Calif., 5–9 Dec.
Schwandner, F.M., Realmuto, V.J., Carn, S.A., Kahn, B., Oda, T., Kuze, A., Kataoka, F., Krings, T., Rayner, P.J., Shiomi, K., 2015. CO_2 plume detection, verification, and flux determination using OCO-2 data: volcanoes and power plants. Geophys. Res. Abstr. 17 (abstract EGU2015-7665, Presented at EGU General Assembly 2015).
Sharma, K., Blake, S., Self, S., Krueger, A.J., 2004. SO_2 emissions from basaltic eruptions, and the excess sulfur issue. Geophys. Res. Lett. 31, L13612. http://dx.doi.org/10.1029/2004GL019688.
Sheng, J.-X., Weisenstein, D.K., Luo, B.-P., Rozanov, E., Stenke, A., Anet, J., Bingemer, H., Peter, T., 2015. Global atmospheric sulfur budget under volcanically quiescent conditions: aerosol-chemistry-climate model predictions and validation. J. Geophys. Res. Atmos. 120, 256–276. http://dx.doi.org/10.1002/2014JD021985.
Shibata, T., Kouketsu, T., 2008. Volcanic clouds from the 2007 eruption of Jebel at tair (Yemen) detected by ground based and space borne Lidar. Sci. Online Lett. Atmos. 4, 93–96 (available at: https://www.jstage.jst.go.jp/article/sola/4/0/4_0_93/_pdf).
Shinohara, H., 2013. Volatile flux from subduction zone volcanoes: insights from a detailed evaluation of the fluxes from volcanoes in Japan. J. Volcanol. Geotherm. Res. 268, 46–63.
Siebert, L., Simkin, T., Kimberly, P., 2010. Volcanoes of the World. third ed. University of California Press, Berkeley and Los Angeles, CA.
Sigmarsson, O., Haddadi, B., Carn, S.A., Moune, S., Gudnason, J., Yang, K., Clarisse, L., 2013. The sulfur budget of the 2011 grímsvötn eruption, Iceland. Geophys. Res. Lett. 40 (23), 6095–6100. http://dx.doi.org/10.1002/2013GL057760.
Smekens, J.-F., Clarke, A.B., Burton, M.R., Harijoko, A., Wibowo, H.E., 2015. SO_2 emissions at Semeru volcano, Indonesia: characterization and quantification of persistent and periodic explosive activity. J. Volcanol. Geotherm. Res. 300, 121–128.
Smets, B., et al., 2014. Detailed multidisciplinary monitoring reveals pre- and co-eruptive signals at Nyamulagira volcano (North Kivu, D.R.C.). Bull. Volcanol. 76 (1). http://dx.doi.org/10.1007/s00445-013-0787-1.
Solomon, S., Daniel, J.S., Neely III, R.R., Vernier, J.-P., Dutton, E.G., Thomason, L.W., 2011. The persistently variable "background" stratospheric aerosol layer and global climate change. Science 333, 866–870.

Spinei, E., Carn, S.A., Krotkov, N.A., Mount, G.H., Yang, K., Krueger, A., 2010. Validation of ozone monitoring instrument SO_2 measurements in the Okmok volcanic cloud over Pullman, WA, July 2008. J. Geophys. Res. 115, D00L08. http://dx.doi.org/10.1029/2009JD013492.

Spiro, P.A., Jacob, D.J., Logan, J.A., 1992. Global inventory of sulfur emissions with $1° \times 1°$ resolution. J. Geophys. Res. 97, 6023–6036.

Stebel, K., Amigo, A., Thomas, H., Prata, A.J., 2015. First estimates of fumarolic SO_2 fluxes from Putana volcano, Chile, using an ultraviolet imaging camera. J. Volcanol. Geotherm. Res. 300, 112–120.

Steinman, B.A., Mann, M.E., Miller, S.K., 2015. Atlantic and Pacific multidecadal oscillations and northern hemisphere temperatures. Science 347, 988–991. http://dx.doi.org/10.1126/science.1257856.

Stoiber, R.E., Williams, S.N., Huebert, B., 1987. Annual contribution of sulfur dioxide to the atmosphere by volcanoes. J. Volcanol. Geotherm. Res. 33, 1–8.

Stothers, R.B., Wolff, J.A., Self, S., Rampino, M.R., 1986. Basaltic fissure eruptions, plume heights, and atmospheric aerosols. Geophys. Res. Lett. 13 (8), 725–728.

Surono, P., Jousset, J., Pallister, M., Boichu, M.F., Buongiorno, A., Budisantoso, F., Costa, S., Andreastuti, F., Prata, D., Schneider, L., Clarisse, H., Humaida, S., Sumarti, C., Bignami, J., Griswold, S.A., Carn, C.O., Lavigne, F., 2012. The 2010 explosive eruption of Java's Merapi volcano — a '100-year' event. J. Volcanol. Geotherm. Res. 241-242, 121–135. http://dx.doi.org/10.1016/j.jvolgeores.2012.06.018.

Symonds, R.B., Rose, W.I., Reed, M.H., 1988. Contribution of Cl- and F-bearing gases to the atmosphere by volcanoes. Nature 334, 415–418. http://dx.doi.org/10.1038/334415a0.

Tabazadeh, A., Turco, R.P., 1993. Stratospheric chlorine injection by volcanic eruptions: HCl scavenging and implications for ozone. Science 260, 1082–1086.

Tamburello, G., Hansteen, T.H., Bredemeyer, S., Aiuppa, A., Tassi, F., 2014. Gas emissions from five volcanoes in northern Chile and implications for the volatiles budget of the central volcanic zone. Geophys. Res. Lett. 41, 4961–4969. http://dx.doi.org/10.1002/2014GL060653.

Teggi, S., Bogliolo, M.P., Buongiorno, M.F., Pugnaghi, S., Sterni, A., 1999. Evaluation of SO_2 emissions from Mt. Etna using diurnal and nocturnal multispectral IR and visible imaging spectrometer thermal infrared remote sensing images and radiative transfer models. J. Geophys. Res. 104 (20), 069–20,079.

Telling, J.W., Flower, V.J.B., Carn, S.A., 2015. A multi-sensor satellite assessment of SO_2 emissions from the 2012–13 eruption of Tolbachik volcano, Kamchatka. J. Volcanol. Geotherm. Res. 98–106.

Textor, C., Graf, H.-F., Herzog, M., Oberhuber, J.M., 2003. Injection of gases into the stratosphere by explosive volcanic eruptions. J. Geophys. Res. 108 (D19), 4606. http://dx.doi.org/10.1029/2002JD002987.

Theys, N., Van Roozendael, M., Dils, B., Hendrick, F., Hao, N., De Mazière, M., 2009. First satellite detection of volcanic bromine monoxide emission after the Kasatochi eruption. Geophys. Res. Lett. 36, L03809. http://dx.doi.org/10.1029/2008GL036552.

Theys, N., Campion, R., Clarisse, L., Brenot, H., van Gent, J., Dils, B., Corradini, S., Merucci, L., Coheur, P.-F., Van Roozendael, M., Hurtmans, D., Clerbaux, C., Tait, S., Ferrucci, F., 2013. Volcanic SO_2 fluxes derived from satellite data: a survey using OMI, GOME-2, IASI and MODIS. Atmos. Chem. Phys. 13, 5945–5968. http://dx.doi.org/10.5194/acp-13-5945-2013.

Theys, N., De Smedt, I., Van Roozendael, M., Froidevaux, L., Clarisse, L., Hendrick, F., 2014. First satellite detection of volcanic OClO after the eruption of Puyehue-Cordón Caulle. Geophys. Res. Lett. 41, 667–672. http://dx.doi.org/10.1002/2013GL058416.

Theys, N., De Smedt, I., van Gent, J., Danckaert, T., Wang, T., Hendrick, F., Stavrakou, T., Bauduin, S., Clarisse, L., Li, C., Krotkov, N., Yu, H., Brenot, H., Van Roozendael, M., 2015. Sulfur dioxide vertical column DOAS retrievals from the Ozone Monitoring Instrument: Global observations and comparison to ground-based and satellite data. J. Geophys. Res. Atmos. 120, 2470–2491. http://dx.doi.org/10.1002/2014JD022657.

Thomas, H.E., Watson, I.M., 2009. Observations of volcanic emissions from space: current and future perspectives. Nat. Hazards 54 (2), 323–354. http://dx.doi.org/10.1007/s11069-009-9471-3.

Thomas, W., Erbertseder, T., Ruppert, T., van Roozendael, M., Verdebout, J., Balis, D., Meleti, C., Zerefos, C., 2005. On the retrieval of volcanic sulfur dioxide emissions from GOME backscatter measurements. J. Atmos. Chem. 50, 295–320.

Thomas, H.E., Watson, I.M., Kearney, C., Carn, S.A., Murray, S.J., 2009. A multi-sensor comparison of Sulphur dioxide emissions from the 2005 eruption of sierra negra volcano, Galápagos islands. Remote Sens. Environ. 113 (6), 1331–1342. http://dx.doi.org/10.1016/j.rse.2009.02.019.

Thomas, H.E., I.M. Watson, S.A. Carn, A.J. Prata, and V.J. Realmuto (2011), A comparison of AIRS, MODIS and OMI sulphur dioxide retrievals in volcanic clouds, Geomatics Nat. Hazard. Risk, 2(3), 217–232. http://dx.doi.org/10.1080/19475705.2011.564212.

Tulet, P., Villeneuve, N., 2011. Large scale modeling of the transport, chemical transformation and mass budget of the sulfur emitted during the April 2007 eruption of Piton de la Fournaise. Atmos. Chem. Phys. 11, 4533–4546. http://dx.doi.org/10.5194/acp-11-4533-2011.

Tupper, A., Kinoshita, K., 2003. Satellite, air and ground observations of volcanic clouds over islands of the southwest Pacific. S. Pac. Study 23 (2), 21–46.

Tupper, A., Wunderman, R., 2009. Reducing discrepancies in ground and satellite-observed eruption heights. J. Volcanol. Geotherm. Res. 186, 22–31.

Tupper, A., et al., 2004. An evaluation of volcanic cloud detection techniques during recent significant eruptions in the western 'ring of fire'. Remote Sens. Environ. 91, 27–46. http://dx.doi.org/10.1016/j.rse.2004.02.004.

Tupper, A., Itikarai, I., Richards, M., Prata, A.J., Carn, S.A., Rosenfeld, D., 2007. Facing the challenges of the international airways volcano watch: the 2004/05 eruptions of Manam, Papua New Guinea. Weather Forecast. 22 (1), 175–191.

Tupper, A., Textor, C., Herzog, M., Graf, H.-F., Richards, M.S., 2009. Tall clouds from small eruptions: the sensitivity of eruption height and fine ash content to tropospheric instability. Nat. Hazards 51, 375–401.

Uchino, O., Sakai, T., Nagai, T., Nakamae, K., Morino, I., Arai, K., Okumura, H., Takubo, S., Kawasaki, T., Mano, Y., Matsunaga, T., Yokota, T., 2012. On recent (2008–2012) stratospheric aerosols observed by Lidar over Japan. Atmos. Chem. Phys. 12, 11975–11984. http://dx.doi.org/10.5194/acp-12-11975-2012.

Urai, M., 2004. Sulfur dioxide flux estimation from volcanoes using advanced spaceborne thermal emission and reflection radiometer — a case study of the Miyakejima volcano, Japan. J. Volcanol. Geotherm. Res. 134, 1–13.

Vaughan, M.A., Powell, K.A., Winker, D.M., Hostetler, C.A., Kuehn, R.E., Hunt, W.H., Getzewich, B.J., Young, S.A., Liu, Z., McGill, M.J., 2009. Fully automated detection of cloud and aerosol layers in the CALIPSO Lidar measurements. J. Atmos. Ocean. Technol. 26, 2034–2050.

Vernier, J.P., et al., 2011. Major influence of tropical volcanic eruptions on the stratospheric aerosol layer during the last decade. Geophys. Res. Lett. 38 (12) (L12,807).

Vernier, J.P., Thomason, L.W., Fairlie, T.D., Minnis, P., Palikonda, R., Bedka, K.M., 2013. Comment on "Large volcanic aerosol load in the stratosphere linked to Asian monsoon transport". Science 339 (6120), 647. http://dx.doi.org/10.1126/science.1227817.

von Glasow, R., Bobrowski, N., Kern, C., 2009. The effects of volcanic eruptions on atmospheric chemistry. Chem. Geol. 263, 131–142.

Wadge, G., Burt, L., 2011. Stress field control of eruption dynamics at a rift volcano: Nyamuragira, D.R. Congo. J. Volcanol. Geotherm. Res. 207, 1–15.

Wallace, P.J., 2005. Volatiles in subduction zone magmas: concentrations and fluxes based on melt inclusion and volcanic gas data. J. Volcanol. Geotherm. Res. 140, 217–240.

Wallace, P.J., Edmonds, M., 2011. The sulfur budget in magmas: evidence from melt inclusions, submarine glasses, and volcanic gas emissions. Rev. Mineral. Geochem. 73, 215–246.

Wallace, P.J., Gerlach, T.M., 1994. Magmatic vapor source for sulfur dioxide released during volcanic eruptions: evidence from mount Pinatubo. Science 265, 497–499.

Wallace, L., Livingston, W., 1992. The effect of the Pinatubo cloud on hydrogen chloride and hydrogen fluoride. Geophys. Res. Lett. 19, 1209–1211.

Walter, D., Heue, K.-P., Rauthe-Schöch, A., Brenninkmeijer, C.A.M., Lamsal, L.N., Krotkov, N.A., Platt, U., 2012. Flux calculation using CARIBIC DOAS aircraft measurements: SO_2 emission of Norilsk. J. Geophys. Res. 117, D11305. http://dx.doi.org/10.1029/2011JD017335.

Wang, J., Park, S., Zeng, J., Ge, C., Yang, K., Carn, S., Krotkov, N., Omar, A.H., 2013. Modeling of 2008 kasatochi volcanic sulfate direct radiative forcing: assimilation of OMI SO_2 plume height data and comparison with MODIS and CALIOP observations. Atmos. Chem. Phys. 13, 1895–1912. http://dx.doi.org/10.5194/acp-13-1895-2013.

Waters, J.W., et al., 2006. The earth observing system microwave limb sounder (EOS MLS) on the aura satellite. IEEE Trans. Geosci. Remote Sens. 44 (5), 1075–1092.

Watson, I.M., Realmuto, V.J., Rose, W.I., Prata, A.J., Bluth, G.J.S., Gu, Y., Bader, C.E., Yu, T., 2004. Thermal infrared remote sensing of volcanic emissions using the moderate resolution imaging spectroradiometer. J. Volcanol. Geotherm. Res. 135, 75–89.

Waythomas, C.F., Scott, W.E., Prejean, S.G., Schneider, D.J., Izbekov, P., Nye, C.J., 2010. The 7–8 August 2008 eruption of Kasatochi Volcano, central Aleutian Islands, Alaska. J. Geophys. Res. 115, B00B06. http://dx.doi.org/10.1029/2010JB007437.

Westrich, H.R., Gerlach, T.M., 1992. Magmatic gas source for the stratospheric SO_2 cloud from the June 15, 1991 eruption of Mount Pinatubo. Geology 20, 867–870.

Wigley, T.M.L., 2006. A combined mitigation/geoengineering approach to climate stabilization. Science 314, 452–454. http://dx.doi.org/10.1126/science.1131728.

Winker, D.M., Vaughan, M.A., Omar, A., Hu, Y., Powell, K.A., Liu, Z., Hunt, W.H., Young, S.A., 2009. Overview of the CALIPSO mission and CALIOP data processing algorithms. J. Atmos. Ocean. Technol. 26, 2310–2323.

Winker, D.M., Liu, Z., Omar, A., Tackett, J., Fairlie, D., 2012. CALIOP observations of the transport of ash from the Eyjafjallajökull volcano in April 2010. J. Geophys. Res. 117, D00U15. http://dx.doi.org/10.1029/2011JD016499.

Wright, R., Carn, S.A., Flynn, L., 2005. A satellite chronology of the May 2003 eruption of Anatahan volcano. J. Volcanol. Geotherm. Res. 146, 102–116.

Yang, K., Krotkov, N.A., Krueger, A.J., Carn, S.A., Bhartia, P.K., Levelt, P.F., 2007. Retrieval of large volcanic SO_2 columns from the aura ozone monitoring instrument: comparison and limitations. J. Geophys. Res. 112, D24S43. http://dx.doi.org/10.1029/2007JD008825.

Yang, K., Krotkov, N.A., Krueger, A.J., Carn, S.A., Bhartia, P.K., Levelt, P.F., 2009a. Improving retrieval of volcanic sulfur dioxide from backscattered UV satellite observations. Geophys. Res. Lett. 36, L03102. http://dx.doi.org/10.1029/2008GL036036.

Yang, K., Liu, X., Krotkov, N.A., Krueger, A.J., Carn, S.A., 2009b. Estimating the altitude of volcanic sulfur dioxide plumes from space-borne hyper-spectral UV measurements. Geophys. Res. Lett. 36, L10803. http://dx.doi.org/10.1029/2009GL038025.

Yang, K., Liu, X., Bhartia, P.K., Krotkov, N.A., Carn, S.A., Hughes, E., Krueger, A.J., Spurr, R., Trahan, S., 2010. Direct retrieval of sulfur dioxide amount and altitude from spaceborne hyper-spectral UV measurements: theory and application. J. Geophys. Res. 115, D00L09. http://dx.doi.org/10.1029/2010JD013982.

Yang, K., Dickerson, R.R., Carn, S.A., Ge, C., Wang, J., 2013. First observations of SO_2 from the satellite Suomi NPP OMPS: widespread air pollution events over China. Geophys. Res. Lett. 40. http://dx.doi.org/10.1002/grl.50952.